VISUAL-INS USING A HUMAN OPERATOR AND CONVERTED MEASUREMENTS

THESIS

Turner J. Montgomery, Captain, USAF

AFIT-ENG-MS-16-M-036

DEPARTMENT OF THE AIR FORCE
AIR UNIVERSITY

AIR FORCE INSTITUTE OF TECHNOLOGY

Wright-Patterson Air Force Base, Ohio

AFIT-ENG-MS-16-M-036

VISUAL-INS USING A HUMAN OPERATOR AND CONVERTED MEASUREMENTS

THESIS

Presented to the Faculty

Department of Electrical and Computer Engineering

Graduate School of Engineering and Management

Air Force Institute of Technology

Air University

Air Education and Training Command

in Partial Fulfillment of the Requirements for the

Degree of Master of Science in Electrical Engineering

Turner J. Montgomery, B.S.E.E.

Captain, USAF

March 2016

AFIT-ENG-MS-16-M-036

VISUAL-INS USING A HUMAN OPERATOR AND CONVERTED MEASUREMENTS

THESIS

Turner J. Montgomery, B.S.E.E.
Captain, USAF

Committee Membership:

Dr. Meir Pachter
Chair

Dr. Scott J. Pierce
Member

Dr. John F. Raquet
Member

AFIT-ENG-MS-16-M-036

Abstract

A method for pilot-assisted Inertial Navigation System (INS) aiding is explored in which the pilot identifies and tracks a ground feature of unknown position over a short measurement epoch using an Electro-Optical (E/O) sensor. One then refers to Visual-INS. In contrast to current research trends, a human operator is entrusted with visually tracking the ground feature. In addition, a less conventional measurement linearization technique is applied to generate "converted" measurements of the feature position from successive bearing measurements and the INS estimated aircraft position. A linear regression algorithm is then applied to the converted measurements providing an estimate of the INS horizontal velocity error and accelerometer biases. At the completion of the measurement epoch, the INS is corrected by subtracting out the estimated errors. Aiding the INS in this manner provides a significant improvement in the accuracy of the INS-provided aircraft navigation state estimates when compared to those of a free/unaided INS. A number of scenarios are simulated including with and without a constrained flight path, with single vs. multiple ground feature tracking sessions, and with a navigation vs. tactical grade INS. Applications for this autonomous navigation approach include navigation in Global Positioning System (GPS) denied environments and/or when RF emitting/receiving sensors are undesirable.

To my wife, for your unwaivering love and support throughout the course of this escapade I am forever grateful. To my daughter, coming home to your laughter and smiles was the highlight of every day. To my daughter joining us in April, your mother and sister put up with a lot this past year-and-a-half, so try to give them a break. This is for you three.

Acknowledgements

I must thank my research advisor, Dr. Meir Pachter, whose top priority is always furthering the eduction of his students, and whithout whom this research could not have happened. This work is a testment to his teaching, mentorship, and patience.

Table of Contents

List of Figures

List of Tables

VISUAL-INS USING A HUMAN OPERATOR AND CONVERTED MEASUREMENTS

I. Introduction

"I hate GPS. The idea that we are all hooked to a satellite... in a semi-synchronous orbit that doesn't work in certain circumstances... is ridiculous."

—Ashton Carter, U.S. Secretary of Defense [1]

Modern navigation is dominated by Global Navigation Satellite System (GNSS), predominately the Global Positioning System (GPS) operated by the U.S. Air Force. Its ease of use, the low cost and small form-factor of its user segment, and its long-term accuracy are among the many reason few aircraft, water vessels, or even land vehicles—military or civilian—navigate without it. The GPS is truly remarkable; however, as Secretary Carter lamented in the quote from a June 2014 interview, it is not without flaws. The long-term outlook of military navigation, he went on to assert, is not in expensive and inherently vulnerable orbiting satellites but in highly-accurate gyroscope and accelerometer Micro-Electrical Mechanical Sensors (MEMS) integrated into a new class of Inertial Navigation System (INS) [5].

Although many experts do not see GPS going away anytime soon, there is a clear need for alternative Position Navigation and Timing (PNT) technology to supplement the GPS, a view shared by many top Air Force leaders. General William Shelton and Gen John Hyten, former and current commanders of US Air Force Space Command (AFSPC), respectively, both recognize the risk of GPS dependency. As they have stated, the U.S. Air Force and her sister services must get off the GPS-only solution by implementing a more resilient/robust, multi-faceted approach to PNT. Advanced MEMS-based inertial systems are part of the

---

[1]from a June 2014 interview with the podcast a16z [5].

solution, but not the lone solution. Furthermore, although in active development at DARPA and elsewhere, adequate MEMS technology is likely years away and is not a short-term solution [12, 33]. Therein lies the ultimate purpose of this research: develop a short-term solution for a robust navigation system that supplements GPS. This research proposes and develops an INS system aided by vision in the form of a human-aided monocular Electro-Optical (E/O) system, which will provide a sufficiently accurate navigation solution when the GPS is compromised. This research will demonstrate, via MATLAB simulation, the developed method and characterize its effectiveness.

1.1 Problem and Approach

In exploring GPS alternatives, one must consider the INS. The INS is essential to the navigation of modern aircraft. It provides a self-contained, truly autonomous navigation solution impervious to jamming, spoofing, and environmental factors. However, the free or unaided INS suffers from drift or error growth over time rendering it unreliable for long-duration navigation. The rate of error growth depends on the quality of the INS. Alone, the INS is not a viable navigation system. However, when integrated with other instrumentation, the INS error can be constrained, and it can provide a very accurate and reliable navigation solution over long durations. Unsurprisingly, the GPS itself is a popular choice for INS aiding. As earlier mentioned, the user segment hardware is small and inexpensive, and navigation solution it provides is very accurate with errors commonly less than a few meters —depending on Geometric Dilution of Precision (GDOP), the environment, and other factors. However, GPS availability is not always assured. The GPS is vulnerable to jamming and spoofing; consequently, when integrated into the navigation solution, it compromises the autonomy and integrity of the overall navigation system.

Research efforts seeking alternative, passive aiding sources have recently turned to optical sensors and computer vision. The increase in computing power and development of auto-

mated feature tracking software, such as Scale Invariant Feature Transformation (SIFT), combined with the availability of digital cameras, makes Visual-INS (V-INS) an enticing option [7]. Furthermore, optical sensors are passive, non-radiating and are not susceptible to traditional Electronic Warfare (EW) attacks and are not dependent on outside sources of information, an aircraft navigation system to maintain autonomy. The possibility of tightly coupled INS and vision navigation systems has been explored with promising results [6, 23, 40]. However, current computer vision and Simultaneous Localization and Mapping (SLAM) techniques often struggle in "dynamic environments, in environments with too many or very few salient features, during erratic movements of the camera and when partial or total occlusions of the sensor occur" [7]. It is generally the same problem that also plagues Automatic Target Recognition (ATR); automated imaging algorithms struggle in operational enthronements [30]. Consequently, it remains an active field of research. Near-term solutions may employ human-aided techniques to overcome the shortcomings of the purely automated systems.

This work seeks a V-INS unencumbered by the limitations of current fully autonomous solutions, one which may be implemented in aircraft immediately with minimal system modification. It diverges from contemporary research in that the pilot or navigator is in the loop and, over a short measurement epoch, manually tracks a single ground feature relying on the innate pattern recognition ability of humans. In this way, serious drawbacks of automated feature tracker are avoided, in particular, the inevitability of false matches and image registration problems. Using an available E/O imaging system (e.g., Sniper or LANTIRN), the pilot/navigator, when manually tracking the ground feature while the aircraft is flown by the autopilot, obtains isochronal measurements of the bearings to a ground feature, from which the aircraft's horizontal velocity components' errors and accelerometer biases are estimated. At the end of the measurement epoch, the minimum variance estimate of the aircraft horizontal velocity error is calculated in batch using linear regression, and the

horizontal velocity measurements provided by the INS are corrected. Thus, the INS provided estimates of horizontal velocity will be improved. Since velocity is the derivative of position, an improved estimate of the aircraft's future position is also obtained. In addition, because velocity is the integral of acceleration, by estimating the accelerometers' biases, the future error in velocity will by reduced even more, consequently the error in position is further reduced.

The proposed V-INS operates under the assumption that the position of the tracked ground features is unknown. However, if the position of the ground features is known, the V-INS could also supplement the traditional INS update technique of obtaining position fixes from check points. If the feature position is known, INS would receive both a position and velocity update. This would substantially decrease the position error at the end of the scenario when compared to either the V-INS or check point position alone. In addition, the more measurement epochs accomplished, the greater the aiding benefit. Demonstration and evaluation of the herein developed V-INS was accomplished using MATLAB simulations. Multiple aiding scenarios were simulated, including one which exploits the correlation between the INS position and velocity errors, one which includes multiple measurement epochs, and one which replaces the navigation-grade INS with a less accurate tactical-grade inertial system.

The human-in-the-loop V-INS navigation method was previously investigated in [19] where the measurement equation was linearized—the measurement equation associated with bearing measurements is nonlinear. In this paper the measurement equation is "linearized" by reverting to the use of converted measurements generated from the distance of the aircraft from the ground feature; the INS-provided aircraft position and the measured bearings and altitude are taken at face value. This is an adaption of "linearization" method which is sometimes used in radar tracking and referred to as converted measurements [14]. Only the measurement errors are linearized.

1.2 Thesis Organization

Following the introduction, Chapter II delivers a brief review of the navigation concepts and underlying modeling and estimation principles considered in this research. It next provides a sample of current research in the area of INS and visual aiding tracing developments/contributions over the last decade and explains how this research ties in and advances the field. In Chapter III the human-in-the-loop V-INS aiding method is developed and the stochastic system models derived. The simulations designed to demonstrate and evaluate/characterize the V-INS are described. Chapter IV presents the simulation results and attempts to analyze and explain the observed performance. Finally, Chapter V summarizes the research emphasizing its potential impact on real-world operations and suggests specific ideas to advance the research.

II. Background

Chapter II begins by providing the physical and mathematical background necessary to develop the key aspects of the research herein. It presents a high-level review of relevant concepts in the fields of navigation (particularly inertial navigation), computer vision, state space and stochastic modeling, and estimation that are essential to the research. The second portion of the chapter presents a brief review of current V-INS research is provided. This serves to both bring the reader up to speed regarding research trends of the last decade and demonstrate and differentiate the contributions of this research to the larger V-INS field. The bulk of this chapter is derived from [36] [2] [18] [4] [1]; each provide an excellent and highly recommended discussion of their respective topics.

2.1   Notation

The following list defines the notation used throughout this work.

Variables

Scalars (lowercase, italicized): x

Vectors (lowercase, boldface): $\mathbf{x}$

Matrices (capitalized, boldface): $\mathbf{X}$

Estimated value: $\hat{x}$ (hat accent)

Element of a matrix (i^{th} row and the jth column): $\mathbf{X}_{(i,j)}$

Mathematical Operators

Transpose: $[\cdot]^{\text{T}}$

Expectation: $E[\cdot]$

Time derivative: $[\dot{\cdot}]$

Matrix exponential: $e^{[\cdot]}$

Reference Frames

Vector frame of reference: $\mathbf{x}^{(b)}$ (superscript frame identifier in parentheses)

Relative vector motion: ω_{ib} (motion of the right subscript relative to the left subscript)

Direction Cosine Matrix (DCM): $\mathbf{C}_b^i$ (rotate from subscript frame to superscript frame)

Aircraft body frame identifier: b

Earth-Centered Earth-Fixed frame identifier: e

Earth-Centered inertial frame identifier: i

North-East-Down (NED) navigation frame identifier: n

Camera frame identifier: c

2.2 Reference Frames and Coordinate Transforms

Modern navigation, especially inertial navigation, requires well-defined coordinate reference frames which give spacial relevance to physical navigation states. Coordinate transforms allow vectors represented in a particular reference frame to be represented relative to a different reference frame. The reference frames used in this research are orthogonal, right-handed Cartesian frames. Each is identified and defined below.

Inertial Frame.

The inertial frame is the frame of Sir Isac Newton, the static frame in which Newton's laws of motion are rooted. Though the true inertial frame has no fixed origin, for Earthbound

navigation it is the convention (and quite convenient) to place an inertial frame origin at the Earth's center. Conventionally, the x-axis is aligned with the first star of the constellation Ares, the z-axis is aligned with the Earth's polar axis, and the y-axis is orthogonal to both, see Figure 1.

Earth-Centered Earth-Fixed Frame.

The Earth Centered Earth Fixed (ECEF) is fixed to the Earth and rotates with respect to the Earth-Centered inertial frame. Its origin is at the Earth's center of mass. The z-axis is aligned with the Earth's polar axis, the x-axis extends through the intersection of the Equator and Prime Meridian, and the y-axis is orthogonal to both following the right-handed convention. It rotates with the Earth ($\omega_{ie} = \frac{2\pi \text{ rad}}{23.93 \text{ hr}}$), see Figure 1.

Navigation Frames.

Navigation frames are local, geographic frames in which relative measurements of a navigation system's position, velocity, and orientation are made. The *vehicle-fixed* navigation frame has its origin at the navigation system, and the axes (x, y, and z) are conventionally defined in either the East-North-Up (ENU) or the NED direction. The *down* and *up* directions are aligned with and opposite to the gravity vector, respectively. The frame is attached to and moves with the navigation system. In contrast, the Earth-fixed navigation frame has its origin located at a predefined point, often on the Earth's surface and at the vehicle's starting location. Like the vehicle-fixed frame, its axes are aligned in the ENU or NED directions, but it does not move with the vehicle, see Figure 1.
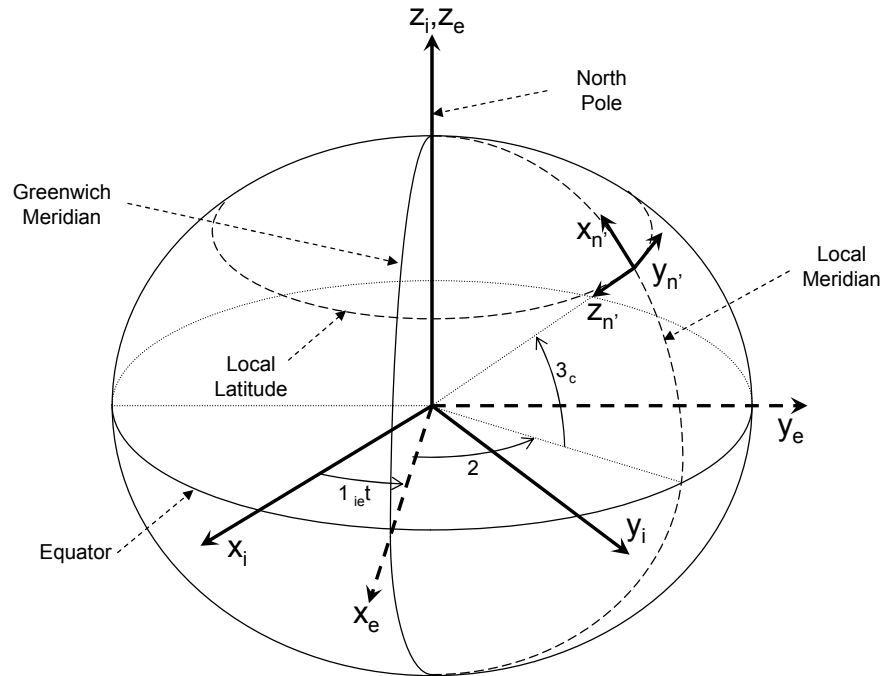
Figure 1. Earth-Fixed Inertial Frame, Earth-Centered Earth-Fixed Frame, and NED Navigation Frame denoted with subscripts [40]

Body Frame.

Body frames are tied to the reference vehicle. They shares an origin with the vehicle-fixed navigation frame, but axes are aligned with physical components of the vehicle. Conventionally for aircraft, the body frame of fixed-wing aircraft have the x-axis aligned with the fuselage pointing out the nose, the y-axis aligned with the right wing, and the z-axis pointing down orthogonal to the others, as indicated in Figure 2.
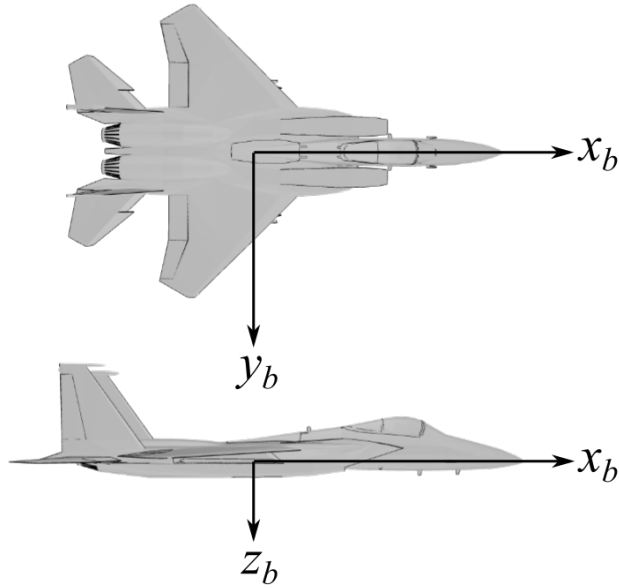
Figure 2. Aircraft Body Frame

Camera Frame and Image Frame.

The camera frame is a reference frame with origin at the optical center of the camera or E/O sensor. Its z-axis extends out of the camera aligned with the focal length and perpendicular to the focal plane or the image frame. An object in the image frame is the two-dimensional projection of that object from the three-dimensional world and may be referenced relative to the camera frame; the object's z axes coordinate is equal to the camera focal length [10], see Figure 3. Conventionally, the x-axis points up and the y-axis points to the right; although, this may vary among different texts.
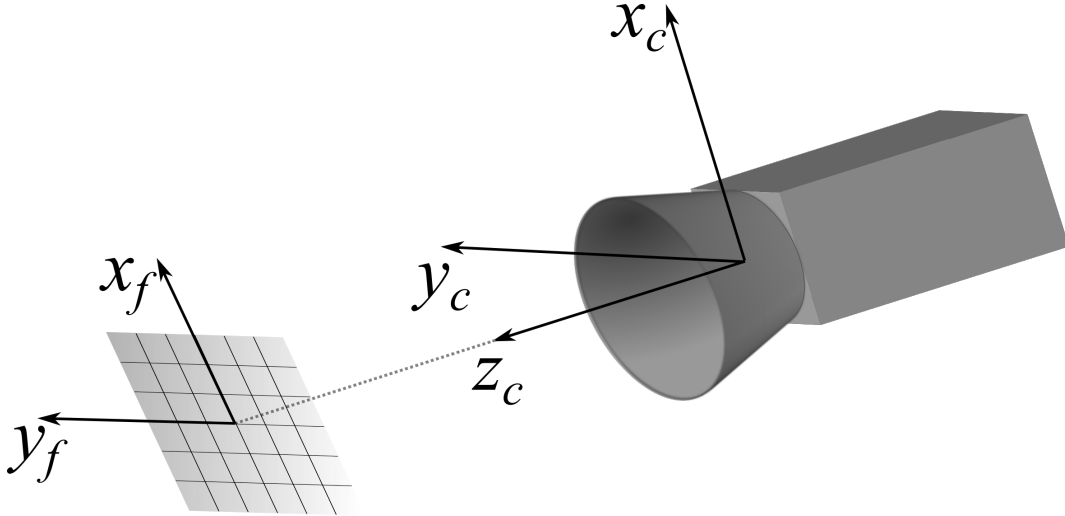
Figure 3. Camera Frame (right) and Image Frame (left)

Coordinate Transforms.

Often vector quantities given relative to a particular reference frame require conversion to another reference frame. This is quite common in navigation when vehicle position, velocity, acceleration, or orientation are not available in the desired frame. For example, an INS, as described in a later section, measures specific force along vehicle's body frame, which must first be transformed into the inertial frame in order to navigate. Coordinate transforms allow the transformation of vectors from one reference frame to another. Common transform methods include Euler angle rotations, DCMs, and quaternions. In this research only the DCM is used.

2.3   Dead Reckoning, Inertial, and Vision Navigation

Dead Reckoning.

Dead Reckoning (DR) is one of the earliest and simplest forms of navigation. It provides a method for determining one's position, direction or heading to destination, and time of arrival from basic measurements of velocity, heading, and time [38]. Prior to the development

of accurate, seafaring clocks in the mid-18th century, DR was the primary means of long distance sea navigation and was used by explorers such as Columbus. In 1927 Charles Lindbergh completed his illustrious, nonstop transatlantic flight from New York to Paris using DR, a testament to its efficacy [15]. In its simplest form, DR consists of estimating the distance traveled from a known starting point by multiplying one's ground speed by time traveled. The distance traveled, combined with ground track angle, gives one's new position relative to the starting point.

In practice, DR is complicated by many factors, most notably wind drift. The wind vector (wind speed and direction) affects an aircraft's ground speed and track. Aviators in the pioneering decades of powered flight were limited to airspeed indicators and magnetic compasses, however, which measure only air speed and true heading (the direction in which the aircraft is pointed), respectively. The relationship between the aircraft ground speed and track (ground vector), wind vector, and air speed and true heading (air vector) is illustrated in the "wind triangle" in Figure 4.
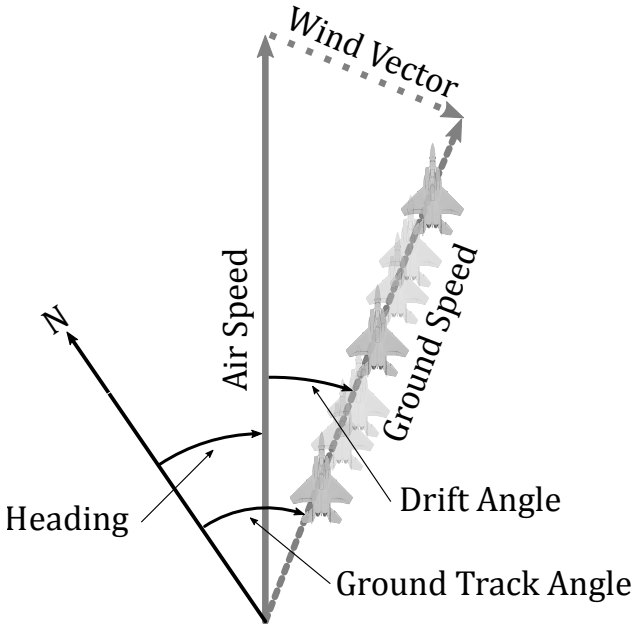
Figure 4. The wind triangle consists of three vectors: air vector, ground vector, and wind vector. Having two vectors allows for the third to be mathematically computed.

To compute the ground vector, aviators required both the air speed (available from on-board air speed indicator and magnetic compass) and the wind vector. Local weather reports could provide current wind conditions, but these were not always accurate and could change quickly rendering the measurements useless, especially for missions of long duration. One method used by aviators to determine the wind vector and ground speed from within the cockpit while in flight involved making a series of measurements of a fixed landmark using a drift indicator or driftmeter. A variety of such instruments existed; the simplest consisted of lines marked on the aircraft, usually on the wings or tail, at increasing angles as in Figure 5a [27]. By noting the drift line corresponding to the path of a landmark, the aviator obtained an estimate of the wind direction. More advanced drift meters were later developed including the Gatty drift indicator in 1930, Figure 5b, and the gyro-stabilized B-6 driftmeter, Figure 5c, in the 1940s and used into the mid 1960s. Instrument stabilization increased the accuracy of readings, especially in turbulent air.
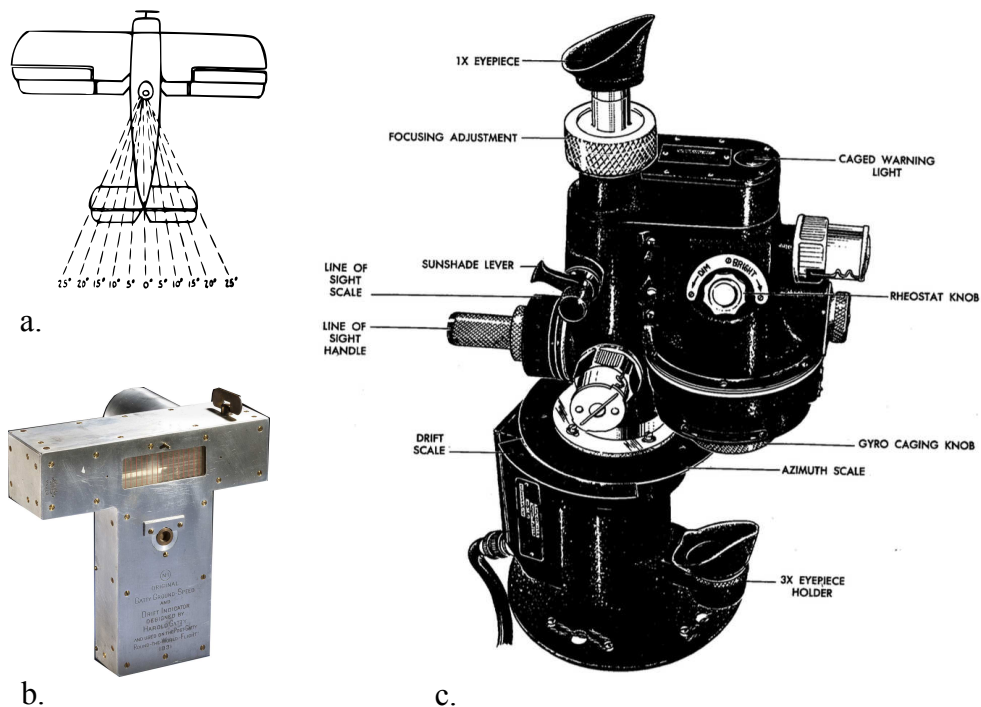
Figure 5. a. Drift lines on the tail [27] b. Gatty drift indicator[1] c. B-6 driftmeter [38]

Despite differences in design and accuracy, drift indicator functioned on the same principles. The schematics of a conceptual driftmeter sight plate are shown in Figure 6. It consists of a transparent plate with several parallel "drift lines" perpendicular to two outer "timing lines". The instrument is positioned to provided the navigator with a view of the terrain directly beneath the aircraft. To measure wind drift and ground speed, the pilot first holds a steady heading and airspeed. As the aircraft overflies a landmark, the navigator rotates the plate to align the drift lines with the landmark's path. The angle of the rotation as measured on the plate is the aircraft's drift angle due to wind. The navigator also notes the time taken for the landmark to cross between the two timing lines, from which he or she may calculate the ground speed geometrically using the aircraft's absolute altitude (height above ground level) and the distance between the timing lines on the transparent plate. Without such measurements, relying solely on the air speed indicator, the aircraft would "drift" significantly from DR calculated track.
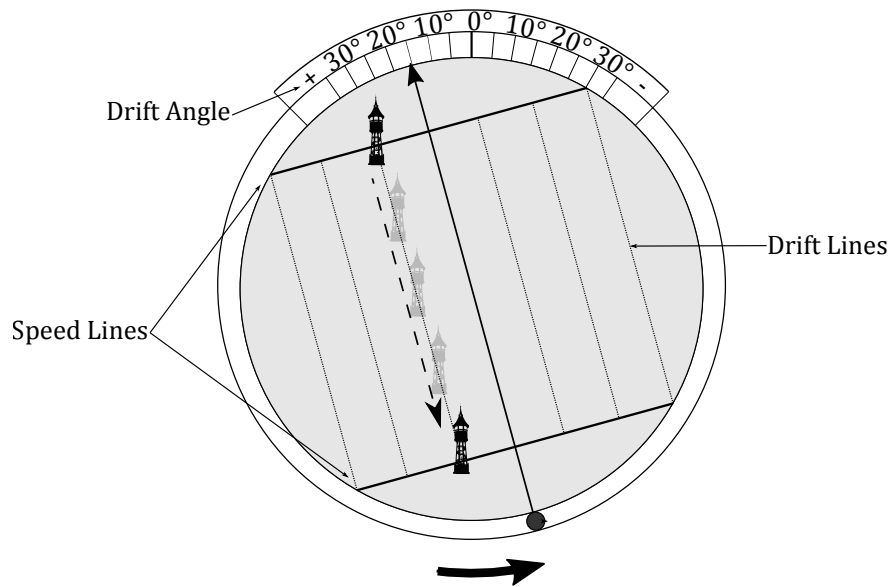
Figure 6. The navigator rotates the plate of the driftmeter until the drift lines are aligned with the path of a stationary landmark

---

[1]National Air and Space Museum, Smithsonian Institution:
http://timeandnavigation.si.edu/multimedia-asset/prototype-gatty-drift-indicator

It is noteworthy that even with the ability to determine the ground speed and track, DR navigation suffered from other errors including error in instrumentation accuracy. Because DR is essentially an integration of velocity, even a small error in the ground speed will cause, over time, errors to accumulate in position. Therefore, DR navigation required additional aiding to be viable for all but short flights. Among the many DR navigation aiding methods available to aviators of the mid 20th century included map reading (or piloting), celestial navigation, and radio based systems (i.e., radar fixes, long range (LORAN), and VHF Omni directional Radio (VOR)) [38].

The Inertial Navigation System.

The INS is a modern day, high-tech DR system. Although they may vary greatly in form, cost, and accuracy, any INS comprises the same fundamental design: three orthogonally arranged accelerometers and three orthogonally arranged gyroscopes. The foundations of the INS are set in the development of the laws of force and motion in the 18th century and the development and demonstration of gyroscopes in the late 19th and early 20th centuries. By the late 1930, technological advancements in accelerometer and gyroscopic sensors improved enough to permit the first practical inertial guidance systems, which was used on the German V2 rockets during World War II [21]. Development continued, and by the 1960s, the INS was standard aboard US military aircraft, ship, and submarines [36].

Early INS models consisted of expensive, bulky platform-stabilized and gimbaled sensors that were difficult to maintain. However, solid-state technology led to the development of the strapdown INS. The strapdown INS costs far less than traditional gimbaled systems. In addition, they are much smaller and lighter, do not suffer from gimbal lock, and have fewer moving parts requiring less maintenance. Optical gyroscopes, including the ring laser type first developed in the 1960s, helped pave the way for the strapdown system. In the last three decades, advancements in MEMS technology have enabled more accurate, smaller silicon chip

based accelerometers and gyroscopes. The relative low cost and small form-factor combined with high accuracy of strapdown systems make them the dominant design of modern day. Nearly all modern aircraft use a version of the strap-down INS, and it is a strapdown INS considered in this research[2]. A brief development of fundamental INS mechanization and error analysis follows providing sufficient background to develop the research herein. For a far more in-depth discussion of the INS seek [2, 36].

Inertial Navigation Systems: Fundamental Strapdown Mechnization.

The INS mechanization equations provide the desired vehicle navigation states (position, velocity, and attitude) from the accelerometer and gyroscope outputs and fundamental kinematics and laws of motion. The accelerometers found in the INS measure specific force along their respective axes and the gyroscopes measure angular rate of change. The specific force is a combination of all forces acting on an aircraft (or any vehicle), including its own propulsion and gravity. The accelerometers make no distinction between acceleration due to gravity and acceleration from other sources. However, by subtracting out an estimate of the gravity component the acceleration of the aircraft is obtained. By integrating the vehicle acceleration, the velocity is obtained, and by integerating a second time, the vehicle position is obtained. In their simplest form, relative to an inertial frame, the dynamics can be expressed as in Equation (1) and Equation (2), where $\mathbf{v}$ is the vehicle velocity and $\mathbf{p}$ is vehicle position. The vectors $\mathbf{f}$ and $\mathbf{g}$ are the specific force and gravity acceleration, respectively. Integrating Equation (1) and Equation (2) yields vehicle velocity and position, respectively.

$$\dot{\mathbf{v}}^{(i)} = \mathbf{f}^{(i)} + \mathbf{g} \tag{1}$$

---

[2]It is worth noting that the most accurate platform stabilized mechanical systems outperform strapdown systems from an accuracy standpoint. However, technological advancement continues to close that gap.

$$\dot{\mathbf{p}}^{(i)} = \mathbf{v}^{(i)} \tag{2}$$

The accelerometers, however, measure specific force in the body frame, $\mathbf{f}^{(b)}$. Thus, to obtain specific force in the inertial frame, the vector must be rotated into the inertial frame. This may be accomplished by pre-multiplying the vector by a DCM:

$$\mathbf{f}^{(i)} = \mathbf{C}_b^i \mathbf{f}^{(b)} \tag{3}$$

where $\mathbf{C}_b^i$ is derived from the gyroscope measurements of angular rate of change by solving the ordinary differential equation[3]:

$$\dot{\mathbf{C}}_b^i = \mathbf{C}_b^i \Omega_{ib}^b \tag{4}$$

The matrix Ω_{ib}^b is the skew symmetric matrix form of the vector $\omega_{ib}^b = (\omega_x, \ \omega_y, \ \omega_z)^{\mathrm{T}}$, the angular rate of change around each axis as measured by the corresponding gyroscope:

$$\Omega_{ib}^b = \begin{bmatrix} 0 & -\omega_z & \omega_y \\ \omega_z & 0 & -\omega_x \\ -\omega_y & \omega_x & 0 \end{bmatrix} \tag{5}$$

The reference frame in which one navigates dictates the form of mechanization equations. In practice, terrestrial navigation occurs on a rotating reference frame; thus, a more careful analysis is required to account for the forces apparent from the motion of the reference frame itself. Thus, the phantom Coriolis acceleration and centripetal acceleration must be accounted for:

$$\dot{\mathbf{v}}^{(n)} = \mathbf{C}_b^n \mathbf{f}^{(b)} - [2\omega_{ie}^{(n)} + \omega_{en}^{(n)}] \times \mathbf{v}_e^{(n)} + \mathbf{g}_1^{(n)} \tag{6}$$

---

[3]See [2] for a full derivation

where $\mathbf{g}_1^{(n)}$ is the sum of gravity and the centripetal force. The DCM, $\mathbf{C}_b^n$, rotates the accelerometer indicated specific force from the aircraft body reference frame into the navigation frame.

Inertial Navigation Systems: General Error Equations.

The errors sources associated with the strapdown INS are well documented. They include inertial alignment errors, inertial sensor errors, and computational error. The dynamic error equation may be developed using the perturbation of the INS dynamic mechanization equations previously described, and full derivation are found in [2, 36]. Once again, a local-level navigation reference frame is considered. It turns out these equation are quite useful for aiding an INS, precisely what this research accomplishes with computer vision. As will be described, they provide for the modeling and propagation of INS error states, which when integrated with an aiding source allow for a far more accurate navigation solution estimate than the INS provides alone. In fact, the use of error states is used for essentially all terrestrial navigation when using an aided INS [18]. In general, the equations model the errors of nine navigation states (comprising the popular Pinson INS error model [18]): position, velocity, and attitude.

Position Error

$$\delta\dot{\mathbf{p}}^{(n)} = \delta\mathbf{v}^{(n)} \tag{7}$$

Velocity Error

$$\begin{aligned}
\delta\dot{\mathbf{v}}^{(n)} = \ & [\mathbf{f}^{(n)}\times]\boldsymbol{\psi} + \mathbf{C}_b^n\delta\mathbf{f}^{(b)} - (2\omega_{ie}^{(n)} + \omega_{en}^{(n)}) \times \delta\mathbf{v} \\
& - (2\delta\omega_{ie}^{(n)} + \delta\omega_{en}^{(n)}) \times \mathbf{v} - \delta\mathbf{g}
\end{aligned} \tag{8}$$

Attitude Error

$$\delta\dot{\boldsymbol{\psi}} \approx -\omega_{\text{in}}^{(n)} \times \delta\boldsymbol{\psi} + \delta\omega_{\text{in}}^{(n)} - \mathbf{C}_{\text{b}}^{\text{n}}\delta\omega_{\text{ib}}^{(b)} \tag{9}$$

The attitude error term is a vector of the misalignment angles:

$$\delta\boldsymbol{\psi} = (\delta\phi, \delta\theta, \delta\psi)^{\text{T}} \tag{10}$$

which indicate the angle errors about each axes in $\mathbf{C}_b^n$ provided by the INS.

Modeling and estimating the INS error states as opposed to the direct state dynamics is commonplace. The equations are linear, and the high-frequency dynamics of the vehicle need not be modeled, as the INS provides very accurate high-frequency information. The low-frequency error dyanmics require far less computational power due to their low sampling rate.

Vision Navigation.

Visual navigation is conducted with optical sensors and encapsulates a broad assortment of navigation techniques. Digital cameras and other E/O sensors (e.g., infrared) are the most popular choice in recent decades due to the power of computers in processing digital imagery. Figure 7 illustrates a simple digital imaging model in which reflected light enters the sensor through a lens and is focused onto a photon detector and converted to a digital signal.

19
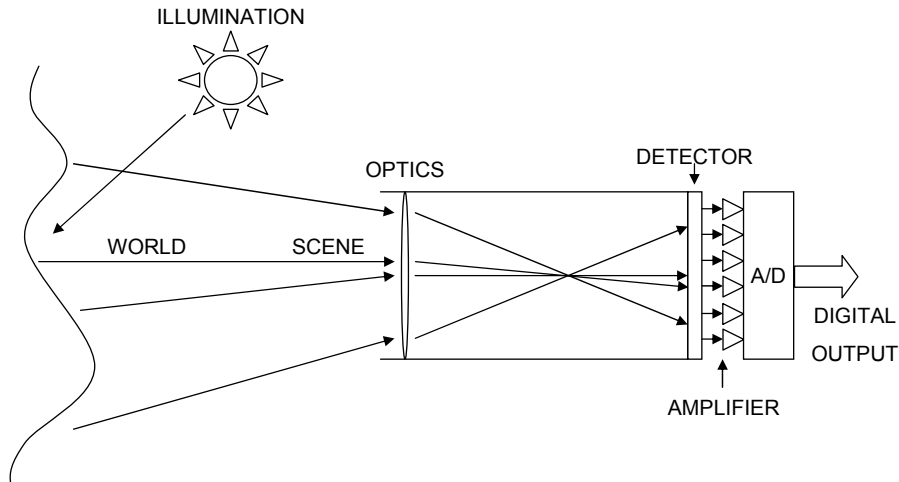
Figure 7. Digital Imaging Model [40]

Multiple vision navigation technologies and techniques exists. [1] proposes a vision navigation classification structure which serves to guide this background discussion. To begin, consider two conditions: known and unknown environments. In the former, the navigation system has a database of known landmarks. Vision navigation in such an environment primarily consists of comparing and matching landmarks in live images with those in the database. The vehicle position and pose are estimated from the stored position of the landmarks, akin to obtaining position fixes from check points. In contrast, operating in an unknown environment means navigation systems have no previous knowledge of the environment or landmarks. Subdividing further, vision navigation systems either operate alone or as part of an integrated, multi-sensor navigation system. This research considers the latter operating in an unknown environment.

Most vision navigation systems operating in unknown environments, regardless of a standalone or integrated design, rely on one of two approaches, Visual Odometry (VO) or SLAM. In VO camera motion is estimated from a series of two-dimensional images using optical flow or feature tracking. At its heart, it is a measurement of velocity, from which position is obtained through integration. SLAM implements feature tracking VO, estimating the vehicle

trajectory, but also estimates the location of all feature landmarks along the way building a map of the environment. In this way, SLAM accounts for the correlation that exists between camera pose and the position of observed features making it more accurate than a purely VO based system but at the cost of computational burden. Both operate on the basic DR principle and accordingly require a known starting point. Like DR or INS navigation systems, errors accumulate with time. Reliable, longterm/long-duration navigation requires aiding of some variety, such as an INS.

Vision navigation approaches require relating the projection of objects in a 2-dimensional image to their position in a world coordinate frame. The pinhole camera model is widely used when representing the relationship between the three-dimensional (3D) scene and two-dimensional projected image [8, 16, 24, 40]. Implementing the fundamental equation of the thin lens, the position of a feature or landmark in the world scene as projected onto the image plane is given by

$$\mathbf{s}^{image} = \left(\frac{f}{s_z^c}\right)\mathbf{s}^c \tag{11}$$

where f is the camera focal length, $\mathbf{s}^c$ is the feature position in the camera reference frame, and s_z^c is the z-axis component of the feature position. The image plane may be notionally inverted and moved to the front of the camera one focal length away, as illustrated in Figure 8, which produces an upright image projection. The position of the feature thus may be derived, with scale ambiguity, from the projected image. That is, the feature may rest in an infinite number of positions along the line of site. Techniques may be employed to resolve the scale including a binocular camera setup or a target ranging sensor. In this research, knowledge of aircraft altitude is employed to that effect.
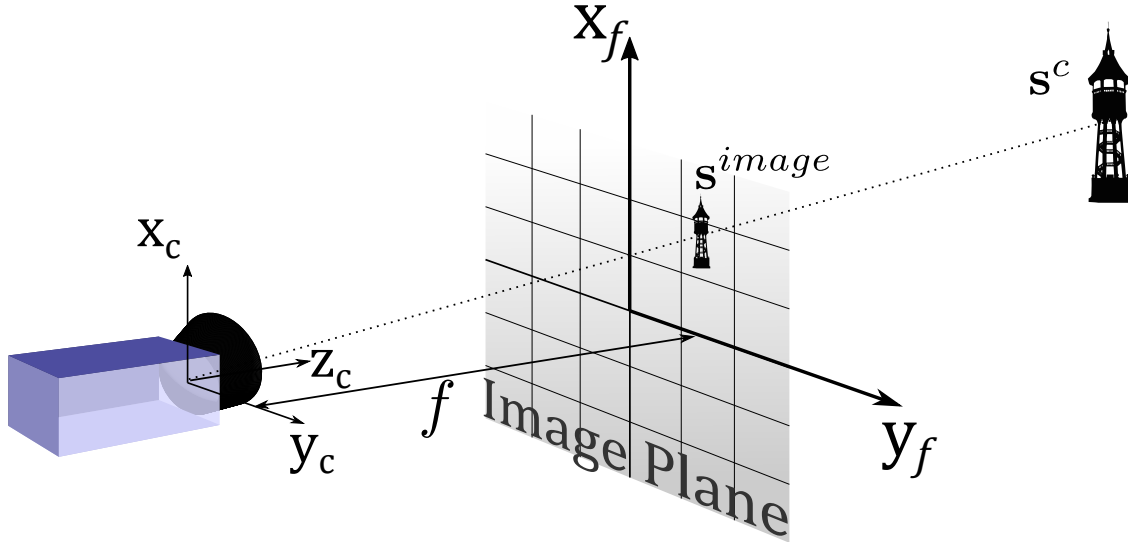
Figure 8. Pinhole Camera Projection Model

2.4   System Modeling

In order to analyze a system, be it tangible or otherwise, it is helpful to model it. By modeling a system mathematically, one can master it—that is, determine the outputs given a set of inputs or determine the inputs that provide the desired outputs. Often, as in the case of navigation, we concern ourselves with the way systems behave with time, the dynamics of a system. Navigation systems, as well as many other physical and non-physical systems, are conventionally modeled in continuous time with systems of differential equations. Further-more, we define system "states" as the quantities/information from the system we desire to analyze. If a system's dynamics are linear, it may be converted to a system of first-order differential equations and modeled in state-space form using matrices with Equation (12), the dynamics equation, and Equation (13), the output or measurement equation.

$$\dot{\mathbf{x}}(t) = \mathbf{A}\mathbf{x}(t) + \mathbf{\Gamma}\mathbf{u}(t) \tag{12}$$

$$\mathbf{z}(t) = \mathbf{H}\mathbf{x}(t) + \mathbf{D}\mathbf{u}(t) \tag{13}$$

where the vectors $\mathbf{x}(t)$, $\mathbf{u}(t)$, and $\mathbf{z}(t)$ are the system's states, inputs, and outputs, respectively. The outputs are typically sensor measurements (e.g., an altimeter outputs a measurements of altitude). The matrices $\mathbf{A}$, $\boldsymbol{\Gamma}$, $\mathbf{H}$, and $\mathbf{D}$ are known as the system or dynamics matrix, the input matrix, the output or observation matrix, and the direct input matrix, respectively, and define the linear relationships among states, outputs, and inputs. Linear systems are especially convenient because the mathematics behind their analysis, control, and estimation are well understood and relatively simple to implement.

The solution to the linear system dynamic equation is given by

$$\mathbf{x}(t) = e^{\mathbf{A}(t-t_0)}\mathbf{x}(t_0) + \int_{t_0}^{t} e^{-\mathbf{A}(t-\tau)}\boldsymbol{\Gamma}\mathbf{u}(\tau)d\tau \tag{14}$$

Unfortunately, the systems found in the real world are never perfectly linear. However, they can often be approximated with linear systems to a useful degree of accuracy through linearization.

Model in Discrete Time.

It is worth noting that the previous development used continuous time. However, any system which incorporates a digital computer will generally require discrete modeling, as is the case with this research. An approximation of the discrete time state-space dynamics converted from continuous time is given by the following difference equation [34]:

$$\mathbf{x}_k = \mathbf{A}_{k-1}\mathbf{x}_{k-1} + \boldsymbol{\Gamma}_{k-1}\mathbf{u}_{k-1} \tag{15}$$

where

$$\mathbf{A}_{k-1} = e^{\mathbf{A}(t_k - t_{k-1})} \tag{16}$$

and

$$\mathbf{\Gamma}_{k-1} = \int_{t_{k-1}}^{t_k} e^{\mathbf{A}(t_k - \tau)} \mathbf{\Gamma} d\tau \tag{17}$$

the subscript 'k' denote the digital time step. It must be assumed that the matrix $\mathbf{A}$ is constant during the small time step interval, Δt, as is the case in the research herein.

Stochastic Modeling.

The systems described thus far are *deterministic*; that is, the system inputs are completely known, the model is perfect, and the solution is exact. This rarely, if ever, happens in the real world. Linearization introduces error into the model, for example, and sensors always exhibit a degree of measurement error. Stochastic modeling, in contrast, adds randomness or noise to the system which account for the unknowns and errors in the model and sensors and more accurately portrays real-world systems. The type of noise added depends on the system, but Gaussian white noise is very common in navigation modeling because the majority of errors (e.g., gyroscope and accelerometers biases) tend to be Gaussian distributed. Equations (18) and (19) show the addition of noise to the linear system's dynamics and measurement equations.

The noise input matrix, $\mathbf{G}$, maps the vector of white noise sources, $\mathbf{w}(t)$, to the states and primarily accounts for model error and system disturbances. The sensor noise vector, $\mathbf{v}(t)$, accounts for error in the sensor measurements.

$$\dot{\mathbf{x}}(t) = \mathbf{A}\mathbf{x}(t) + \mathbf{\Gamma}\mathbf{u}(t) + \mathbf{G}\mathbf{w}(t), \quad \mathbf{w}(t) \sim \mathcal{N}(0, \mathbf{Q}(t)) \tag{18}$$

$$\mathbf{z}(t) = \mathbf{H}\mathbf{x}(t) + \mathbf{v}(t), \quad \mathbf{v}(t) \sim \mathcal{N}(0, \mathbf{R}(t)) \tag{19}$$

The noise sources are zero mean with strengths defined by the covariance matrices $\mathbf{Q}$ and $\mathbf{R}$. Unlike deterministic system, which have an exact solution, the states in stochastic sys-

tems exist as probability distribution. Accordingly, the solutions to stochastic systems with Gaussian distributed noise are completely described by their expected value and covariance.

2.5   Estimation

In a perfect, deterministic world system models are free of imperfections and always provide the exact solution; consequently, sensors and measurement models would serve no purpose and life would be quite dull. However, unavoidable uncertainty in the models and measurements means that exact solutions are unobtainable. The best one can do is estimate the truth value from all the information at hand, namely the measurements and system model, and calculate the corresponding uncertainty, the estimate covariance or standard deviation. Estimation is a gargantuan field in its own right, and there are a plethora of texts on the subject. This section provides a high-level review of the techniques used in this research. For a thorough explanation, three great resources include [4, 18, 34], from which this section is derived.

Linear Regression.

Regression analysis involves modeling the relationship between sets of independent and dependent variables, often called the regressors and predictors, respectively. Linear Regression (LR) applies specifically to situations in which this relationship is linear. LR finds utility in many navigation problems as a method to reduce error in state estimates given multiple observations. The relationship may be expressed in the following form

$$\mathbf{z} = \mathbf{H}\boldsymbol{\theta} + \boldsymbol{\nu} \tag{20}$$

where $\mathbf{z}$ is the predictor, $\boldsymbol{\theta}$ is the regressor, $\mathbf{H}$ is the regression matrix, and $\boldsymbol{\nu}$ is error. Typically, the predictor variables are provided in the form of measurements and the regressor

variables are those we wish to estimate. Numerous methods for estimating the regressors exist. The simplest is probably the method of ordinary least squares (OLS), an unbiased[4] and minimum-variance optimal estimate, which minimizes the sum square of the residual [4]. In this research, the residual is defined as the difference between the measurement and a prediction of what the measurement should be from the system model [18]. The OLS method is valid for Gaussian distributed noise. The regressor variable or parameter is estimated as follows:

$$\hat{\boldsymbol{\theta}} = (\mathbf{H}^\mathrm{T}\mathbf{H})^{-1}\mathbf{H}^\mathrm{T}\mathbf{z} \tag{21}$$

One drawback of OLS is the necessary assumption that all measurements are equally "good", an impractical condition in many real-world scenarios. A small modification to the above equation allows the "weighting" of measurements, giving more value/credence to the more accurate measurements. This form, called weighted least squares, is given in Equation (22).

$$\hat{\boldsymbol{\theta}} = (\mathbf{H}^\mathrm{T}\mathbf{W}\mathbf{H})^{-1}\mathbf{H}^\mathrm{T}\mathbf{W}\mathbf{z} \tag{22}$$

where $\mathbf{W}$ is the weighting matrix. To obtain the optimal, minimum variance estimate (as well as the maximum likelihood estimate it turns out) the inverse of the measurement covariance matrix is used for the weighting matrix [4]. That is, $\mathbf{W} = \mathbf{R}^{-1}$. The estimate uncertainty or covariance is given by

$$\mathbf{P}_{\hat{\boldsymbol{\theta}}} = (\mathbf{H}^\mathrm{T}\mathbf{R}^{-1}\mathbf{H})^{-1} \tag{23}$$

---

[4]The expected value of the regressors estimate equals the regressors: $E[\hat{\boldsymbol{\theta}}] = \boldsymbol{\theta}$

Kalman Filter.

The LR method, as described above, assumes all measurements are available at the time of estimation. However, this is not always the case, especially in dynamic navigation scenarios. The Kalamn filter essentially applies a recursive weighted least squares algorithm, acting on measurements as soon as they become available and updating the estimate accordingly. The filter need only store information from the latest estimate update; it does not need to keep track of all measurements or navigation states for the entire mission duration. When dealing with a lot of measurements, this form of recursive estimation is essential as the amount of data and computational power required to process all stored states, measurements, and covariances quickly grows intractable. As with least squares LR, the traditional Kalman filter requires the dynamics model and measurement equations to be linear and all noise to be white, Gaussian distributed.

The key component to Kalman filtering is the Kalman gain matrix. Essentially, it contains the combined uncertainty information from all previous estimates and is needed to carry-on estimation with new measurements. The Kalman gain provides the minimum mean squared error estimate and is calculated as follows [5]:

$$\mathbf{K}_{k+1} = \mathbf{P}_{k+1}^{-} \mathbf{H}_{k+1}^{T} (\mathbf{H}_{k+1} \mathbf{P}_{k+1}^{-} \mathbf{H}_{k+1}^{T} + \mathbf{R})^{-1} \tag{24}$$

The process begins with initialized states and state covariance matrix, usually at time step $k = 0$. The states and covariance are then propagated in time using the state transition matrix at each time step, as in Equation (25). The Kalman gain is also computed at each time step. Only the most recent state and covariances, along with the Kalman gain, are stored.

---

[5]The superscript '$-$' indicates an estimate or estimate covariance which was propagated to a given timestep but not yet "updated" with newly available information or measurements. The superscript '$+$' indicates an estimate or estimate covariance which has incorporated the latest information or measurements available at a given timestep.

$$\hat{\mathbf{x}}_{k+1}^{-} = \mathbf{\Phi}\hat{\mathbf{x}}_{k}^{+}$$

$$\mathbf{P}_{k+1}^{-} = \mathbf{\Phi}\mathbf{P}_{k}^{+}\mathbf{\Phi}^{T} + \mathbf{Q}_{d}, \quad \text{for} \quad k = 0, 1, 2, ... \tag{25}$$

the state transition matrix, $\mathbf{\Phi}$, is just the discrete dynamic matrix as calculated in Equation (16) that propagates the states from 0 to the next digital time step, $k + 1$.

When new measurements are available, the estimates are updated using the Kalman gain and Equation (26).

$$\hat{\mathbf{x}}_{k+1}^{+} = \hat{\mathbf{x}}_{k+1}^{-} + \mathbf{K}_{k+1}(\bar{\mathbf{z}}_{k+1} - \mathbf{H}_{k+1}\hat{\mathbf{x}}_{k+1}^{-})$$

$$\mathbf{P}_{k+1}^{+} = (\mathbf{I} - \mathbf{K}_{k+1}\mathbf{H}_{k+1})\mathbf{P}_{k+1}^{-}, \quad \text{for} \quad k = 0, 1, 2, ... \tag{26}$$

Non-Linear Estimation.

The methods discussed up to this point assume all linear models; however they can be extended to included non-linear models. There are multiple techniques to deal with problems of non-linearity. Non-linear least squares, for example, uses Taylor series approximations to linearize the system dynamics or measurement equations. Among its many practical applications includes GPS navigation in which it is used iteratively to estimate user position. The Extended Kalman Filter (EKF) is essentially the recursive analog of the non-linear weighted least squares. Additional methods may be found in [3, 4, 17].

Another method to deal with non-linearity is to convert the model parameters in such a way that the model itself need not be linearized, only the error. This can provide a more accurate estimate and decrease computational burden, depending on the scenario. For example, a radar system tracking a target provides measurement in polar coordinates while the target dynamics are often modeled in Cartesian coordinates. Thus, the measurement model is inherently non-linear as the following example demonstrates: A typical, 2-dimensional non-

linear measurement model for the described tracking scenario might be given as in equations (27) and (28),

$$R(x, y) = \sqrt{x^2(t) + y^2(t)} + \delta R(t) \tag{27}$$

$$\theta(x, y) = \tan^{-1}\left(\frac{y(t)}{x(t)}\right) + \delta\theta(t) \tag{28}$$

where R is range and θ is azimuth to target, and the error in the respective measurements, δR and $\delta\theta$, may be modeled as white Gaussian noise of strengths σ_R^2 and σ_θ^2.

An alternative linear measurement equation may be generated using the clean variables as follows:

$$x_k = R_k \cos\theta_k \tag{29}$$

$$y_k = R_k \sin\theta_k \tag{30}$$

Now, the physical measurements are $R_{m_k} = R_k + \delta R_k$ and $\theta m_k = \theta_k + \delta\theta_k$, where the subscript m denotes a measured value yielding equations (31) and (32)

$$x_k = (R_{m_k} - \delta R_k)\cos(\theta_{m_k} - \delta\theta_k) \tag{31}$$

$$y_k = (R_{m_k} - \delta R_k)\sin(\theta_{m_k} - \delta\theta_k) \tag{32}$$

Expanding, neglecting small terms, and rearranging yields

$$R_{m_k}\cos\theta_{m_k} = x_k + \cos\theta_{m_k} \cdot \delta R_k - R_{m_k}\sin\theta_{m_k} \cdot \delta\theta_k \tag{33}$$

$$R_{m_k}\sin\theta_{m_k} = y_k + \sin\theta_{m_k} \cdot \delta R_k + R_{m_k}\cos\theta_{m_k} \cdot \delta\theta_k \tag{34}$$

Thus, the measurement given to the KF is, in matrix notation

$$\mathbf{z_k} = R_{m_k} \begin{pmatrix} \cos\theta_{m_k} \\ \sin\theta_{m_k} \end{pmatrix} \tag{35}$$

The observation matrix is

$$\mathbf{H} = \begin{bmatrix} 1 & 0 & 0 & 0 \\ 0 & 0 & 1 & 0 \end{bmatrix} \tag{36}$$

and the Kalman filter's "linear" measurement equation is

$$\mathbf{z_k} = \mathbf{H} \begin{pmatrix} x_k \\ y_k \end{pmatrix} + \begin{pmatrix} \nu_{1k} \\ \nu_{2k} \end{pmatrix} \tag{37}$$

where ν_k is measurement noise:

$$\nu_k \triangleq \begin{pmatrix} \nu_{1k} \\ \nu_{2k} \end{pmatrix} = \begin{bmatrix} \cos\theta_m & -R_m\sin\theta_m \\ \sin\theta_m & +R_m\cos\theta_m \end{bmatrix} \begin{pmatrix} \delta R \\ \delta\theta \end{pmatrix} \tag{38}$$

Define the matrix

$$\mathbf{M_k} = \begin{bmatrix} \cos\theta_m & -R_m\sin\theta_m \\ \sin\theta_m & +R_m\cos\theta_m \end{bmatrix} \tag{39}$$

The covariance of the measurement noise $E(\nu_k\nu_k^{\mathrm{T}})$ is then

$$\mathbf{R_k} = \mathbf{M_k} \begin{bmatrix} \sigma_R^2 & 0 \\ 0 & \sigma_\theta^2 \end{bmatrix} \mathbf{M_k}^{\mathrm{T}} \tag{40}$$

With a linear dynamics and measurement model, the target may be tracked using a linear Kalman filter. The sensor noise strength matrix, $\mathbf{R}_k$, is dynamic, however, and will change with each new measurement. Such methods are discussed in [14], and a similar method

of measurement conversion and error linearization is employed in this research. As will be explained in great detail in Chapter 3, this research employs a combination of the Kalman filter and batch LR using converted measurement.

2.6   Review of Related Research

Since the proliferation of the INS in the mid 20th century, researchers have sought to overcome its inherent limitations through aiding with additional sensors and navigation instruments. Aiding methods including external velocity measurements, celestial tracking, and basic map reading or using known check points were explored as early as the 1950s [35]. The LORAN-C navigation system was used extensively to reduce INS drift through the 1970s and 1980s, particularly on long-distance missions. Shortly after the development of the GPS in the 1970s and 1980s however, the GPS became the dominant INS aiding method and remains so to this day [32]. The unrivaled accuracy and precision of GPS combined the low unit cost and small size of the user segment solidified its predominance in modern navigation. Unlike the INS, the GPS is not self contained, and its availability is not always assured. Although modernization efforts have strengthened the GPS, it remains vulnerable to spoofing and jamming. Environmental factors also affect the GPS. Multi-path in urban environment can significantly reduce accuracy as can reduced satellite visibility from trees, buildings, and other obstructions. Realizing the vulnerabilities of the GPS, governments and researchers seek an alternative, and vision aided INS is one such alternative. Although first proposed as early as the late 1970s [32], vision aiding of INSs has only recently garnered extensive research bolstered by the advancement of computer vision technology in the 1990s. Due in part to the growing popularity the Unmanned Aerial Vehicle (UAV), the majority of research focuses on automated vision navigation.

What follows is a brief chronological review of germane research contributions to the field over the last fifteen years. The focus is on visual landmark or ground feature tracking applied

to aiding INS systems, specifically involving stationary landmarks of unknown position. It is not exhaustive but presents the primary foundations of the research herein.

Pachter, Polat, and Porter: INS Aiding using Passive, Bearings-only Vision Measurements.

In [25], Polat, under the guidance of his adviser, Dr. Pachter, broke new ground in 2002 with his work on INS aiding using bearing-only measurements of unknown ground features taken with a theoretical gimbaled E/O telescope tracker. Though aiding using position updates from known landmarks, check points, was commonplace, scant modern research explored using unknown landmarks. He assumed no GPS availability and proposed and simulated a method in which five aircraft's angular navigation variables (roll, pitch, yaw, heading and flight path) are estimated using bearings-only measurements to a single, uncharted ground feature. The measurement provided a direct measurement of the aircraft angle of attack and side slip angles, assuming no wind. His simulations demonstrated significant improvement to the estimate of the aforementioned parameters; however, he obtained little direct improvement to positional aircraft navigation state estimates without prior information about the landmark, e.g. position coordinates or range.

Alec Porter expanded on the work of Polat [26], again working under Dr. Pachter. Using a comparable setup, he demonstrated an improvement in the estimated positional navigation state when including measurements form an independent altitude sensor. The advance of digital camera technology and computer vision, however, vectored later research toward automated feature tracking and optical flow techniques using digital camera imagery.

Veth and Neilsen: INS Aiding with SLAM.

In [40], Veth was one of the first researchers to explore a SLAM approach to passive INS aiding with vision. It automated the task of manual feature tracking, applying deep

vision/INS integration. He developed an improved solution to the feature tracking corre-
spondence problem, see Section 2.3, using the aircraft INS and EKF to predict the location
of features in successive image frames. The method constrained the feature detection er-
rors, improving upon similar visual landmark tracking research such as [9]. Experiments
demonstrated navigation state estimates several orders of magnitude smaller using the inte-
grated vision INS than with the free-running INS using low-cost complementary metal-oxide
semiconductor cameras and both a tactical-grade and consumer-grade MEMS Inertial Mea-
surement Unit (IMU).

Neilsen, in [23], expanded on the work of Veth. He implemented the same SIFT algorithm
as Veth but with a monocular camera setup and in a more robust, militaristic environment.
Examining the aided system observability Grammian, Neilsen showed that the setup required
two or more ground features with a priori known locations to achieve full observability and
full INS aiding. In contrast, when limited to a single camera, observability is unachievable
when the position of the tracked ground features are unknown, regardless of the number
of features tracked. Furthermore, Neilsen witnessed no aiding (position/velocity estimate
improvement) when tracking features of unknown position using only bearing measurements
(supporting the earlier results of Polat and Porter [25] [26]). However, by integrating inde-
pendent measurements of altitude and heading, the research showed improved performance.

Mulat, Relyea, and Quarnermyne: Bearing-only Measurement Observability and Monocular SLAM.

In [22, 28, 31] research focused on the observability of feature tracking and the aiding
of an INS through "bootstrapping". Examining the dynamic observability Grammian, it
was ascertained that that full navigation state observability is attainable when at least
two known ground features are tracked. Specifically, [31] performed an in-depth covariance
annalysis. Two assumptions were made: 1) the location of at least two ground features was

known at scenario start and 2) at least two ground features were available in every frame thereafter. It showed that the growth in INS position errors significantly slowed, by 99.5% for horizontal position error, though not eliminated when continuously tracking at least two ground features of unknown position. The technique relied on the SIFT automated feature tracking algorithm and successful image correspondence. A significant contribution of the work was the geometry-based, non-linear measurement equation relating the ground feature in the image plane to the aircraft position:

$$
\begin{pmatrix} x_p \\ y_p \\ z_p \end{pmatrix} = \begin{pmatrix} x \\ y \\ z \end{pmatrix} + \frac{|r_{LOS}|}{\sqrt{x_f^2 + y_f^2 + f^2}} \mathbf{C}_b^n \begin{pmatrix} x_f \\ y_f \\ -f \end{pmatrix} \tag{41}
$$

It is the general measurement equation used by proceeding researchers at AFIT and the basis for the measurement equation used in this research.

Recent SLAM Research.

The latest research into V-INS when considering only landmarks/ground features of unknown position continues to focus near exclusively on improving SLAM for autonomous aircraft. Many recent improvements have been made. In [32], researchers used multiple passes made around landmarks of unknown position to constrain INS divergence/error. The navigation state vector is augmented with multiple estimates of the same landmarks decreasing the estimate covariance of each, thereby constraining the INS divergence. The technique, although demonstrated in a binocular setup, should also apply to the monocular case. Although insightful, one drawback is the required "circling" of landmarks which is not feasible in many applications.

In [16] researchers improved upon the traditional EKF SLAM approach implementing a factored EKF. Flight test confirmed the approach improved numerical stability without

noticeably taxing the navigation computer. Although research continues to improve the SLAM technique in a variety of ways, the specific problem of feature tracking and image correspondence is often overlooked or assumed "solved" as in [32]. In addition, successful flight tests typically occur in highly controlled environments [16] [24]. This implies much research into the correspondence problem is still required for reliability in many real-world applications. Indeed, [13] demonstrated successful motion estimation of a ground system implementing an monocular V-INS, but among their conclusions, researchers highlight the need for solutions to a score of problems including complex visual environments, moving objects, and environmental aberrations. Similarly, in [30] Ratches discusses the problems computer vision has in operational and unpredictable environments underscoring the continued need for human-aided/human-in-the-loop implementation in real-world systems.

Mirabile: Pilot-Assisted V-INS.

In [20], Mirabile and Pachter broke from traditional V-INS methods replacing the automated SLAM approach with a human operator, presumably the aircraft pilot or navigator. By allowing a human operator to select and track the ground feature, the approach side-stepped hurdles innate to current computer vision technology including the image registration/correspondence problem. Aiding was accomplished through a ground speed measurement. Development was based on the idea of early navigators using driftmeters. Mirabile first showed that a ground speed measurement, such as one obtained by a navigator employing a driftmeter, could reduce error at the end of a one-hour flight by up to 60%, if the flight path was constrained. He also demonstrated the validity/robustness of his the simplified INS error model in scenarios of varied aircraft acceleration.

Mirabile continued development considering next an updated E/O system. He tracked a single ground feature while flying wing-level with constant velocity during a short, 10-second epoch and incorporated a barometer for z-channel stabilization. He employed the

same measurement equation of his predecessors, originally derived in [22, 31], and used the linear Kalman filter for estimation. Although theoretically valid for a ground feature located anywhere within the E/O system field of view, only grounds features directly beneath the aircraft were simulated, he examined only aiding in the x (or east) channel. Although the navigation states are not all observable, a respectable reduction in estimate uncertainty at the end of the scenario when compared to a free-running INS was demonstrated. Monte Carlo trials were not executed, but the single-run results he presented demonstrated aiding. Among other advancements, this research will use Monte Carlo trials to strengthen the validity of simulation results.

Advancing the Research.

This work follows directly from that of [19] and Mirabile's immediate predecessors. His results demonstrated the feasibility of the human-in-the-loop V-INS approach. This research develops and implements an alternative approach to the measurement equation. Instead of conventional linearization, the measurement equation is "linearized" by reverting to the use of converted measurements in which the sensor outputs are manipulated algebraically to yield a linear measurement to INS navigation error state relationship. In this way, only the "small" measurement error terms must be linearized, which may be accomplished through perturbation analysis. Theoretically, linearizing only the error terms in the measurement equation, instead of the measurement equations themselves, reduces the overall modeling error, and consequently, the estimation error. This is an adaption of a "linearization" method which is sometimes used in radar tracking and referred to as converted measurements [14].

The new measurement model allows a more accurate V-INS navigation solution. In addition to a new measurement model, the overall method is matured with a more robust simulation, including the addition of ground feature not directly below the aircraft. Estimation of the y-direction error is added, providing a more complete, 3D simulation. Monte

36

Carlo trials are also executed. Such a thorough exploration should provide the results and risk reduction necessary to justify continued research, including simulations enhanced with real-world flight data followed by flight tests.

III. Methodology

The intent of this research is to develop, demonstrate, and characterize a human-in-the-loop, bearings-only measurement approach to the V-INS. The herein developed V-INS will provide an alternative, inertial-based navigation system that is entirely passive and self-contained, which the system accomplishes using a barometer and monocular E/O system to aid an INS. Furthermore, the V-INS will employ a human to assist with E/O operation. This chapter entails a complete, step-by-step development of the V-INS. It then describes the simulations designed to demonstrate and characterize the V-INS.

3.1   V-INS Method Development

Development of the human-in-the-loop V-INS begins with defining a baseline flight scenario in which the system is employed and simulated. This baseline scenario will aid the development of the INS error model and measurement equation. The scenario also provided a model for simulation development; the simulation demonstrated the V-INS and provided for its characterization. Following the initial round of simulations, the baseline scenario was altered to demonstrate other facets of the V-INS method including the benefits of undertaking multiple measurement epochs and the aiding potential of the visual system when paired with a less accurate tactical-grade INS.

Baseline Navigation Scenario.

The baseline navigation scenario considers an aircraft, equipped with a navigation-grade INS, during a one-hour flight along an arbitrary, unconstrained flight path. Because the flight duration is only one hour, the aircraft navigates in a simplified terrestrial navigation frame (Earth-fixed) on a theoretical flat, non-rotating earth. These assumptions significantly impacts the error model development, as will be seen shortly. The aircraft is equipped with

the V-INS system, as well as a basic autopilot capability. The scenario may start in midflight and need not begin at takeoff; however, the navigation system must acquire a precise aircraft Position Velocity Attitude (PVA) solution and near-perfect INS alignment at scenario start. When the scenario begins, the pilot navigates only with the INS, aided by the barometer. A navigation grade INS always requires aiding from an independent altitude source to maintain stability in the vertical channel [2, 36]. A Kalman Filter (KF) integrates the unaided INS solution with the barometer altitude measurements. Although a number of altimeters are available, a barometer maintains the passive nature of the V-INS and does not transmit Radio Frequency (RF). Coined the "free"-INS, the baro-aided INS model will exhibit immediate, unbounded error growth in the horizontal x and y channels but maintains a stable vertical z channel solution.

The V-INS navigation solution comes only from the "free"-INS for the entire one-hour scenario, except for a single velocity update from its E/O sensor approximately halfway through the flight. This velocity update is generated from isochronal, bearing measurements of a stationary ground feature. The pilots uses the E/O sensor's digital display to identify and select the ground feature and manually tracks it over a short, 10-second, measurement epoch as illustrated in Figure 9. The V-INS interprets the measurements and generates the INS PVA update. The measurement equation, as will be seen shortly, requires the aircraft maintain constant velocity (ground speed), constant altitude, steady heading, and wings-level flight for the duration of the measurement epoch. The pilot may accomplish this by engaging the autopilot. Any error that occurs due to the autopilot during the short measurement epoch will be small and Gaussian in nature. The autopilot generates an airspeed hold; therefore, to maintain a constant velocity/ground speed the research assumes the wind field is constant during the measurement epoch. Although different flight dynamics will induce varying amounts of error growth, they will not effect the accuracy of this velocity update.
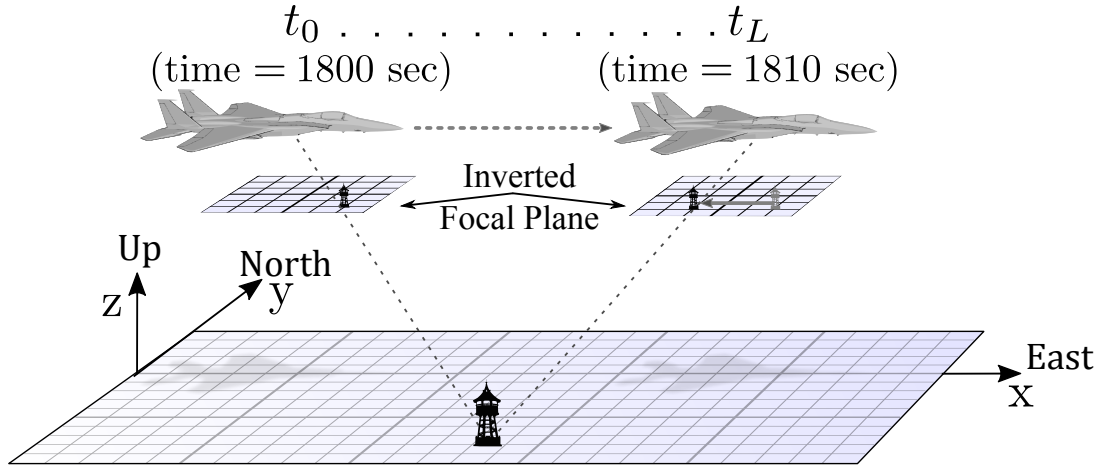
Figure 9. Measurement Epoch in ENU frame: As the aircraft flies East and the pilot tracks the ground feature on the E/O display, measurements of the feature location (x_{f_ℓ}, y_{f_ℓ}) in the focal plane are recorded and sent to the navigation computer.

Following the measurement epoch, the pilot may disengage the autopilot and continue the flight plan for the remainder of the one hour scenario. At the end of one hour scenario, the aircraft V-INS position and velocity errors are decreased compared to the errors of the "free"-INS acting alone.

INS Error Dynamics and Initialization.

The development of the INS error dynamics is presented, followed by the measurement equation development. The aircraft flightpath determines the INS error dynamics and, therefore, drive the growth of error during the flight. The error dynamics developed herein serve two purposes: (1) they provide a means for modeling and simulating the INS error growth during the flight; (2) they drive the derivation of the measurement equation. The ground speed estimate obtained from the measurements through LR is independent of the flight path dynamics prior to the measurement epoch. Therefore, the flight path need only be constrained during the short measurement epoch. For simplicity, however, the scenarios simulated herein considers an aircraft in straight, constant velocity and level flight in an eastward direction at a steady altitude for the duration of the flight, not just the measurement

40

epoch. Because the per-measurement epoch flight path does not affect the ground speed measurement, using a simple flight path to derive the dynamics model does not detract from the legitimacy of the V-INS development or its simulations.

This research employs an unaided INS error state dynamics model, like the one described in Section 2.3, derived from the navigation scenario and based on the Pinson INS error model. The error model is used by the V-INS in generating INS error updates both for the "free"-INS and when integrating the E/O measurements. It is also used to propagate the INS error in the simulations. The nine standard Pinson states (position, velocity, and platform misalignment errors) are augmented with the accelerometer and gyroscope biases—the greatest contributers to INS error—for a total of 15 error states:

$$\delta \mathbf{p}^{(n)} = \begin{pmatrix} \delta x \\ \delta y \\ \delta z \end{pmatrix}, \text{ the aircraft position errors (nav. frame)}$$

$$\delta \mathbf{v}^{(n)} = \begin{pmatrix} \delta v_x \\ \delta v_y \\ \delta v_z \end{pmatrix}, \text{ the aircraft velocity errors (nav. frame)}$$

$$\delta \boldsymbol{\psi} = \begin{pmatrix} \delta \phi \\ \delta \theta \\ \delta \psi \end{pmatrix}, \text{ the notional platform tilt errors}$$

$$\delta \mathbf{b}^{(b)} = \begin{pmatrix} \delta b_x \\ \delta b_y \\ \delta b_z \end{pmatrix}, \text{ the accelerometer biases (body frame)}$$

$$\delta\boldsymbol{\omega}^{(b)} = \begin{pmatrix} \delta\omega_x \\ \delta\omega_y \\ \delta\omega_z \end{pmatrix}, \text{ the gyro biases (body frame)}$$

which comprise the complete error state vector $\delta\mathbf{x}$:

$$\delta\mathbf{x} = \left(\delta\mathbf{p}^{(n)}, \quad \delta\mathbf{v}^{(n)}, \quad \delta\boldsymbol{\psi}, \quad \delta\mathbf{f}^{(b)}, \quad \delta\boldsymbol{\omega}_{ib}^{(b)} \right)^{\mathrm{T}} \tag{42}$$

The model neglects INS accelerometer and gyroscope drift, justified given the short scenario duration.

Development of the error state dynamics begins with the "platform"[1] misalignment errors. Equation (9), from Section 2.3, may be simplified due to the flat, non-rotating earth assumption yielding

$$\delta\dot{\boldsymbol{\psi}} \approx -\mathbf{C}_b^n \delta\omega_{ib}^b \tag{43}$$

The continuous time velocity error state dynamics, first described in Equation (8), are simplified to Equation (44) where the Coriolis terms are neglected and the gravity vector is assumed known.

$$\delta\dot{\mathbf{v}}^{(n)} = [\mathbf{f}^{(n)}\times]\boldsymbol{\psi} + \mathbf{C}_b^n \delta\mathbf{b}^{(b)} \tag{44}$$

where $[\mathbf{f}^{(n)}\times]$ is the skew symmetrix matrix form of the specific force vector, $\mathbf{f}^{(n)}$, defined, in the case of constant altitude and wings-level flight, in the east direction by

---

[1]Although there is no actual platform, because we consider a strapdown INS, these are the errors that would be present if the gyroscopes and accelerometers were platform mounted.

$$\mathbf{f}^{(n)} = \begin{pmatrix} f_x^{(n)} \\ f_y^{(n)} \\ f_z^{(n)} \end{pmatrix} = \begin{pmatrix} a_x \\ 0 \\ 0 \end{pmatrix} - \begin{pmatrix} 0 \\ 0 \\ -g \end{pmatrix} = \begin{pmatrix} a_x \\ 0 \\ g \end{pmatrix} \tag{45}$$

where g is the acceleration of gravity and a_x the aircraft acceleration along the x-axis; in the considered scenarios, $a_x = 0$. During the measurement epoch, while the autopilot is engaged, the aircraft velocity is constant. The aircraft position error state dynamics are modeled as the time derivative of the velocity error.

$$\delta \dot{\mathbf{p}}^{(n)} = \delta \mathbf{v}^{(n)} \tag{46}$$

Finally, the accelerometer and gyroscope errors are modeled as zero-mean, Gaussian constant biases:

$$\delta \dot{\mathbf{b}} = 0, \quad \delta \mathbf{b}(0) \sim \mathcal{N}(0, \sigma_b^2) \tag{47}$$

$$\delta \dot{\boldsymbol{\omega}} = 0, \quad \delta \boldsymbol{\omega}(0) \sim \mathcal{N}(0, \sigma_\omega^2) \tag{48}$$

The variance values (σ_b^2 and σ_ω^2) are chosen to induce an unaided INS position error of 1 km/hr, typical of a navigation grade INS [36, 39], and later 100 km/hr typical of a tactical grade INS. Combining the dynamics equations from the above into matrix form, which allows for easy computation, yields

$$\delta \dot{\mathbf{x}}(t) = \mathbf{A} \delta \mathbf{x}(t), \quad \text{where } \delta \mathbf{x} = (\delta \boldsymbol{p}, \ \delta \boldsymbol{v}, \ \delta \boldsymbol{\psi}, \ \delta \boldsymbol{b}, \ \delta \boldsymbol{\omega})^{\mathrm{T}} \tag{49}$$

and

$$\mathbf{A} = \begin{bmatrix} \mathbf{0_3} & \mathbf{I_3} & \mathbf{0_3} & \mathbf{0_3} & \mathbf{0_3} \\ \mathbf{0_3} & \mathbf{0_3} & -\mathbf{F}^{(n)} & \mathbf{C}_b^n & \mathbf{0_3} \\ \mathbf{0_3} & \mathbf{0_3} & \mathbf{0_3} & \mathbf{0_3} & \mathbf{C}_b^n \\ \mathbf{0_3} & \mathbf{0_3} & \mathbf{0_3} & \mathbf{0_3} & \mathbf{0_3} \\ \mathbf{0_3} & \mathbf{0_3} & \mathbf{0_3} & \mathbf{0_3} & \mathbf{0_3} \end{bmatrix}_{15 \times 15} \tag{50}$$

It is worth noting that because the model considers only constant random biases (accelerom-eter and gyroscope biases), the dynamics model has no noise vector component as did the stochastic system described in Section 2.4, Equation (18).

The continuous time dynamics are converted to the their discrete time equivalents by evaluating the matrix exponential of $\mathbf{A}$, Equation (51), which allows computer processing and modeling. In simulating the scenario, this step is executed with built-in MATLAB functions.

$$\mathbf{A_d} = e^{\mathbf{A}\Delta t}, \quad \text{where } \Delta t \triangleq \text{computer system time step} \tag{51}$$

Propagating the INS error requires initialization. The aircraft PVA solution is known precisely at scenario start; the INS errors are exclusively caused by the accelerometers' and gyroscopes' biases. Accordingly, the V-INS error states are initialized as follows:

$$\delta\mathbf{x}_0 = \begin{pmatrix} \delta x_0 & \delta y_0 & \delta z_0 & \delta v_{x_0} & \delta v_{y_0} & \delta v_{z_0} & \delta\phi_0 & \delta\theta_0 & \delta\psi_0 & \delta b_{x_0} & \delta b_{y_0} & \delta b_{z_0} & \delta\omega_{x_0} & \delta\omega_{y_0} & \delta\omega_{z_0} \end{pmatrix}^{\mathrm{T}}$$

$$= \begin{pmatrix} 0_{1\times 9} & \mathcal{N}(0,\sigma_b^2) & \mathcal{N}(0,\sigma_b^2) & \mathcal{N}(0,\sigma_b^2) & \mathcal{N}(0,\sigma_\omega^2) & \mathcal{N}(0,\sigma_\omega^2) & \mathcal{N}(0,\sigma_\omega^2) \end{pmatrix}^{\mathrm{T}} \tag{52}$$

and the covariance at scenario start is

$$\mathbf{P}_{\delta \mathbf{x}_0} = \begin{bmatrix} 0 & 0 & 0 & 0 & 0 & 0 & 0 & 0 & 0 & 0 & 0 & 0 & 0 & 0 & 0 \\ 0 & 0 & 0 & 0 & 0 & 0 & 0 & 0 & 0 & 0 & 0 & 0 & 0 & 0 & 0 \\ 0 & 0 & 0 & 0 & 0 & 0 & 0 & 0 & 0 & 0 & 0 & 0 & 0 & 0 & 0 \\ 0 & 0 & 0 & 0 & 0 & 0 & 0 & 0 & 0 & 0 & 0 & 0 & 0 & 0 & 0 \\ 0 & 0 & 0 & 0 & 0 & 0 & 0 & 0 & 0 & 0 & 0 & 0 & 0 & 0 & 0 \\ 0 & 0 & 0 & 0 & 0 & 0 & 0 & 0 & 0 & 0 & 0 & 0 & 0 & 0 & 0 \\ 0 & 0 & 0 & 0 & 0 & 0 & 0 & 0 & 0 & 0 & 0 & 0 & 0 & 0 & 0 \\ 0 & 0 & 0 & 0 & 0 & 0 & 0 & 0 & 0 & 0 & 0 & 0 & 0 & 0 & 0 \\ 0 & 0 & 0 & 0 & 0 & 0 & 0 & 0 & 0 & 0 & 0 & 0 & 0 & 0 & 0 \\ 0 & 0 & 0 & 0 & 0 & 0 & 0 & 0 & 0 & \sigma_b^2 & 0 & 0 & 0 & 0 & 0 \\ 0 & 0 & 0 & 0 & 0 & 0 & 0 & 0 & 0 & 0 & \sigma_b^2 & 0 & 0 & 0 & 0 \\ 0 & 0 & 0 & 0 & 0 & 0 & 0 & 0 & 0 & 0 & 0 & \sigma_b^2 & 0 & 0 & 0 \\ 0 & 0 & 0 & 0 & 0 & 0 & 0 & 0 & 0 & 0 & 0 & 0 & \sigma_\omega^2 & 0 & 0 \\ 0 & 0 & 0 & 0 & 0 & 0 & 0 & 0 & 0 & 0 & 0 & 0 & 0 & \sigma_\omega^2 & 0 \\ 0 & 0 & 0 & 0 & 0 & 0 & 0 & 0 & 0 & 0 & 0 & 0 & 0 & 0 & \sigma_\omega^2 \end{bmatrix} \tag{53}$$

The "Free"-INS.

In the envisioned scenario, the "free"-INS runs continuously providing the vertically stabilized aircraft navigation solution, which is only aided by the E/O sensor once, after the measurement epoch. The "free"-INS consists of the unaided INS and barometer integrated with a linear KF. The navigation solution is obtained using the INS error model previously developed, and the trivial measurement equation:

$$z_{br_k} = \mathbf{h}_{br_k} \mathbf{x}_k + v_{br_k} \tag{54}$$

where the scalar measurement z_{br}, at time step k, is actually the INS altitude error generated

by differencing the indicated INS altitude, taken at face value, and the altitude provided by barometer:

$$z_{br_k} = z_c - z_{baro} \tag{55}$$

Furthermore, the regressor matrix is a direct mapping from the measurement to the INS altitude error

$$\mathbf{h}_{br} = \begin{bmatrix} 0 & 0 & 1 & 0 & 0 & 0 & 0 & 0 & 0 & 0 & 0 & 0 & 0 & 0 & 0 \end{bmatrix} \tag{56}$$

and the measurement noise, from the barometer sensor, is zero-mean, Gaussian with variance σ_{br}^2:

$$v_{br_k} \sim \mathcal{N}(0, \sigma_{br}^2) \quad \rightarrow \quad r_{br} = \sigma_{br}^2 \tag{57}$$

The "free"-INS error states and covariance are propagated and updated for the duration of the scenario using a linear KF according to Equation (24) through Equation (26). The "free"-INS error states and covariance, at any time step k immedetly following a barometer measurement, are indicated by the variables $\delta \mathbf{x}_k^{+(\text{free})}$ and $\mathbf{P}_k^{+(\text{free})}$.

V-INS.

The estimation of the ground speed/velocity error is the linchpin of the herein developed V-INS navigation method. The V-INS combines the "free"-INS output with the E/O sensor measurement through a LR algorithm at the end of the measurement epoch. Development of the V-INS measurement equation, required for the LR, involves the conversion of the non-linear E/O bearing measurements to linear measurements of INS velocity error. Calculating the change in the ground feature position at each step of the measurement epoch and applying
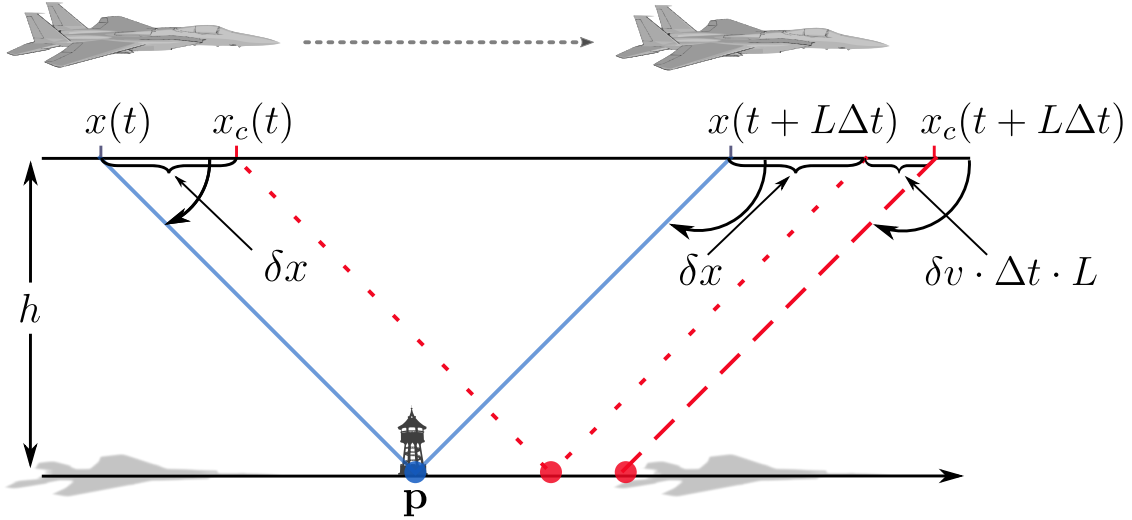
Figure 10. INS Velocity Error Measurement Concept: The change in the calculated feature position, x_c, from time (t) to time $(t + L\Delta t)$ is attributed to the error in the INS indicated velocity, δv [20].

a linear regression algorithm allows an estimate of the aircraft ground speed error as well as the horizontal axes accelerometer biases. Figure 10 depicts the V-INS aiding concept.

The measurement equation employed herein is novel in that the bearing measurements taken with the E/O system and recorded as the position coordinate (x_f, y_f) of the ground feature in the E/O system's focal plane are converted so their relationship with the INS error states is linear. Thus, only the measurement error terms need be linearized, which is accomplished using conventional perturbation techniques. This allows the application of LR, which tends to be less computationally intensive than the EKF or particle filter methods, as well as more accurate.

Development begins with a measurement equation relating the position of the ground feature, as referenced in the E/O inverse focal plane, to the INS error states in the local-level navigation frame. The measurement made by the E/O system are illustrated in Figure 11 and guide the model development.
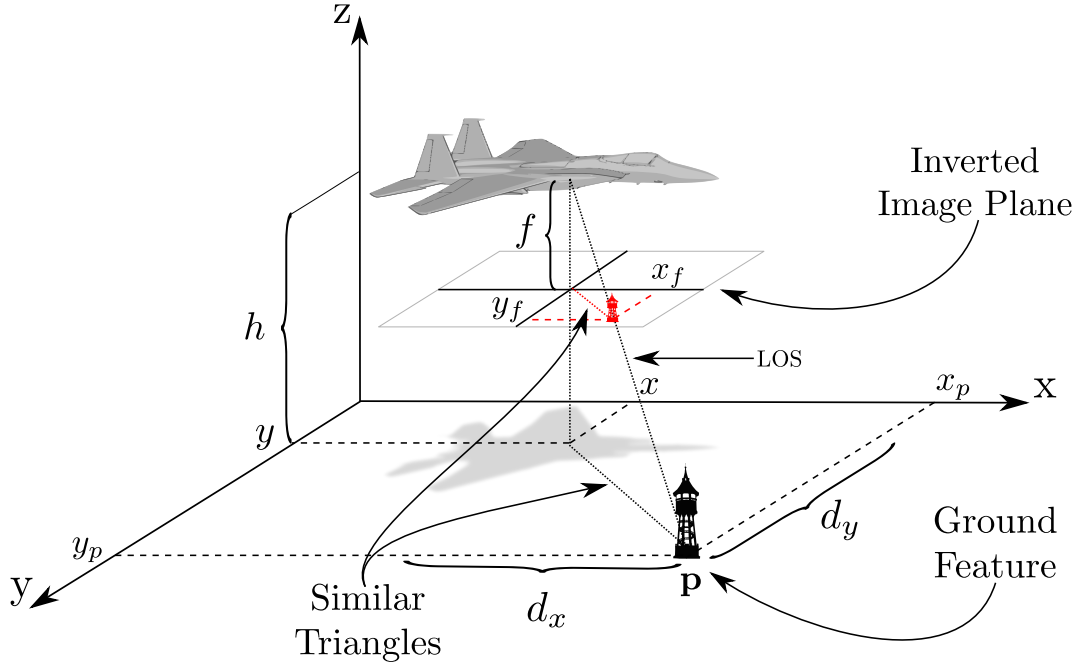
Figure 11. Measurement Geometry: The selected ground feature is projected onto the focal plane at coordinates (x_f, y_f).

Working in the navigation frame, the position of the feature, $\mathbf{x}_p$, is equal to the position of the aircraft, $\mathbf{x}$, plus the distance of the feature from the aircraft, $\mathbf{d}$:

$$\begin{pmatrix} x_p \\ y_p \\ z_p \end{pmatrix} = \begin{pmatrix} x \\ y \\ z \end{pmatrix} + \begin{pmatrix} d_x \\ d_y \\ d_z \end{pmatrix} \tag{58}$$

The derivation depends on two key assumptions. For the duration of the measurement epoch, (1) the aircraft is on a constrained flight path (flying due east with wings level and at a constant velocity and steady altitude) and (2) the wind field is constant.

The pilot/navigator takes the bearing measurement to the selected ground feature, which is interpreted by the E/O imaging system as a pixel whose two-dimensional image plane coordinates are x_f and y_f. Exploiting the similar triangle relationship between the camera and navigation frames, the ratio of the nav frame and camera frame line-of-sight magnitudes is

equal to the ratio of the three ground feature distance components and the feature projection components in the camera frame:

$$\frac{r_{LOS}}{r_f} = \frac{d_x}{x_f} = \frac{d_y}{y_f} = \frac{d_z}{z_f} \tag{59}$$

Accordingly, the distance component values are proportional to the projected feature location in the image frame:

$$\begin{pmatrix} d_x \\ d_y \\ d_z \end{pmatrix} = \frac{r_{LOS}}{r_f} \cdot \begin{pmatrix} x_f \\ y_f \\ z_f \end{pmatrix} \tag{60}$$

Substituting the above yields the non-linear measurement equation

$$\begin{pmatrix} x_p \\ y_p \\ z_p \end{pmatrix} = \begin{pmatrix} x \\ y \\ z \end{pmatrix} + \frac{|r_{LOS}|}{\sqrt{x_f^2 + y_f^2 + f^2}} \mathbf{C}_b^n \begin{pmatrix} x_f \\ y_f \\ -f \end{pmatrix} \tag{61}$$

The DCM, $\mathbf{C}_b^n$, is identity in the presented scenario because the aircraft body is aligned with the navigation frame (i.e., wings level and easterly heading). Furthermore, because the barometer provides the "height above ground level" altitude, knowledge of the elevation at the aircraft position is assumed, which allows the altitude of the ground feature to be constrained and the equation simplified. The z component of Equation (61) may be isolated and rearranged as follows:

$$\frac{|r_{LOS}|}{\sqrt{x_f^2 + y_f^2 + f^2}} = \frac{z_p - z}{\begin{pmatrix} 0 & 0 & 1 \end{pmatrix} \mathbf{C}_b^n \begin{pmatrix} x_f \\ y_f \\ -f \end{pmatrix}} \tag{62}$$

Now, substituting this back into Equation (61) yields

$$\begin{pmatrix} x_p \\ y_p \end{pmatrix} = \begin{pmatrix} x \\ y \end{pmatrix} + \frac{z_p - z}{\begin{pmatrix} 0 & 0 & 1 \end{pmatrix} \mathbf{C_b^n} \begin{pmatrix} x_f \\ y_f \\ -f \end{pmatrix}} \begin{bmatrix} 1 & 0 & 0 \\ 0 & 1 & 0 \end{bmatrix} \mathbf{C_b^n} \begin{pmatrix} x_f \\ y_f \\ -f \end{pmatrix} \tag{63}$$

Equation (63) ties together the aircraft INS navigation states, ground object position, and the E/O bearing measurements $(x_f, y_f)^{\mathrm{T}}$. The equation is clearly nonlinear; thus, we convert the measurement to provide a linear measurement equation. Through conversion, the INS navigation error states are realized. The measurement equation is first rearranged and the right-hand side (RHS) is linearized using the perturbation method and written in the form of Equation (64), where the subscript c indicates a value provided by the baro-aided "free"-INS taken at face value, and the subscript m indicates a measured valued provided by the E/O sensor, namely the position of the ground feature in the E/O sensor inverted focal plane (x_{f_m}, y_{f_m}). The full derivation is provided in Appendix A.

$$
\begin{pmatrix} x \\ y \end{pmatrix} - \begin{pmatrix} x_p \\ y_p \end{pmatrix} = \frac{z_c - z_p}{\begin{pmatrix} 0 & 0 & 1 \end{pmatrix} (\mathbf{C}_b^n)_c \begin{pmatrix} x_{fm} \\ y_{fm} \\ -f \end{pmatrix}} \begin{bmatrix} 1 & 0 & 0 \\ 0 & 1 & 0 \end{bmatrix} (\mathbf{C}_b^n)_c \begin{pmatrix} x_{fm} \\ y_{fm} \\ -f \end{pmatrix}
$$

$$
- \frac{1}{\begin{pmatrix} 0 & 0 & 1 \end{pmatrix} \mathbf{C}_b^n \begin{pmatrix} x_f \\ y_f \\ -f \end{pmatrix}} \begin{bmatrix} 1 & 0 & 0 \\ 0 & 1 & 0 \end{bmatrix} \mathbf{C}_b^n \begin{pmatrix} x_f \\ y_f \\ -f \end{pmatrix} \delta z
$$

$$
+ \frac{z - z_p}{\begin{pmatrix} 0 & 0 & 1 \end{pmatrix} \mathbf{C}_b^n \begin{pmatrix} x_f \\ y_f \\ -f \end{pmatrix}} \begin{bmatrix} 1 & 0 & 0 \\ 0 & 1 & 0 \end{bmatrix} \begin{bmatrix} 0 & \delta\psi & -\delta\theta \\ -\delta\psi & 0 & \delta\phi \\ \delta\theta & -\delta\phi & 0 \end{bmatrix} \begin{pmatrix} x_f \\ y_f \\ -f \end{pmatrix}
$$

$$
- \frac{z - z_p}{[\begin{pmatrix} 0 & 0 & 1 \end{pmatrix} \mathbf{C}_b^n \begin{pmatrix} x_f \\ y_f \\ -f \end{pmatrix}]^2} \begin{pmatrix} 0 & 0 & 1 \end{pmatrix} \begin{bmatrix} 0 & \delta\psi & -\delta\theta \\ -\delta\psi & 0 & \delta\phi \\ \delta\theta & -\delta\phi & 0 \end{bmatrix} \begin{pmatrix} x_f \\ y_f \\ -f \end{pmatrix} \begin{bmatrix} 1 & 0 & 0 \\ 0 & 1 & 0 \end{bmatrix} \mathbf{C}_b^n \begin{pmatrix} x_f \\ y_f \\ -f \end{pmatrix}
$$

$$
- \frac{z - z_p}{\begin{pmatrix} 0 & 0 & 1 \end{pmatrix} \mathbf{C}_b^n \begin{pmatrix} x_f \\ y_f \\ -f \end{pmatrix}} \begin{bmatrix} 1 & 0 & 0 \\ 0 & 1 & 0 \end{bmatrix} \mathbf{C}_b^n \begin{pmatrix} \delta x_f \\ \delta y_f \\ 0 \end{pmatrix}
$$

$$
+ \frac{z - z_p}{[\begin{pmatrix} 0 & 0 & 1 \end{pmatrix} \mathbf{C}_b^n \begin{pmatrix} x_f \\ y_f \\ -f \end{pmatrix}]^2} \begin{pmatrix} 0 & 0 & 1 \end{pmatrix} \mathbf{C}_b^n \begin{pmatrix} \delta x_f \\ \delta y_f \\ 0 \end{pmatrix} \begin{bmatrix} 1 & 0 & 0 \\ 0 & 1 & 0 \end{bmatrix} \mathbf{C}_b^n \begin{pmatrix} x_f \\ y_f \\ -f \end{pmatrix}
$$

$$
\tag{64}
$$

The body to navigation frame DCM, $\mathbf{C}_b^n$, is identity due to the scenario flight conditions; accordingly, Equation (64) is simplified yielding Equation (65).

$$
\begin{pmatrix} x \\ y \end{pmatrix} - \begin{pmatrix} x_p \\ y_p \end{pmatrix} = \frac{z_c - z_p}{\begin{pmatrix} 0 & 0 & 1 \end{pmatrix} \left(\mathbf{C_b^n}\right)_c \begin{pmatrix} x_{fm} \\ y_{fm} \\ -f \end{pmatrix}} \begin{bmatrix} 1 & 0 & 0 \\ 0 & 1 & 0 \end{bmatrix} \left(\mathbf{C_b^n}\right)_c \begin{pmatrix} x_{fm} \\ y_{fm} \\ -f \end{pmatrix} + \begin{pmatrix} \frac{x_f}{f} \\ \frac{y_f}{f} \end{pmatrix} \delta z
$$

$$
- (z - z_p) \begin{pmatrix} \frac{y_f}{f}\delta\psi + \delta\theta \\ -\frac{x_f}{f}\delta\psi - \delta\phi \end{pmatrix} - (z - z_p)\left(\frac{x_f}{f}\delta\theta - \frac{y_f}{f}\delta\theta \right)
$$

$$
+ (z - z_p) \begin{pmatrix} \frac{x_f}{f} \\ \frac{y_f}{f} \end{pmatrix} + (z - z_p) \begin{pmatrix} \frac{\delta x_f}{f} \\ \frac{\delta y_f}{f} \end{pmatrix}
$$

$$(65)$$

The measurement equation remains a bit unwieldy. Letting matrix, $\mathbf{M}$, equal the INS error state coefficients aids in readability for continued development.

$$
\mathbf{M} = \begin{bmatrix} 0 & 0 & \frac{x_f}{f} & 0 & 0 & 0 & (z_p - z)\frac{x_f}{f}\frac{y_f}{f} & (z - z_p)\left(1 + \frac{x_f}{f}\right) & (z - z_p)\frac{y_f}{f} & 0_{1\times6} \\ 0 & 0 & \frac{y_f}{f} & 0 & 0 & 0 & (z_p - z)\left[1 + \left(\frac{y_f}{f}\right)^2\right] & (z - z_p)\frac{x_f}{f}\frac{y_f}{f} & (z_p - z)\frac{x_f}{f} & 0_{1\times6} \end{bmatrix}
$$

$$(66)$$

or, allowing that $z - z_p$ equal aircraft altitude, h:

$$
\mathbf{M} = \begin{bmatrix} 0 & 0 & \frac{x_f}{f} & 0 & 0 & 0 & -h\frac{x_f}{f}\frac{y_f}{f} & h\left(1 + \frac{x_f}{f}\right) & h\frac{y_f}{f} & 0_{1\times6} \\ 0 & 0 & \frac{y_f}{f} & 0 & 0 & 0 & -h\left[1 + \left(\frac{y_f}{f}\right)^2\right] & h\frac{x_f}{f}\frac{y_f}{f} & -h\frac{x_f}{f} & 0_{1\times6} \end{bmatrix}
$$

$$(67)$$

Thus, the measurement equation may be written as follows:

$$
\begin{pmatrix} x \\ y \end{pmatrix} - \begin{pmatrix} x_p \\ y_p \end{pmatrix} = \frac{z_c - z_p}{\begin{pmatrix} 0 & 0 & 1 \end{pmatrix} (\mathbf{C_b^n})_c \begin{pmatrix} x_{f_m} \\ y_{f_m} \\ -f \end{pmatrix}} \begin{bmatrix} 1 & 0 & 0 \\ 0 & 1 & 0 \end{bmatrix} (\mathbf{C_b^n})_c \begin{pmatrix} x_{f_m} \\ y_{f_m} \\ -f \end{pmatrix}
$$

$$
+ \mathbf{M}\delta x + h \begin{pmatrix} \frac{\delta x_f}{f} \\ \frac{\delta y_f}{f} \end{pmatrix}
$$

(68)

The horizontal aircraft position coordinates, x and y, are perturbed. Again, the subscript 'c' denotes the calculated value as indicated by the INS, which is taken at face value.

$$
\begin{pmatrix} x_c \\ y_c \end{pmatrix} - \begin{pmatrix} \delta x \\ \delta y \end{pmatrix} - \begin{pmatrix} x_p \\ y_p \end{pmatrix} = \frac{z_c - z_p}{\begin{pmatrix} 0 & 0 & 1 \end{pmatrix} (\mathbf{C_b^n})_c \begin{pmatrix} x_{f_m} \\ y_{f_m} \\ -f \end{pmatrix}} \begin{bmatrix} 1 & 0 & 0 \\ 0 & 1 & 0 \end{bmatrix} (\mathbf{C_b^n})_c \begin{pmatrix} x_{f_m} \\ y_{f_m} \\ -f \end{pmatrix}
$$

$$
+ \mathbf{M}\delta x + h \begin{pmatrix} \frac{\delta x_f}{f} \\ \frac{\delta y_f}{f} \end{pmatrix}
$$

(69)

To further simplify, let $\boldsymbol{\zeta}$ equal the first term on the RHS of the equation plus the calculated horizontal aircraft position:

$$
\boldsymbol{\zeta} = -\frac{z_c - z_p}{\begin{pmatrix} 0 & 0 & 1 \end{pmatrix} (\mathbf{C_b^n})_c \begin{pmatrix} x_{f_m} \\ y_{f_m} \\ -f \end{pmatrix}} \begin{bmatrix} 1 & 0 & 0 \\ 0 & 1 & 0 \end{bmatrix} (\mathbf{C_b^n})_c \begin{pmatrix} x_{f_m} \\ y_{f_m} \\ -f \end{pmatrix} + \begin{pmatrix} x_c \\ y_c \end{pmatrix}
$$

(70)

53

which is a measurement of the horizontal ground feature position. Taking a series of these measurements provides a measurement of ground speed. Substituting back into Equation (69) yields

$$
\begin{pmatrix} \delta x \\ \delta y \end{pmatrix} + \begin{pmatrix} x_p \\ y_p \end{pmatrix} = \boldsymbol{\zeta} - \mathbf{M}\boldsymbol{\delta}\mathbf{x} - h \begin{pmatrix} \frac{\delta x_f}{f} \\ \frac{\delta y_f}{f} \end{pmatrix} \tag{71}
$$

At this point, the x-channel and y-channel components are decoupled and the ground speed for each is estimated separately. Accordingly, let $\mathbf{m}_1^{\mathrm{T}}$ denote the first row of matrix $\mathbf{M}$, corresponding to the x-channel, and $\mathbf{m}_2^{\mathrm{T}}$ the second row, corresponding to the y-channel. Consider $L+1$ measurements, $\boldsymbol{\zeta}_\ell$, processed by the aircraft navigation system yielding the x and y channel components: ζ_{x_ℓ} and ζ_{y_ℓ}, for $\ell = 0, 1, \ldots, L$. For the x-channel this yields

$$
\delta x_\ell + x_p = \zeta_{x_\ell} - \mathbf{m}_{1_\ell}^{\mathrm{T}}\boldsymbol{\delta}\mathbf{x}_\ell - h\left(\frac{\delta x_f}{f}\right)_\ell, \quad \text{for } \ell = 0, 1, \ldots, L \tag{72}
$$

and for the y-channel

$$
\delta y_\ell + y_p = \zeta_{y_\ell} - \mathbf{m}_{2_\ell}^{\mathrm{T}}\boldsymbol{\delta}\mathbf{y}_\ell - h\left(\frac{\delta y_f}{f}\right)_\ell, \quad \text{for } \ell = 0, 1, \ldots, L \tag{73}
$$

Subtracting the measurements for $\ell = 1, 2, ..., L$ from the measurement at $\ell = 0$ yields L measurements of the change in the ground feature position error:

$$
\delta x_\ell - \delta x_0 = \zeta_{x_\ell} - \zeta_{x_0} + \mathbf{m}_{1_0}^{\mathrm{T}}\boldsymbol{\delta}\mathbf{x}_0 + h\left(\frac{\delta x_f}{f}\right)_0 - \mathbf{m}_{1_\ell}^{\mathrm{T}}\boldsymbol{\delta}\mathbf{x}_\ell - h\left(\frac{\delta x_f}{f}\right)_\ell \tag{74}
$$

and

$$
\delta y_\ell - \delta y_0 = \zeta_{y_\ell} - \zeta_{y_0} + \mathbf{m}_{2_0}^{\mathrm{T}}\boldsymbol{\delta}\mathbf{y}_0 + h\left(\frac{\delta y_f}{f}\right)_0 - \mathbf{m}_{2_\ell}^{\mathrm{T}}\boldsymbol{\delta}\mathbf{y}_\ell - h\left(\frac{\delta y_f}{f}\right)_\ell \tag{75}
$$

It is worth noting that for the special case of tracking a known ground feature, the measure-

54

ment z_{1_0} is the known position of the feature, and z_{1_ℓ} remains derived from Equation (70)[2]. In either case, the feature is stationary, thus we attribute the change in its measured position error to the velocity error in the INS, as well as the INS accelerometer bias using the equation for linear motion. That is,

$$\delta x_\ell - \delta x_0 = \delta v_{x_0} \ell \Delta t + \frac{1}{2} b_x \ell^2 \Delta t^2, \quad \text{for } \ell = 1, 2, ..., L \tag{76}$$

and equivalently for the y-channel

$$\delta y_\ell - \delta y_0 = \delta v_{y_0} \ell \Delta t + \frac{1}{2} b_y \ell^2 \Delta t^2, \quad \text{for } \ell = 1, 2, ..., L \tag{77}$$

substituting into Equations (74) and (75) yields

$$\zeta_{x_\ell} - \zeta_{x_0} = \delta v_{x_0} \ell \Delta t + \frac{1}{2} b_x \ell^2 \Delta t^2 + \mathbf{m}_{1_0}^{\mathrm{T}} \delta \mathbf{x}_0 + h \left(\frac{\delta x_f}{f} \right)_0 - \mathbf{m}_{1_\ell}^{\mathrm{T}} \delta \mathbf{x}_\ell - h \left(\frac{\delta x_f}{f} \right)_\ell \tag{78}$$

and equivalently

$$\zeta_{y_\ell} - \zeta_{y_0} = \delta v_{y_0} \ell \Delta t + \frac{1}{2} b_y \ell^2 \Delta t^2 + \mathbf{m}_{2_0}^{\mathrm{T}} \delta \mathbf{y}_0 + h \left(\frac{\delta y_f}{f} \right)_0 - \mathbf{m}_{2_\ell}^{\mathrm{T}} \delta \mathbf{y}_\ell - h \left(\frac{\delta y_f}{f} \right)_\ell \tag{79}$$

for $\ell = 1, 2, \ldots, L$. Thus, a linear measurement equation of ground speed error in the x and y directions is obtained for each E/O bearing measurement increment of ℓ. The regressors variable are the INS velocity error and accelerometer bias, and the error terms are a combination of the E/O sensor uncertainty and the error introduced when using the INS output to determine the relative feature position. Employing the general linear regression form described in 2.5, Equation (20), yields

---

[2]The measurement error terms if the ground feature position is known would also differ as they would depend on the precision of known feature coordinates

$$\mathbf{z}_x = \Delta t \cdot \mathbf{H}\theta_x + \mathbf{v}_x \tag{80}$$

$$\mathbf{z}_y = \Delta t \cdot \mathbf{H}\theta_y + \mathbf{v}_y \tag{81}$$

where the converted measurements are $\mathbf{z}_x = \begin{pmatrix} z_{x_1} - z_{x_0} \\ z_{x_2} - z_{x_0} \\ \vdots \\ z_{x_L} - z_{x_0} \end{pmatrix}$ and $\mathbf{z}_y = \begin{pmatrix} z_{y_1} - z_{y_0} \\ z_{y_2} - z_{y_0} \\ \vdots \\ z_{y_L} - z_{y_0} \end{pmatrix}$.

The linear regressor matrix $\mathbf{H} = \begin{bmatrix} 1 & \frac{1}{2}\Delta t \\ 2 & 2\Delta t \\ \vdots & \vdots \\ L & \frac{1}{2}L^2\Delta t \end{bmatrix}_{L\times 2}$.

The INS velocity error and acceleration bias are the regressor parameters:

$$\boldsymbol{\theta}_x = \begin{pmatrix} \delta v_x \\ \delta b_x \end{pmatrix} \quad \text{and} \quad \boldsymbol{\theta}_y = \begin{pmatrix} \delta v_y \\ \delta b_y \end{pmatrix}$$

The uncertainty or error terms on the converted measurement are Gaussian distributed:

$$\mathbf{v}_x = \begin{pmatrix} \mathbf{m}_{1_0}^{\mathrm{T}}\delta\mathbf{x}_0 + h\left(\frac{\delta x_f}{f}\right)_0 - \mathbf{m}_{1_1}^{\mathrm{T}}\delta\mathbf{x}_1 - h\left(\frac{\delta x_f}{f}\right)_1 \\ \mathbf{m}_{1_0}^{\mathrm{T}}\delta\mathbf{x}_0 + h\left(\frac{\delta x_f}{f}\right)_0 - \mathbf{m}_{1_2}^{\mathrm{T}}\delta\mathbf{x}_2 - h\left(\frac{\delta x_f}{f}\right)_2 \\ \vdots \\ \mathbf{m}_{1_0}^{\mathrm{T}}\delta\mathbf{x}_0 + h\left(\frac{\delta x_f}{f}\right)_0 - \mathbf{m}_{1_L}^{\mathrm{T}}\delta\mathbf{x}_L - h\left(\frac{\delta x_f}{f}\right)_L \end{pmatrix}, \quad \mathbf{v}_y = \begin{pmatrix} \mathbf{m}_{2_0}^{\mathrm{T}}\delta\mathbf{x}_0 + h\left(\frac{\delta y_f}{f}\right)_0 - \mathbf{m}_{2_1}^{\mathrm{T}}\delta\mathbf{x}_1 - h\left(\frac{\delta y_f}{f}\right)_1 \\ \mathbf{m}_{2_0}^{\mathrm{T}}\delta\mathbf{x}_0 + h\left(\frac{\delta y_f}{f}\right)_0 - \mathbf{m}_{2_2}^{\mathrm{T}}\delta\mathbf{x}_2 - h\left(\frac{\delta y_f}{f}\right)_2 \\ \vdots \\ \mathbf{m}_{2_0}^{\mathrm{T}}\delta\mathbf{x}_0 + h\left(\frac{\delta y_f}{f}\right)_0 - \mathbf{m}_{2_L}^{\mathrm{T}}\delta\mathbf{x}_L - h\left(\frac{\delta y_f}{f}\right)_L \end{pmatrix},$$
$$\tag{82}$$

We now have a linear measurement model and may use LR to estimate the desired INS error states, δv and δb. The measurement error covariance, $\mathbf{R}$, for each direction is derived

from the measurement equation error terms of Equation (78) and Equation (79) at every measurement step. That is,

$$\mathbf{R}_x = E[(\mathbf{v}_{1_x} + \mathbf{v}_{2_x}) \cdot (\mathbf{v}_{1_x} + \mathbf{v}_{2_x})^{\mathrm{T}}] - E[(\mathbf{v}_{1_x} + \mathbf{v}_{2_x})]^2$$

$$= E[\mathbf{v}_{1_x} \mathbf{v}_{1_x}^{\mathrm{T}}] + E[\mathbf{v}_{2_x} \mathbf{v}_{2_x}^{\mathrm{T}}] \tag{83}$$

and

$$\mathbf{R}_y = E[(\mathbf{v}_{1_y} + \mathbf{v}_{2_y}) \cdot (\mathbf{v}_{1_y} + \mathbf{v}_{2_y})^{\mathrm{T}}] - E[(\mathbf{v}_{1_y} + \mathbf{v}_{2_y})]^2$$

$$= E[\mathbf{v}_{1_y} \mathbf{v}_{1_y}^{\mathrm{T}}] + E[\mathbf{v}_{2_y} \mathbf{v}_{2_y}^{\mathrm{T}}] \tag{84}$$

where $E[\cdot]$ is the expectation operator. The equation error components of $\mathbf{R}_x$ are

$$\mathbf{v}_{x_1} = \begin{pmatrix} \mathbf{m}_{1_0}^{\mathrm{T}} \delta\mathbf{x}_0 - \mathbf{m}_{1_1}^{\mathrm{T}} \delta\mathbf{x}_1 \\ \mathbf{m}_{1_0}^{\mathrm{T}} \delta\mathbf{x}_0 - \mathbf{m}_{1_2}^{\mathrm{T}} \delta\mathbf{x}_2 \\ \vdots \\ \mathbf{m}_{1_0}^{\mathrm{T}} \delta\mathbf{x}_0 - \mathbf{m}_{1_L}^{\mathrm{T}} \delta\mathbf{x}_L \end{pmatrix}_{L\times 1} \quad \text{and} \quad \mathbf{v}_{x_2} = h \begin{pmatrix} \left(\frac{\delta x_f}{f}\right)_0 - \left(\frac{\delta x_f}{f}\right)_1 \\ \left(\frac{\delta x_f}{f}\right)_0 - \left(\frac{\delta x_f}{f}\right)_2 \\ \vdots \\ \left(\frac{\delta x_f}{f}\right)_0 - \left(\frac{\delta x_f}{f}\right)_L \end{pmatrix}_{L\times 1} \tag{85}$$

Similarly, the equation error components of $\mathbf{R}_y$ are

$$\mathbf{v}_{y_1} = \begin{pmatrix} \mathbf{m}_{2_0}^{\mathrm{T}} \delta\mathbf{x}_0 - \mathbf{m}_{2_1}^{\mathrm{T}} \delta\mathbf{x}_1 \\ \mathbf{m}_{2_0}^{\mathrm{T}} \delta\mathbf{x}_0 - \mathbf{m}_{2_2}^{\mathrm{T}} \delta\mathbf{x}_2 \\ \vdots \\ \mathbf{m}_{2_0}^{\mathrm{T}} \delta\mathbf{x}_0 - \mathbf{m}_{2_L}^{\mathrm{T}} \delta\mathbf{x}_L \end{pmatrix}_{L\times 1} \quad \text{and} \quad \mathbf{v}_{y_2} = h \begin{pmatrix} \left(\frac{\delta y_f}{f}\right)_0 - \left(\frac{\delta y_f}{f}\right)_1 \\ \left(\frac{\delta y_f}{f}\right)_0 - \left(\frac{\delta y_f}{f}\right)_2 \\ \vdots \\ \left(\frac{\delta y_f}{f}\right)_0 - \left(\frac{\delta y_f}{f}\right)_L \end{pmatrix}_{L\times 1} \tag{86}$$

calculated seperately for each direction, $\mathbf{R}_x$ and $\mathbf{R}_y$. The derivations for these covariance matrices are provided in Appendix B.

Admittedly, Equations (76) and (77) do not completely describe the aircraft motion as the accelerometer bias is not the sole contributer to velocity error: from Equation (44), aircraft velocity error is coupled with additional states, notably the INS tilt error. The tilt errors may contribute significantly to the velocity error. However, even though the velocity error is attributed solely to the accelerometer biases, a significant reduction in the error is still achievable using this method.

In order to improve the accelerometer bias estimates, we apply a final adjustment to the matrices $\mathbf{H}$ and $\mathbf{R}$, augmenting them with prior information on the accelerometer bias error uncertainty, as provided by the accelerometer's specifications included in the accelerometer's data sheet.

$$\mathbf{H} \longrightarrow \begin{bmatrix} \mathbf{H} \\ (0,1) \end{bmatrix} \quad \mathbf{R} \longrightarrow \begin{bmatrix} \mathbf{R} & 0_{L\times 1} \\ 0_{1\times L} & \sigma_b^2 \end{bmatrix} \tag{87}$$

Error Estimation.

The E/O sensor provides a ground speed update at half-time which ultimately leads to a superior navigation solution. Using linear regression [4], the minimum variance estimate for the velocity error and accelerometer bias are calculated according to

$$\hat{\boldsymbol{\theta}}_x = \begin{pmatrix} \hat{\delta v}_x \\ \hat{\delta b}_x \end{pmatrix} = (\mathbf{H}^{\mathrm{T}}\mathbf{R}_x^{-1}\mathbf{H})^{-1}\mathbf{H}^{\mathrm{T}}\mathbf{R}_x^{-1}\mathbf{z}_x \tag{88}$$

and

$$\hat{\boldsymbol{\theta}}_y = \begin{pmatrix} \hat{\delta v}_y \\ \hat{\delta b}_y \end{pmatrix} = (\mathbf{H}^{\mathrm{T}}\mathbf{R}_y^{-1}\mathbf{H})^{-1}\mathbf{H}^{\mathrm{T}}\mathbf{R}_y^{-1}\mathbf{z}_y \tag{89}$$

Furthermore, the parameter estimation error covariance for each direction is given by

$$\mathbf{P}_{\hat{\boldsymbol{\theta}}_x} = E[(\hat{\boldsymbol{\theta}}_x - \boldsymbol{\theta}_x)(\hat{\boldsymbol{\theta}}_x - \boldsymbol{\theta}_x)^{\mathrm{T}}] = (\mathbf{H}^{\mathrm{T}}\mathbf{R}_x^{-1}\mathbf{H})^{-1} \quad \text{and}$$

$$\mathbf{P}_{\hat{\boldsymbol{\theta}}_y} = E[(\hat{\boldsymbol{\theta}}_y - \boldsymbol{\theta}_y)(\hat{\boldsymbol{\theta}}_y - \boldsymbol{\theta}_y)^{\mathrm{T}}] = (\mathbf{H}^{\mathrm{T}}\mathbf{R}_y^{-1}\mathbf{H})^{-1}$$

V-INS Update.

The INS navigation error states are updated at the end of the measurement epoch (at approximately $k = 1810$ sec) by subtracting out the new velocity error and accelerometer bias estimates obtained through the LR algorithm[3]:

$$\delta\hat{\mathbf{x}}_k = \delta\mathbf{x}_k^{(\text{free})} - \begin{pmatrix} 0 & 0 & 0 & \delta\hat{v}_x & \delta\hat{v}_y & 0 & 0 & 0 & 0 & \delta\hat{b}_x & \delta\hat{b}_y & 0 & 0 & 0 & 0 \end{pmatrix}^{\mathrm{T}}$$

The covariance is also update by replacing the applicable "free"-INS velocity error and accelerometer bias covariance elements (elements in red and underlined):

---

[3]If an accurate flight INS error model exists, the estimates can be fed into the Kalman filter of the "free"-INS as opposed to being simply subtracted from the INS solution, which would provide a more accurate solution as it allows the Kalman filter to automatically account for error state correlation. The benefits are evident later in this document when simulations are run to demonstrate the position/velocity error correlation, see Section 4.2 pg. 81

$$
\mathbf{P}_{\delta \hat{\mathbf{x}}_k} =
\begin{bmatrix}
\mathbf{P}^{+(\text{free})}_{k(1,1)} & \mathbf{P}^{+(\text{free})}_{k(1,2)} & \mathbf{P}^{+(\text{free})}_{k(1,3)} & \mathbf{P}^{+(\text{free})}_{k(1,4)} & \mathbf{P}^{+(\text{free})}_{k(1,5)} & \mathbf{P}^{+(\text{free})}_{k(1,6)} & \mathbf{P}^{+(\text{free})}_{k(1,7)} & \mathbf{P}^{+(\text{free})}_{k(1,8)} \\
\mathbf{P}^{+(\text{free})}_{k(2,1)} & \mathbf{P}^{+(\text{free})}_{k(2,2)} & \mathbf{P}^{+(\text{free})}_{k(2,3)} & \mathbf{P}^{+(\text{free})}_{k(2,4)} & \mathbf{P}^{+(\text{free})}_{k(2,5)} & \mathbf{P}^{+(\text{free})}_{k(2,6)} & \mathbf{P}^{+(\text{free})}_{k(2,7)} & \mathbf{P}^{+(\text{free})}_{k(2,8)} \\
\mathbf{P}^{+(\text{free})}_{k(3,1)} & \mathbf{P}^{+(\text{free})}_{k(3,2)} & \mathbf{P}^{+(\text{free})}_{k(3,3)} & \mathbf{P}^{+(\text{free})}_{k(3,4)} & \mathbf{P}^{+(\text{free})}_{k(3,5)} & \mathbf{P}^{+(\text{free})}_{k(3,6)} & \mathbf{P}^{+(\text{free})}_{k(3,7)} & \mathbf{P}^{+(\text{free})}_{k(3,8)} \\
\mathbf{P}^{+(\text{free})}_{k(4,1)} & \mathbf{P}^{+(\text{free})}_{k(4,2)} & \mathbf{P}^{+(\text{free})}_{k(4,3)} & \underline{\mathbf{P}_{\hat{\theta}_x(1,1)}} & \mathbf{P}^{+(\text{free})}_{k(4,5)} & \mathbf{P}^{+(\text{free})}_{k(4,6)} & \mathbf{P}^{+(\text{free})}_{k(4,7)} & \mathbf{P}^{+(\text{free})}_{k(4,8)} \\
\mathbf{P}^{+(\text{free})}_{k(5,1)} & \mathbf{P}^{+(\text{free})}_{k(5,2)} & \mathbf{P}^{+(\text{free})}_{k(5,3)} & \mathbf{P}^{+(\text{free})}_{k(5,4)} & \underline{\mathbf{P}_{\hat{\theta}_y(1,1)}} & \mathbf{P}^{+(\text{free})}_{k(5,6)} & \mathbf{P}^{+(\text{free})}_{k(5,7)} & \mathbf{P}^{+(\text{free})}_{k(5,8)} \\
\mathbf{P}^{+(\text{free})}_{k(6,1)} & \mathbf{P}^{+(\text{free})}_{k(6,2)} & \mathbf{P}^{+(\text{free})}_{k(6,3)} & \mathbf{P}^{+(\text{free})}_{k(6,4)} & \mathbf{P}^{+(\text{free})}_{k(6,5)} & \mathbf{P}^{+(\text{free})}_{k(6,6)} & \mathbf{P}^{+(\text{free})}_{k(6,7)} & \mathbf{P}^{+(\text{free})}_{k(6,8)} \\
\mathbf{P}^{+(\text{free})}_{k(7,1)} & \mathbf{P}^{+(\text{free})}_{k(7,2)} & \mathbf{P}^{+(\text{free})}_{k(7,3)} & \mathbf{P}^{+(\text{free})}_{k(7,4)} & \mathbf{P}^{+(\text{free})}_{k(7,5)} & \mathbf{P}^{+(\text{free})}_{k(7,6)} & \mathbf{P}^{+(\text{free})}_{k(7,7)} & \mathbf{P}^{+(\text{free})}_{k(7,8)} \\
\mathbf{P}^{+(\text{free})}_{k(8,1)} & \mathbf{P}^{+(\text{free})}_{k(8,2)} & \mathbf{P}^{+(\text{free})}_{k(8,3)} & \mathbf{P}^{+(\text{free})}_{k(8,4)} & \mathbf{P}^{+(\text{free})}_{k(8,5)} & \mathbf{P}^{+(\text{free})}_{k(8,6)} & \mathbf{P}^{+(\text{free})}_{k(8,7)} & \mathbf{P}^{+(\text{free})}_{k(8,8)} \\
\mathbf{P}^{+(\text{free})}_{k(9,1)} & \mathbf{P}^{+(\text{free})}_{k(9,2)} & \mathbf{P}^{+(\text{free})}_{k(9,3)} & \mathbf{P}^{+(\text{free})}_{k(9,4)} & \mathbf{P}^{+(\text{free})}_{k(9,5)} & \mathbf{P}^{+(\text{free})}_{k(9,6)} & \mathbf{P}^{+(\text{free})}_{k(9,7)} & \mathbf{P}^{+(\text{free})}_{k(9,8)} \\
\mathbf{P}^{+(\text{free})}_{k(10,1)} & \mathbf{P}^{+(\text{free})}_{k(10,2)} & \mathbf{P}^{+(\text{free})}_{k(10,3)} & \underline{\mathbf{P}_{\hat{\theta}_x(2,1)}} & \mathbf{P}^{+(\text{free})}_{k(10,5)} & \mathbf{P}^{+(\text{free})}_{k(10,6)} & \mathbf{P}^{+(\text{free})}_{k(10,7)} & \mathbf{P}^{+(\text{free})}_{k(10,8)} \\
\mathbf{P}^{+(\text{free})}_{k(11,1)} & \mathbf{P}^{+(\text{free})}_{k(11,2)} & \mathbf{P}^{+(\text{free})}_{k(11,3)} & \mathbf{P}^{+(\text{free})}_{k(11,4)} & \underline{\mathbf{P}_{\hat{\theta}_y(2,1)}} & \mathbf{P}^{+(\text{free})}_{k(11,6)} & \mathbf{P}^{+(\text{free})}_{k(11,7)} & \mathbf{P}^{+(\text{free})}_{k(11,8)} \\
\mathbf{P}^{+(\text{free})}_{k(12,1)} & \mathbf{P}^{+(\text{free})}_{k(12,2)} & \mathbf{P}^{+(\text{free})}_{k(12,3)} & \mathbf{P}^{+(\text{free})}_{k(12,4)} & \mathbf{P}^{+(\text{free})}_{k(12,5)} & \mathbf{P}^{+(\text{free})}_{k(12,6)} & \mathbf{P}^{+(\text{free})}_{k(12,7)} & \mathbf{P}^{+(\text{free})}_{k(12,8)} \\
\mathbf{P}^{+(\text{free})}_{k(13,1)} & \mathbf{P}^{+(\text{free})}_{k(13,2)} & \mathbf{P}^{+(\text{free})}_{k(13,3)} & \mathbf{P}^{+(\text{free})}_{k(13,4)} & \mathbf{P}^{+(\text{free})}_{k(13,5)} & \mathbf{P}^{+(\text{free})}_{k(13,6)} & \mathbf{P}^{+(\text{free})}_{k(13,7)} & \mathbf{P}^{+(\text{free})}_{k(13,8)} \\
\mathbf{P}^{+(\text{free})}_{k(14,1)} & \mathbf{P}^{+(\text{free})}_{k(14,2)} & \mathbf{P}^{+(\text{free})}_{k(14,3)} & \mathbf{P}^{+(\text{free})}_{k(14,4)} & \mathbf{P}^{+(\text{free})}_{k(14,5)} & \mathbf{P}^{+(\text{free})}_{k(14,6)} & \mathbf{P}^{+(\text{free})}_{k(14,7)} & \mathbf{P}^{+(\text{free})}_{k(14,8)} \\
\mathbf{P}^{+(\text{free})}_{k(15,1)} & \mathbf{P}^{+(\text{free})}_{k(15,2)} & \mathbf{P}^{+(\text{free})}_{k(15,3)} & \mathbf{P}^{+(\text{free})}_{k(15,4)} & \mathbf{P}^{+(\text{free})}_{k(15,5)} & \mathbf{P}^{+(\text{free})}_{k(15,6)} & \mathbf{P}^{+(\text{free})}_{k(15,7)} & \mathbf{P}^{+(\text{free})}_{k(15,8)}
\end{bmatrix}
$$

$$
\begin{bmatrix}
\mathbf{P}^{+(\text{free})}_{k(1,9)} & \mathbf{P}^{+(\text{free})}_{k(1,10)} & \mathbf{P}^{+(\text{free})}_{k(1,11)} & \mathbf{P}^{+(\text{free})}_{k(1,12)} & \mathbf{P}^{+(\text{free})}_{k(1,13)} & \mathbf{P}^{+(\text{free})}_{k(1,14)} & \mathbf{P}^{+(\text{free})}_{k(1,15)} \\
\mathbf{P}^{+(\text{free})}_{k(2,9)} & \mathbf{P}^{+(\text{free})}_{k(2,10)} & \mathbf{P}^{+(\text{free})}_{k(2,11)} & \mathbf{P}^{+(\text{free})}_{k(2,12)} & \mathbf{P}^{+(\text{free})}_{k(2,13)} & \mathbf{P}^{+(\text{free})}_{k(2,14)} & \mathbf{P}^{+(\text{free})}_{k(2,15)} \\
\mathbf{P}^{+(\text{free})}_{k(3,9)} & \mathbf{P}^{+(\text{free})}_{k(3,10)} & \mathbf{P}^{+(\text{free})}_{k(3,11)} & \mathbf{P}^{+(\text{free})}_{k(3,12)} & \mathbf{P}^{+(\text{free})}_{k(3,13)} & \mathbf{P}^{+(\text{free})}_{k(3,14)} & \mathbf{P}^{+(\text{free})}_{k(3,15)} \\
\mathbf{P}^{+(\text{free})}_{k(4,9)} & \underline{\mathbf{P}_{\hat{\theta}_x(1,2)}} & \mathbf{P}^{+(\text{free})}_{k(4,11)} & \mathbf{P}^{+(\text{free})}_{k(4,12)} & \mathbf{P}^{+(\text{free})}_{k(4,13)} & \mathbf{P}^{+(\text{free})}_{k(4,14)} & \mathbf{P}^{+(\text{free})}_{k(4,15)} \\
\mathbf{P}^{+(\text{free})}_{k(5,9)} & \mathbf{P}^{+(\text{free})}_{k(5,10)} & \underline{\mathbf{P}_{\hat{\theta}_y(1,2)}} & \mathbf{P}^{+(\text{free})}_{k(5,12)} & \mathbf{P}^{+(\text{free})}_{k(5,13)} & \mathbf{P}^{+(\text{free})}_{k(5,14)} & \mathbf{P}^{+(\text{free})}_{k(5,15)} \\
\mathbf{P}^{+(\text{free})}_{k(6,9)} & \mathbf{P}^{+(\text{free})}_{k(6,10)} & \mathbf{P}^{+(\text{free})}_{k(6,11)} & \mathbf{P}^{+(\text{free})}_{k(6,12)} & \mathbf{P}^{+(\text{free})}_{k(6,13)} & \mathbf{P}^{+(\text{free})}_{k(6,14)} & \mathbf{P}^{+(\text{free})}_{k(6,15)} \\
\mathbf{P}^{+(\text{free})}_{k(7,9)} & \mathbf{P}^{+(\text{free})}_{k(7,10)} & \mathbf{P}^{+(\text{free})}_{k(7,11)} & \mathbf{P}^{+(\text{free})}_{k(7,12)} & \mathbf{P}^{+(\text{free})}_{k(7,13)} & \mathbf{P}^{+(\text{free})}_{k(7,14)} & \mathbf{P}^{+(\text{free})}_{k(7,15)} \\
\mathbf{P}^{+(\text{free})}_{k(8,9)} & \mathbf{P}^{+(\text{free})}_{k(8,10)} & \mathbf{P}^{+(\text{free})}_{k(8,11)} & \mathbf{P}^{+(\text{free})}_{k(8,12)} & \mathbf{P}^{+(\text{free})}_{k(8,13)} & \mathbf{P}^{+(\text{free})}_{k(8,14)} & \mathbf{P}^{+(\text{free})}_{k(8,15)} \\
\mathbf{P}^{+(\text{free})}_{k(9,9)} & \mathbf{P}^{+(\text{free})}_{k(9,10)} & \mathbf{P}^{+(\text{free})}_{k(9,11)} & \mathbf{P}^{+(\text{free})}_{k(9,12)} & \mathbf{P}^{+(\text{free})}_{k(9,13)} & \mathbf{P}^{+(\text{free})}_{k(9,14)} & \mathbf{P}^{+(\text{free})}_{k(9,15)} \\
\mathbf{P}^{+(\text{free})}_{k(10,9)} & \underline{\mathbf{P}_{\hat{\theta}_x(2,2)}} & \mathbf{P}^{+(\text{free})}_{k(10,11)} & \mathbf{P}^{+(\text{free})}_{k(10,12)} & \mathbf{P}^{+(\text{free})}_{k(10,13)} & \mathbf{P}^{+(\text{free})}_{k(10,14)} & \mathbf{P}^{+(\text{free})}_{k(10,15)} \\
\mathbf{P}^{+(\text{free})}_{k(11,9)} & \mathbf{P}^{+(\text{free})}_{k(11,10)} & \underline{\mathbf{P}_{\hat{\theta}_y(2,2)}} & \mathbf{P}^{+(\text{free})}_{k(11,12)} & \mathbf{P}^{+(\text{free})}_{k(11,13)} & \mathbf{P}^{+(\text{free})}_{k(11,14)} & \mathbf{P}^{+(\text{free})}_{k(11,15)} \\
\mathbf{P}^{+(\text{free})}_{k(12,9)} & \mathbf{P}^{+(\text{free})}_{k(12,10)} & \mathbf{P}^{+(\text{free})}_{k(12,11)} & \mathbf{P}^{+(\text{free})}_{k(12,12)} & \mathbf{P}^{+(\text{free})}_{k(12,13)} & \mathbf{P}^{+(\text{free})}_{k(12,14)} & \mathbf{P}^{+(\text{free})}_{k(12,15)} \\
\mathbf{P}^{+(\text{free})}_{k(13,9)} & \mathbf{P}^{+(\text{free})}_{k(13,10)} & \mathbf{P}^{+(\text{free})}_{k(13,11)} & \mathbf{P}^{+(\text{free})}_{k(13,12)} & \mathbf{P}^{+(\text{free})}_{k(13,13)} & \mathbf{P}^{+(\text{free})}_{k(13,14)} & \mathbf{P}^{+(\text{free})}_{k(13,15)} \\
\mathbf{P}^{+(\text{free})}_{k(14,9)} & \mathbf{P}^{+(\text{free})}_{k(14,10)} & \mathbf{P}^{+(\text{free})}_{k(14,11)} & \mathbf{P}^{+(\text{free})}_{k(14,12)} & \mathbf{P}^{+(\text{free})}_{k(14,13)} & \mathbf{P}^{+(\text{free})}_{k(14,14)} & \mathbf{P}^{+(\text{free})}_{k(14,15)} \\
\mathbf{P}^{+(\text{free})}_{k(15,9)} & \mathbf{P}^{+(\text{free})}_{k(15,10)} & \mathbf{P}^{+(\text{free})}_{k(15,11)} & \mathbf{P}^{+(\text{free})}_{k(15,12)} & \mathbf{P}^{+(\text{free})}_{k(15,13)} & \mathbf{P}^{+(\text{free})}_{k(15,14)} & \mathbf{P}^{+(\text{free})}_{k(15,15)}
\end{bmatrix}_{15 \times 15}
\tag{90}
$$

The effect on the horizontal velocity error is immediate. The effect on the INS horizontal position error is gradual but becomes noticeably more significant as time progresses. The

navigation scenario continues with no further aiding; consequently, if the INS navigation system's aiding session was conducted at halftime (30 min into the flight) then at one hour into the flight the aircraft's positional uncertainty is far less than that of the "free"-INS—this, courtesy of the corrected velocity at halftime and the recalibration of the horizontal accelerometers.
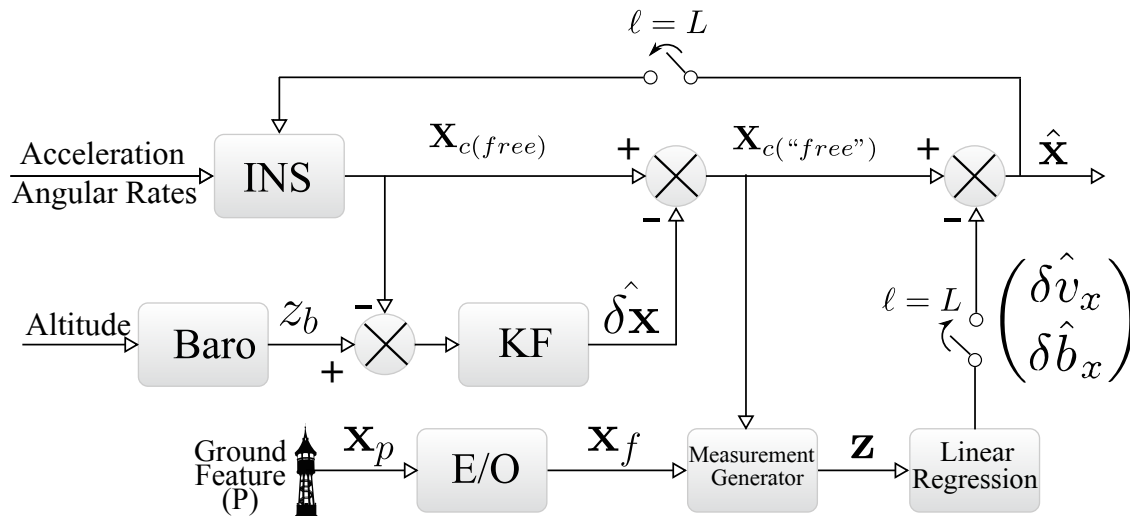
The complete V-INS system is illustrated in Figure 12.

Figure 12. V-INS Navigation System: The unaided (free) INS solution is corrected with a baro and KF yielding the "free"-INS solution. After the measurement epoch, the INS solution is corrected using estimates of the horizontal velocity errors and accelerometer biases from the vision system and LR estimator, and the INS is updated.

Estimation with a Constrained Flightpath.

A special case presents itself if the flight path leading up to the measurement epoch is constrained/known. A constrained scenario (e.g., a constant aircraft velocity, wings level flight) allows the determination of the INS velocity error for the entire flight leading up to the measurement epoch, not just the error at the beginning of the measurement epoch. As was demonstrated in [19], if one knows the flight conditions leading up to the measurement epoch, the correlation between velocity and position error states allows the estimation of the position error in addition to the velocity error and accelerometer bias. Essentially, it allows the system

to account for the position error growth leading up to the measurement epoch, providing a far more accurate navigation solution. However, this limits the practicality of the method since it assumes a constrained flight path for otherwise the INS error equations would be different. Therefore, although the scenario herein considers a constrained pre-measurement epoch flight path, our measurement model assumes no knowledge of the flight path outside of the 10-second measurement epoch and, therefore, no position velocity correlation; the position error is not estimated. Regardless, the V-INS still yields a reduction in the position error over the course of the flight, which comes only from the onetime velocity error estimate; the reduced velocity error after the INS update at the end of the measurment epoch reduces the growth of position error no matter the flight dynamics leading up to or following the measurement epoch. If, however, the entire flight was wings level and at constant altitude and airspeed, the position error may—by exploiting the position/velocity error correlation—be estimated by executing a LR using the estimated INS velocity error and accelerometer bias as follows:

$$
\mathbf{z} \equiv \begin{pmatrix} 0 \\ \hat{\delta v}_x \\ \hat{\delta b}_x \end{pmatrix}, \ \boldsymbol{\theta} \equiv \begin{pmatrix} \delta x \\ \delta v_x \\ \delta b_x \end{pmatrix}, \ \mathbf{H} \equiv \begin{bmatrix} 1 & 0 & 0 \\ 0 & 1 & 0 \\ 0 & 0 & 1 \end{bmatrix}, \tag{91}
$$

$$
\mathbf{R} \equiv \begin{bmatrix} \mathbf{P}_{\delta x \delta x} & \mathbf{P}_{\delta x \delta v_x} & \mathbf{P}_{\delta x \delta b_x} \\ \mathbf{P}_{\delta v_x \delta x} & \mathbf{P}_{\hat{\delta v}_x \hat{\delta v}_x} & \mathbf{P}_{\hat{\delta v}_x \hat{\delta b}_x} \\ \mathbf{P}_{\delta b_x \delta x} & \mathbf{P}_{\hat{\delta b}_x \hat{\delta v}_x} & \mathbf{P}_{\hat{\delta b}_x \hat{\delta b}_x} \end{bmatrix} \tag{92}
$$

where the elements of $\mathbf{R}$ are taken from the error state covariance matrices from the V-INS KF and Equation (90).

Benefit of Additional Measurement Epochs.

The baseline scenario considers a single measurement epoch at halftime; however, additional measurement epochs would theoretically reduce the INS error and increase the accuracy of the navigation solution. The INS velocity error is reset at the end of each measurement epoch restricting it growth. The INS position error growth is also further reduced. Thus, the more measurement epochs, the less time there is for the error to grow. In the original scenario, the INS error is left to grow for 30 minutes, but if a second epoch is added the growth period is restricted to 20 minutes. And at three epochs, the growth is limited to 15 minutes.

Unfortunately, this is likely impractical in the real-world because although a single measurement epoch is a minor and manageable distraction for the pilot, adding additional aiding epochs risks task saturation. Despite the lack of real-world practicality, simulating additional epochs is not difficult, and it provides insight into the benefits of the added measurements. Therefore, an additional scenario in which the pilot engages in six measurement epochs throughout the scenario, roughly every 8.5 minutes was envisioned and simulated. Although inherently impracticable, the addition of measurement epochs may become possible by reducing the pilot involvement during the epoch—e.g., by using an automated tracking system.

3.2 Simulation Design and Setup

The object of the simulations was to demonstrate and charaterize the herein developed V-INS method. They are based on the scenario descried previously and simulates the INS error growth during the one hour flight. Multiple simulation phases were executed to demonstrate different facets of the V-INS method; all simulations used the same flight path (wings level, constant velocity and altitude, heading due east) and assumed the ground feature location was unknown. Phase 1 considered a "free"-running navigation-grade INS with aiding

only from the barometer to verify that the INS horizontal position error is 1 km/hr and to provide a baseline for evaluating the V-INS. Phase 2 employed the full V-INS aiding method tracking a single ground feature for 10 seconds to derive 10 measurement. Phase 3 exploited the correlation between the INS position and velocity errors due to demonstrate the increased aiding potential. Phase 4 removed the position and velocity correlation and introduces five additional measurement epochs. Phase 5, reimplemented Phase 2, but replaced the navigation-grade INS with one of tactical-grade INS with horizontal position errors of 100 km/hr.

V-INS Characterization.

The simulations allow the characterization of the following system attributes:

- Reduction of errors and uncertainty in the INS horizontal position estimates after one hour of flight

- Reduction of errors and uncertainty in the INS horizontal velocity estimates after one hour of flight

- Reduction of errors and uncertainty in the x and y channel INS accelerometer bias estimates after one hour of flight

Due primarily to lack of observability of the INS platform tilt errors and gyroscope biases and the stochastic nature of the system, unaccounted for acceleration can sometimes induce additional error weakening or invalidating the estimates. Thus, it is possible for an individual realization to exhibit increased error. The stochastic nature of the system called for the use of Monte Carlo trials; 10,000 flight scenario were executed to generate the performance data.

Simulated Error States and Covariance.

The MATLAB simulations propagated the 15 INS error states and covariance of both the "free"-INS and the V-INS over the one-hour flight. Prior to the measurement epoch and V-INS updated, these values are identical. The scenario assumes precise knowledge of the aircraft position and pose; thus, the error states and covariance are initialized according to Equations (52) and (53).

For all but the final simulation phase, the accelerometer biases' and gyroscope biases' standard deviation values were chosen to induce a 1 km/hr error horizontal position error in the "free"-INS[4]: $\sigma_b = 1.0906 \times 10^{-4}$ m/sec^2 and $\sigma_\omega = 9.0859 \times 10^{-9}$ rad/sec. This is within the typical error range of a navigation-grade INS [36]. The tactical-grade INS was modeled with accelerometer biases of 1.0906×10^{-4} m/sec^2 and gyroscope biases of 9.0859×10^{-9} rad/sec to induce a 100 km/hr horizontal position error.

Simulated Sensors.

The simulated aircraft E/O sensor design was based on the same camera specifications used in previous vision-aided INS researcher [20, 29, 31, 40]:

- Focal length: 0.0048 m

- Aspect Ratio: 1 (focal plane area: 0.0048^2 m^2)

- Resolution: 9 megapixels

- Error standard deviation: 1 pixel $\Rightarrow \sigma_{x_f} = \sigma_{y_f} = \frac{0.0048}{\sqrt{9 \times 10^6}} = 1.6 \times 10^{-6}$ m

The simulated barometric altimeter sensor specifications was also borrowed from previous research [20] and was based on the Honeywell AM-250 [11]. The altitude error standard deviation, σ_h, was set at 1 m.

---

[4]Derived using the Lyapunov equation and propagating the covariance through time separately for each bias, as was done in previous research [19, 29, 31, 37].

Simulated Measurement Epoch and Estimates.

For all simulation phases, with the exception of Phase 4, the aircraft enters the measurement epoch at the 1800 second mark and begins measurements of the ground feature's bearings at one second intervals for eleven seconds. The ground feature is position 100 m south of the aircraft and approximately 180 km east of the starting position. In this manner, 10 measurements of ground speed error, generated using Equations (76) and (77), provide the linear regression measurements for estimating the x and y-channel INS velocity errors and accelerometer biases with Equations (88) and (89). Equation (90) provides the estimate covariance. Note that Phase 3 also considers the position and velocity error correlation and, therefore, uses Equation (91) to estimate the INS position error. Phase 4 simulates six measurement epochs evenly spaced across the one-hour flight, so that the first epoch begins at around the 514 second mark; all measurements and estimation are carried out as in Phase 2, just multiple times.

Following the measurement epoch, the estimated INS error values are subtracted from the current propagated error states. The new/corrected estimate covariance replaces the former, propagated covariance. This constitutes the INS update, creating the new/corrected V-INS error states. The simulation continues propagating both the "free"-INS and updated V-INS error states and covariances for the remainder of the scenario.

IV. Results

This chapter documents and analyzes the results obtained from the V-INS simulations. It begins with the verification of the barometer aided "free"-INS and accelerometer and gyroscope calibration, simulation Phase 1. The chapter follows with the results and discussion from simulation Phases 2, 3, 4, and 5.

4.1 "Free"-INS Calibration (Phase 1)

Error state plots from a single realization of the "free"-INS, Figures 13-17, depict its propagated state error and covariance over the one-hour scenario. The simulated "free"-INS position error, Figure 13, demonstrates the proper accelerometer and gyroscope bias calibration: The position error in the x and y directions grows to 1000 m over the course of the one-hour scenario. It also demonstrates proper barometer aiding of the z channel as the error is constrained.

Figure 14 displays the INS velocity error growth. As expected, the vertical channel is constrained due to the barometer and KF.

Figure 15 displays the INS "platform" tilt error growth propagated for the one-hour flight. The accelerometer and gyroscope biases cause a total growth in error standard deviation of about 0.33 Mils. As expected, the error is unaffected by the barometer.

Figure 16 and Figure 17 show the random, constant accelerometer and gyroscope biases, respectively. The z-direction accelerometer bias is standard deviation shrinks significantly a short time into the scenario due to the barometer aiding effect.
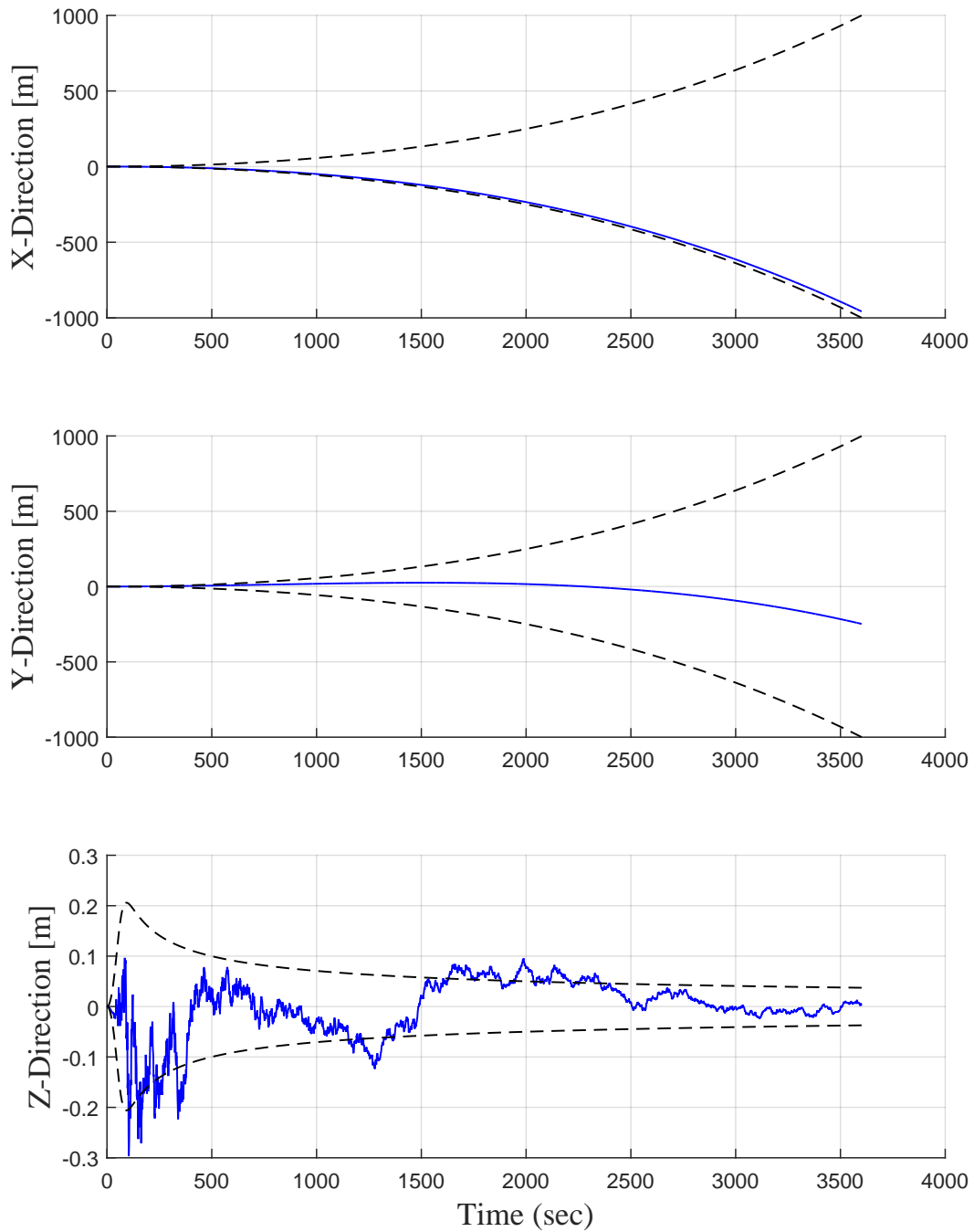
Figure 13. Propagated "Free"-INS Position Error (solid) and standard deviation (dashed)
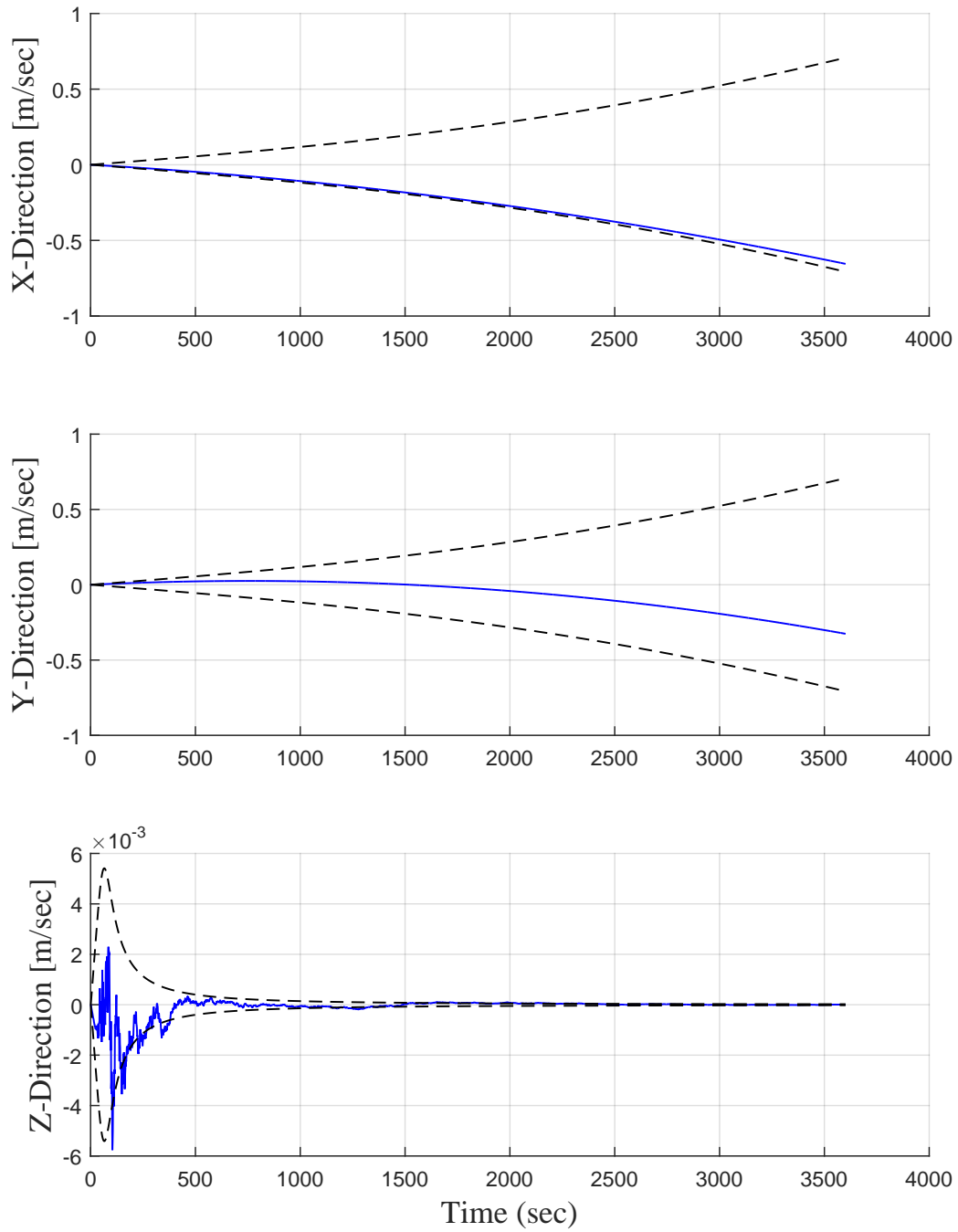
Figure 14. Propagated "Free"-INS Velocity Error (solid) and standard deviation (dashed)

69
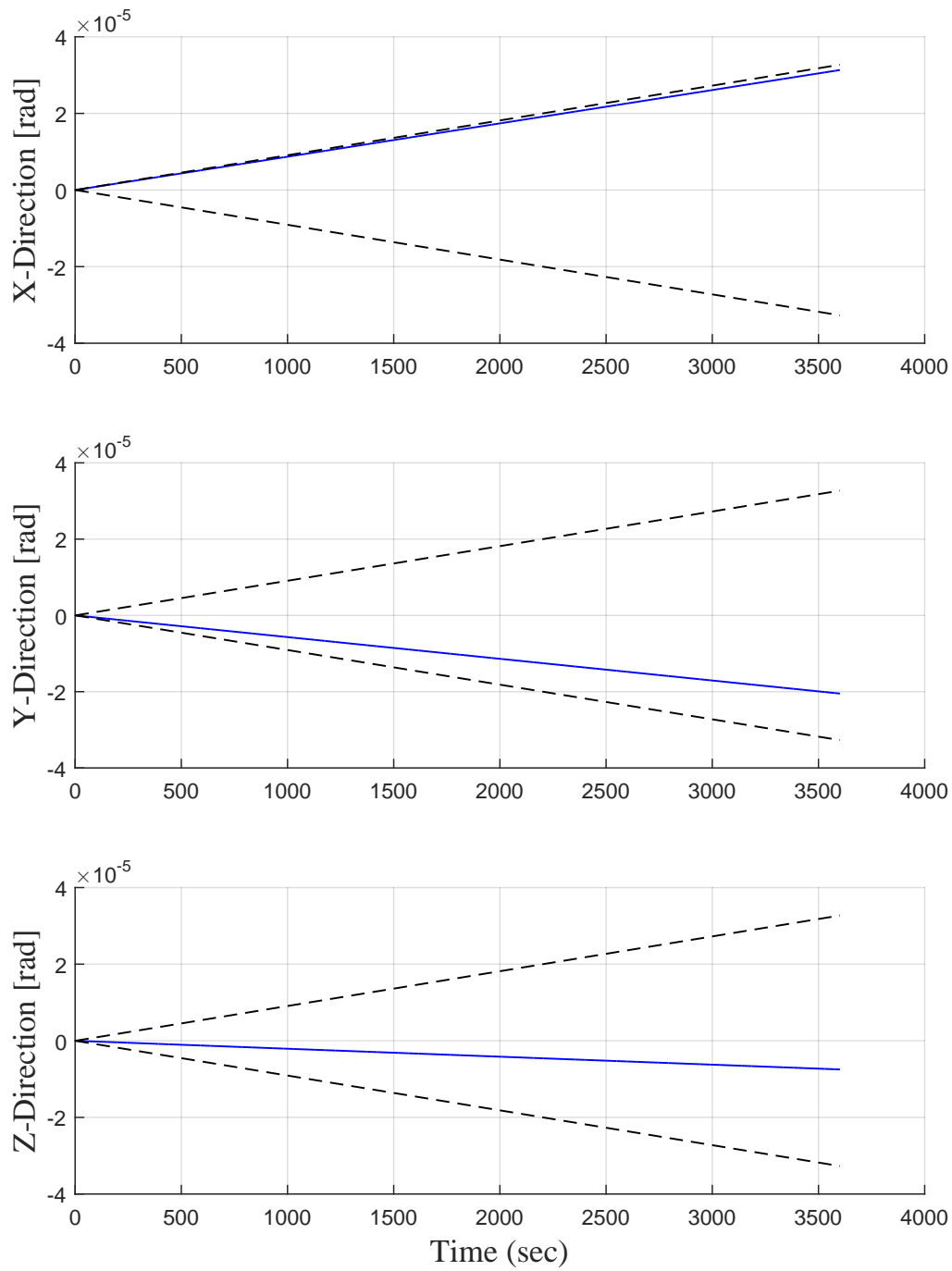
Figure 15. Propagated "Free"-INS Tilt Error (solid) and standard deviation (dashed)

70
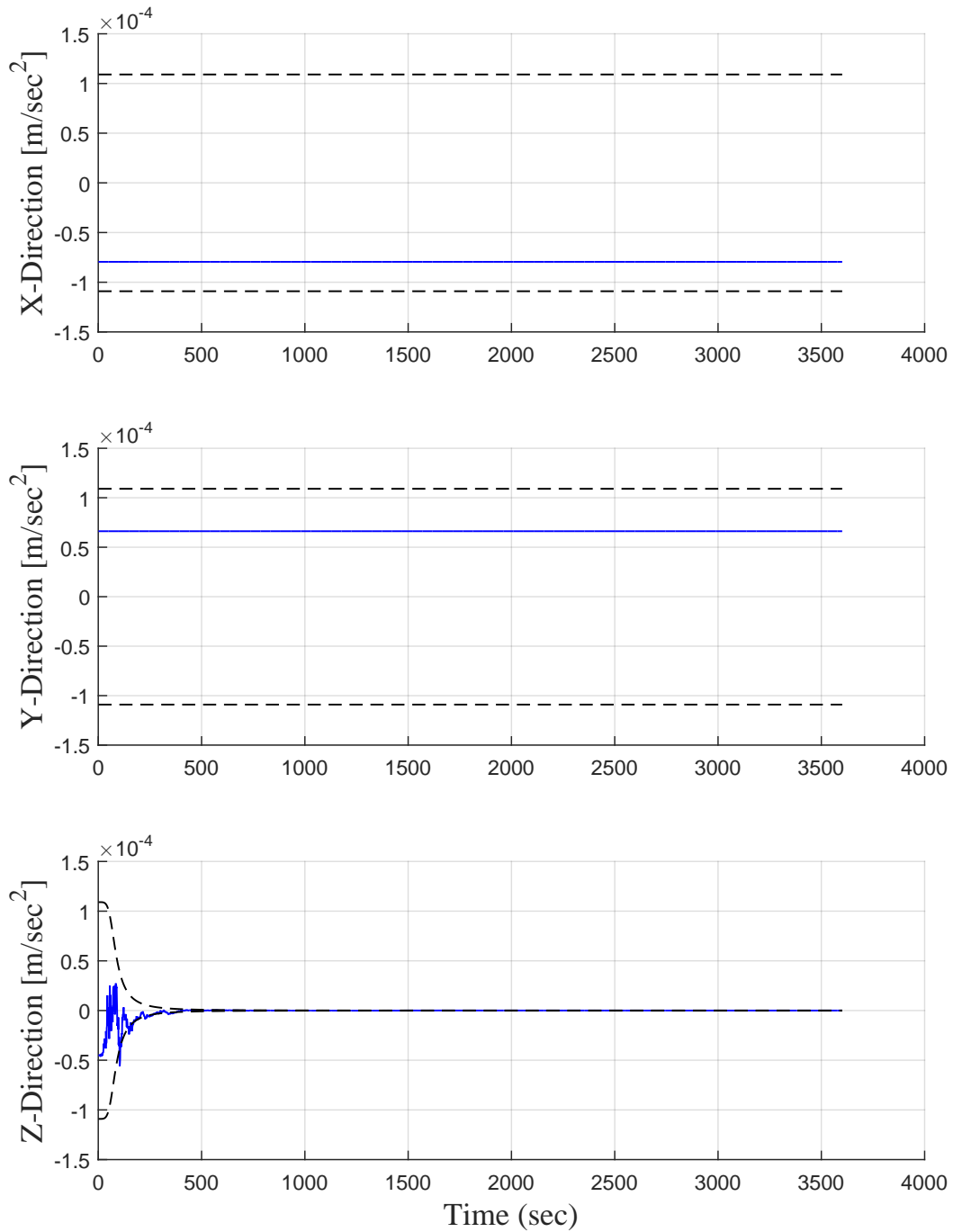
Figure 16. Propagated "Free"-INS Accelerometer Bias (solid) and standard deviation (dashed)

71
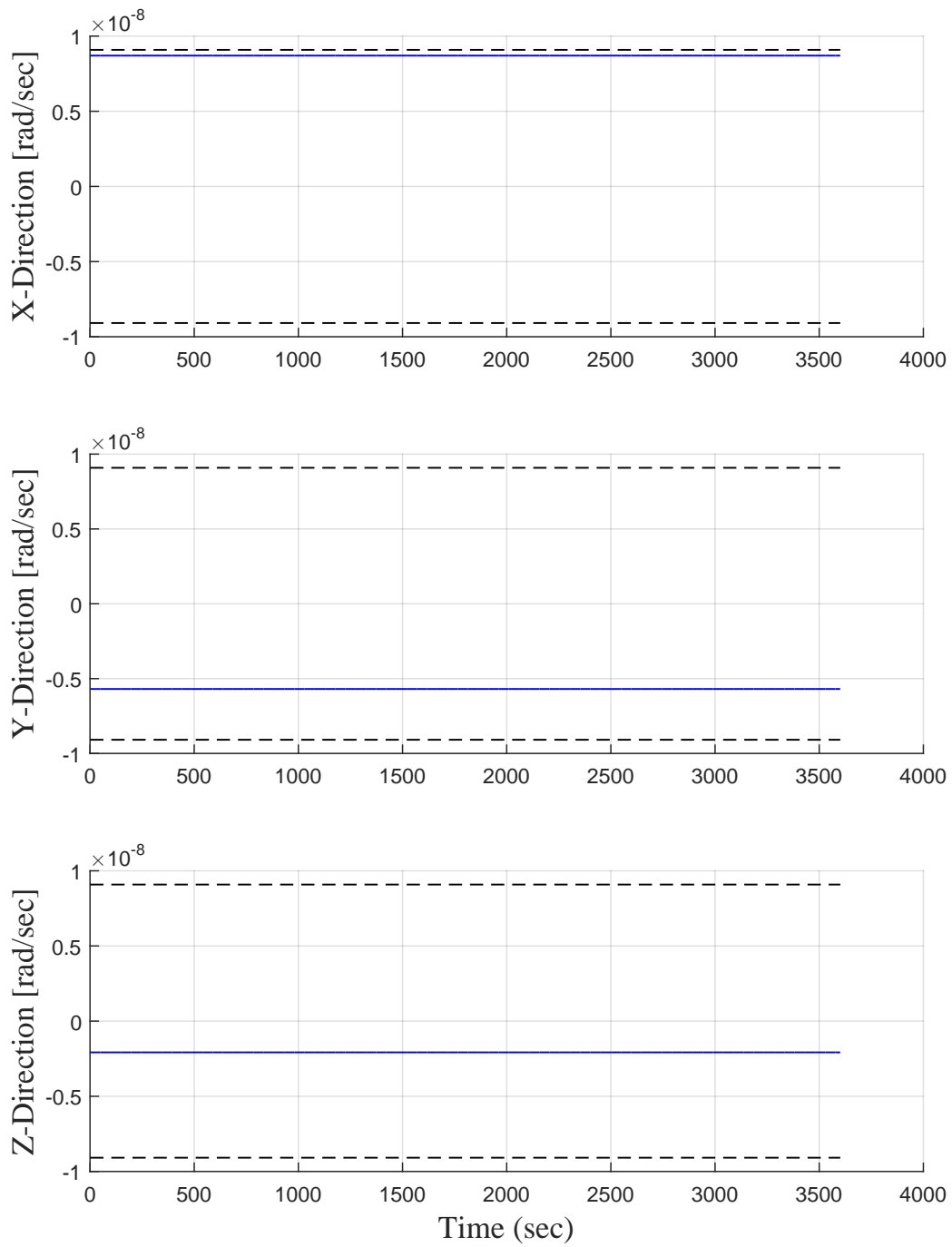
Figure 17. Propagated "Free"-INS Gyroscope Bias (solid) and standard deviation (dashed)

4.2   V-INS Performance (Phase 2)

The following plots compare the 15 error states of the "free"-INS and V-INS from a single, typical realization of the one-hour flight simulation, demonstrating the INS aiding. Each figure depicts error state in the three orthogonal directions (x,y, and z), which correspond to east, north, and altitude in this scenario; each is flanked by its standard deviation.

At its heart, this system works on a ground speed update. Thus, examining the velocity error and accelerometer bias states first provides an illuminating demonstration of the V-INS aiding function. Figure 18 displays the velocity error states in each direction. The measurement epoch occurs from 1800 sec through 1810 sec; the "free"-INS and V-INS errors are identical up until this point. At the 1810 sec mark, the final ground feature measurement is taken, the ground speed and accelerometer bias estimates are obtained via linear regression, and the INS is updated/reset. The ground speed estimate made from the E/O measurements is far more accurate than the "free"-INS estimate. Accordingly, the system exhibits an immediate reduction in the velocity error in both x and y directions; they experience very similar aiding. The estimate standard deviations also drops. Following the V-INS reset, the error instantly begins to grow again. However, because it was reset, the resulting V-INS error remains less than the "free"-INS error for the remainder of the scenario. Accordingly, the INS position error also received aiding from the velocity error estimate as it is simply the integral of the velocity error. There is, of course, no aiding to the vertical, z-direction velocity error as there is no vertical observability from E/O system, alone. The vertical channel is aided by the barometer, and thus, the "free"-INS and V-INS z-direction plots are identical.

Figure 19 compares the accelerometer bias errors. There is a very small decrease in the standard deviation; although it is not noticeable on the plot. As earlier mentioned, because position is simply the integral of the velocity, the reduction in accelerometer bias also con-

tributes to the reduction in the INS position error, see Figure 20. This is apparent in Table 1, which compares the error reduction achieved with and without the accelerometer bias estimated. As will be shown, other scenarios exhibited better estimates of the accelerometer bias.

Figure 20 depicts the position error states in each direction. Aiding from the E/O system occurs in the x and y channels. Although there is never a direct estimate of the INS position error, it still obtains significant aiding from the estimation of INS velocity error and accelerometer bias as it is the integral of the velocity error. Accordingly, there is not an immediate reduction in the position error as was witnessed in the velocity error. However, because the position error following the update propagates with reduced velocity error, its overall growth is dampened. Thus, over the remainder of the scenario, the V-INS position error is much less than the "free"-INS error. As with the velocity error plots, there is additional aiding of the z-channel and the V-INS and "free"-INS plots are identical.

Figure 21 displays the growth of the three INS "platform" tilt error associated with each aircraft axis for the on-hour flight. The tilt errors contribute to the growth in the INS position and velocity errors because they cause incorrectly aligned force vectors, see Equation (44). However, they obtain no aiding from the measurements and their error growth continues unbounded; i.e., the V-INS and "free"-INS plots are identical. The inability to estimate the platform tilt error limits (but certainly does not nullify) the aiding potential of this V-INS.

Figure 22 shows the random, constant gyroscope biases. As with the platform tilt errors, they are not directly estimated and do not receive any aiding from the measurements. Thus, they contribute to the error growth of the position, velocity, and tilt angles for both the V-INS and the "free"-INS, and the plots for each are identical.
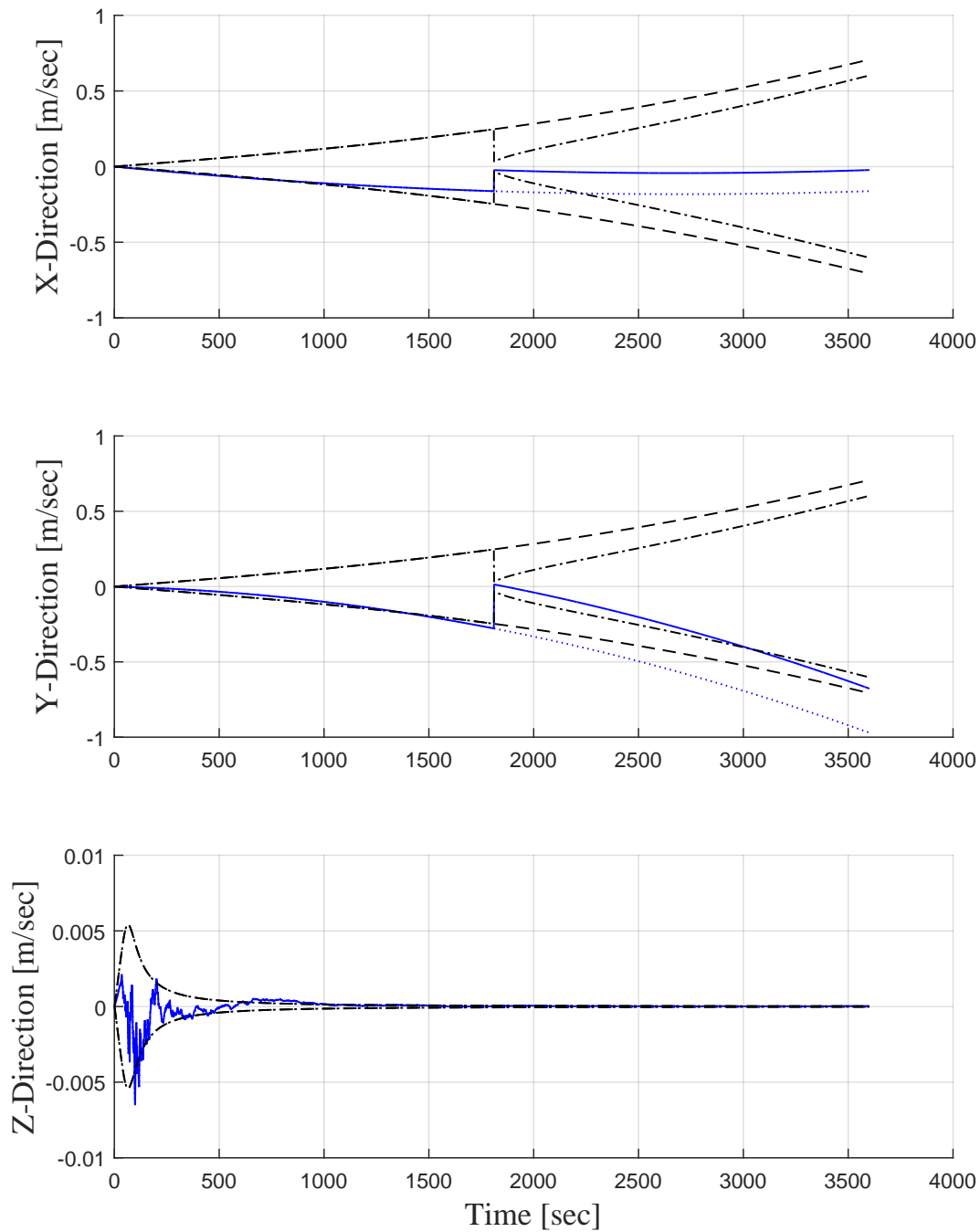
Figure 18. Propagated V-INS velocity error (solid) and standard deviation (dot-dash) compared to the "Free"-INS velocity error (dotted) and standard deviation (dashed)
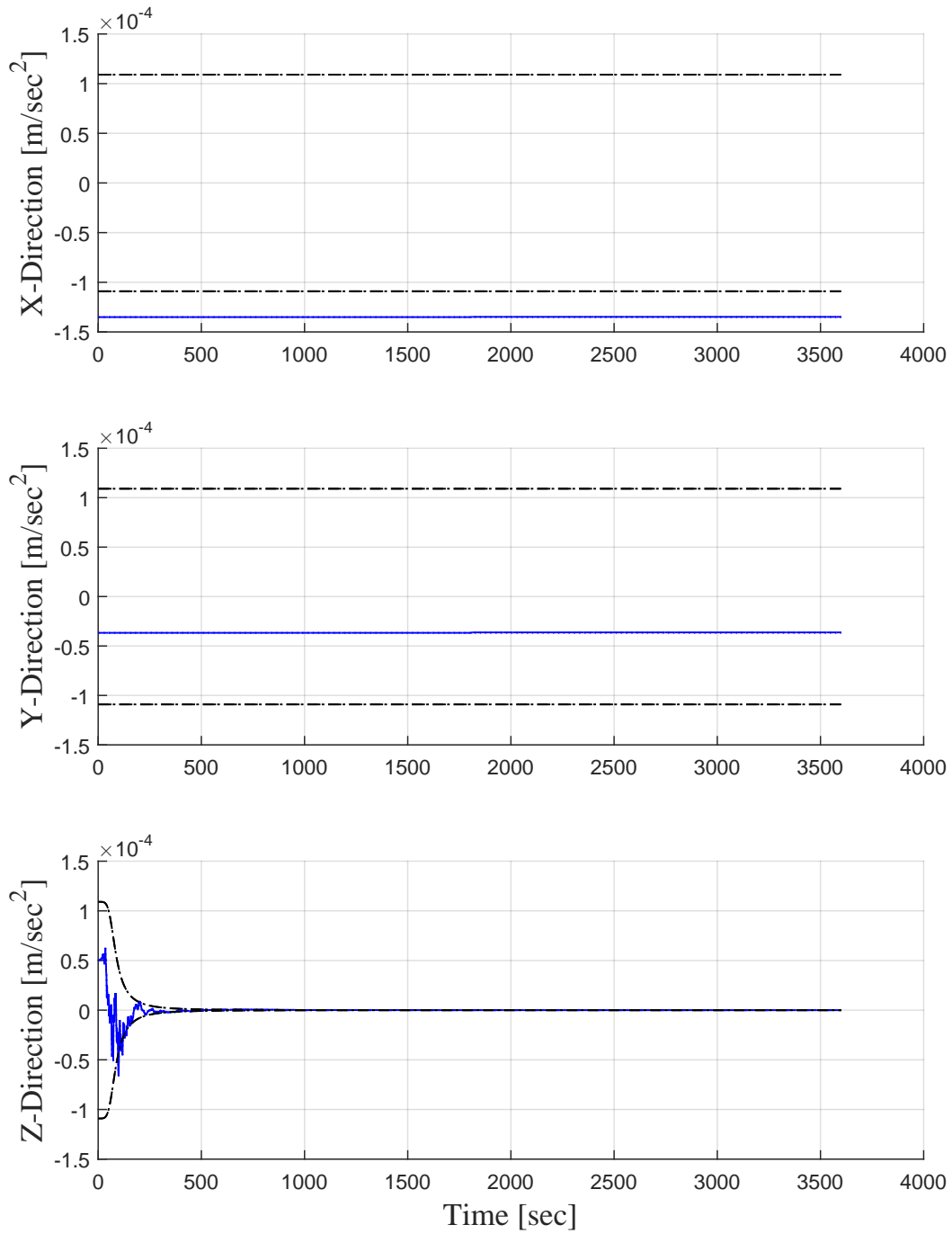
Figure 19. Constant V-INS accelerometer bias (solid) and standard deviation (dot-dash) compared to the "Free"-INS accelerometer bias (dotted) and standard deviation (dashed)
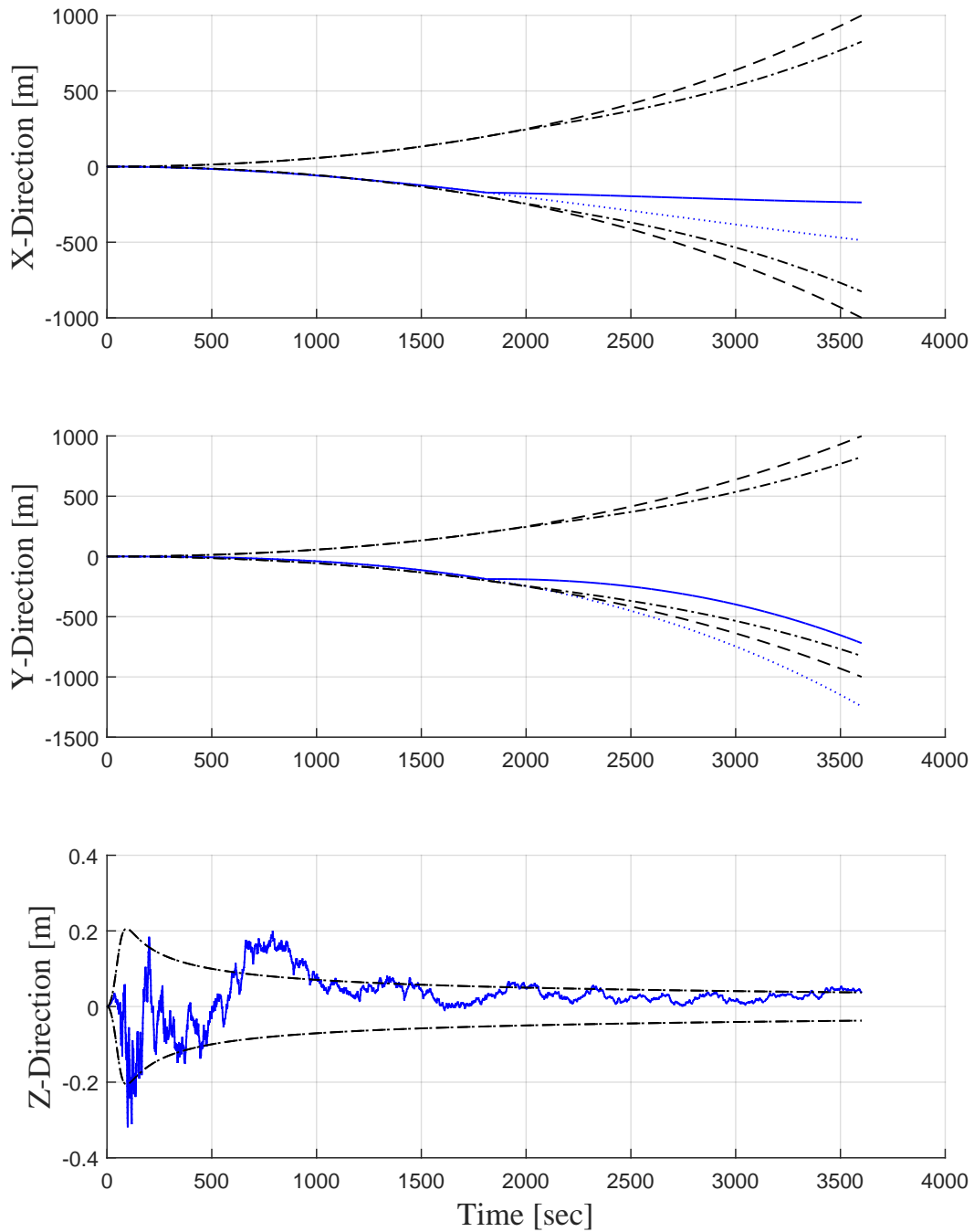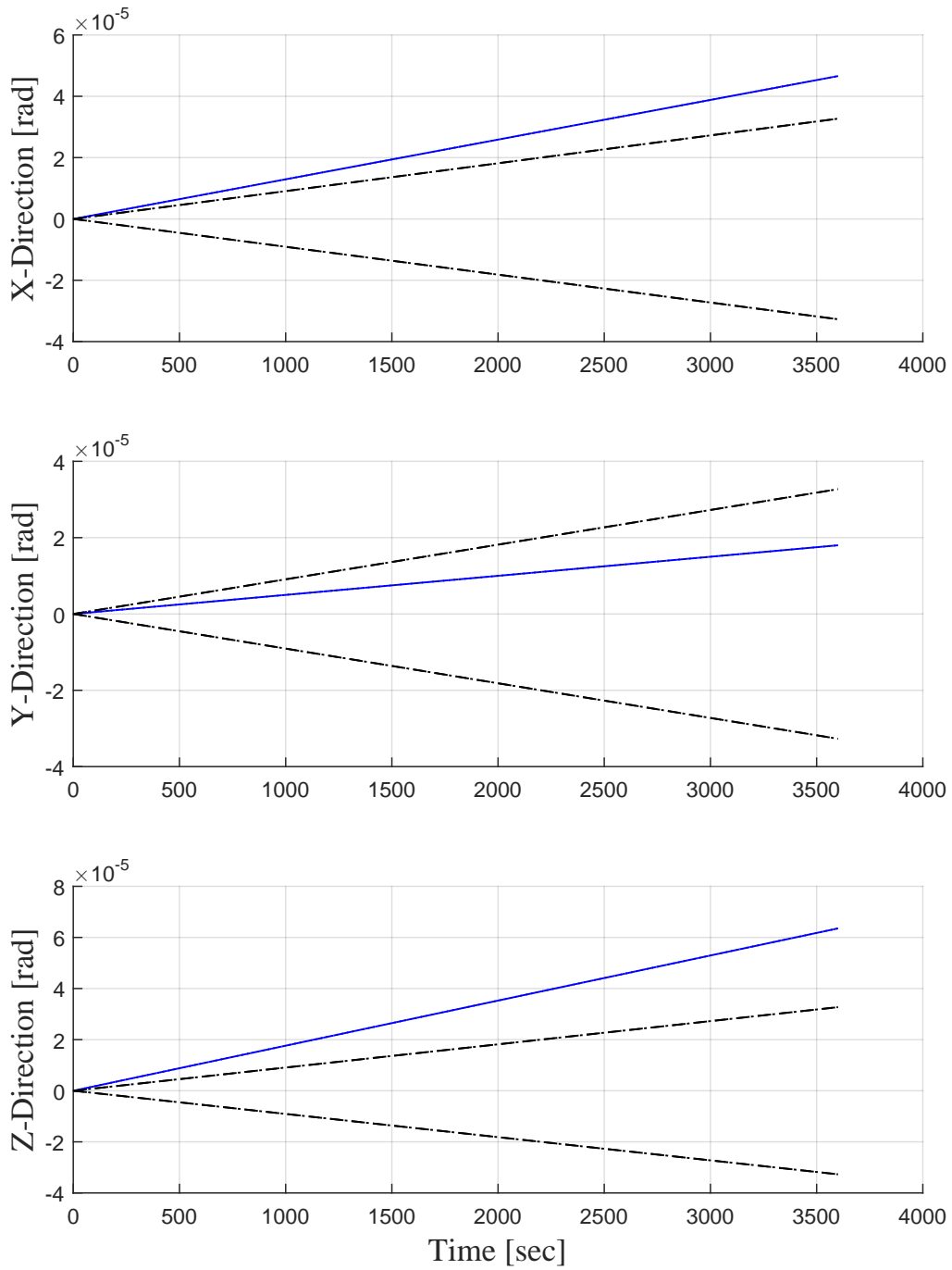
Figure 20. Propagated V-INS positioin error (solid) and standard deviation (dot-dash) compared to the "Free"-INS position error (dotted) and standard deviation (dashed).

77

Figure 21. Propagated "Free"-INS and V-INS Tilt Error (solid) and standard deviation (dotted)
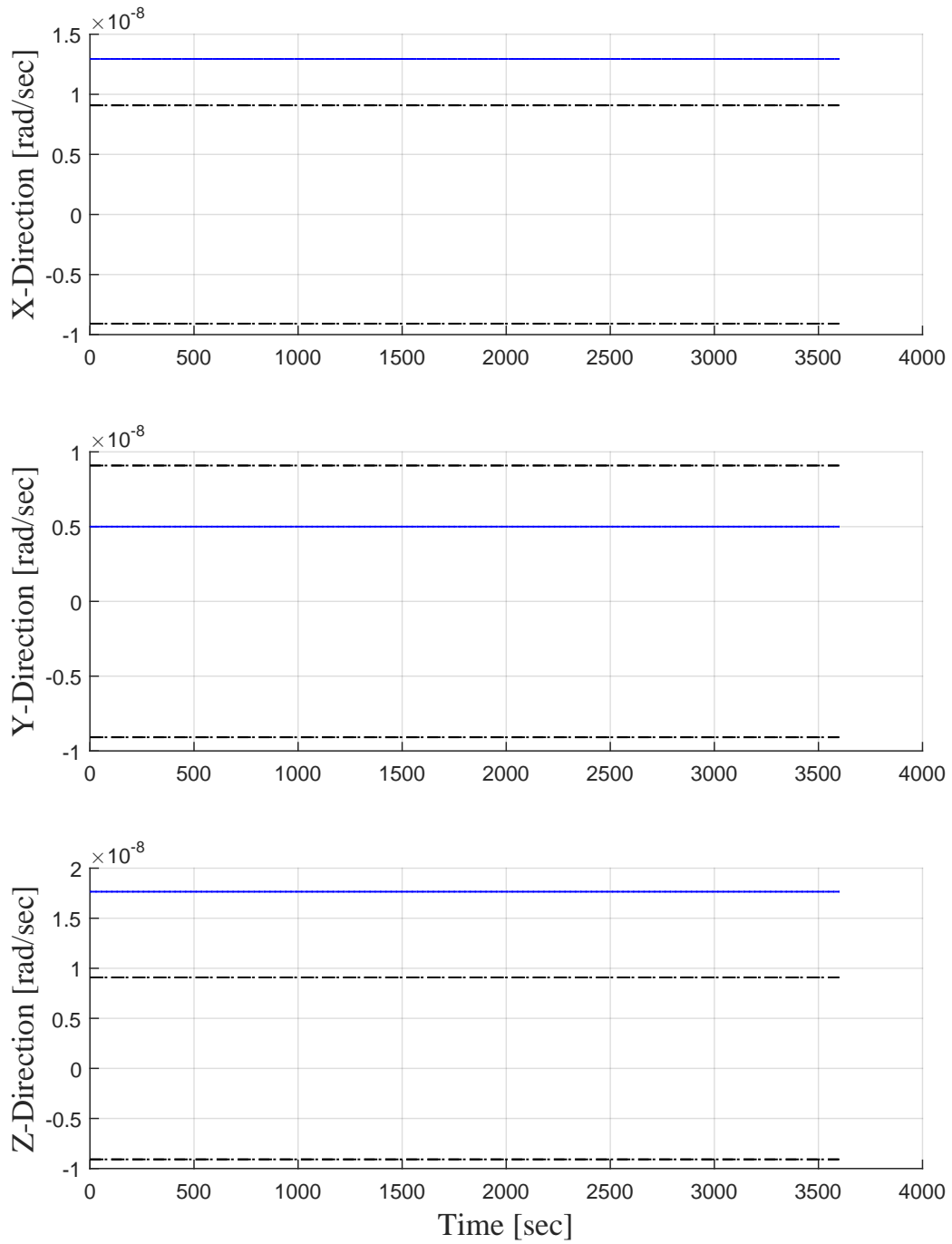
Figure 22. Propagated "Free"-INS Gyroscope Bias (solid) and standard deviation (dotted)

Monte Carlo Results.

To legitimately characterize the aiding potential of this V-INS, 10,000 Monte Carlo trials were executed simulating the navigation scenario and the resulting navigation state errors and covariance values were averaged. Table 1 compares the reduction in state error and standard deviation achieved using the V-INS over the "free"-INS for the horizontal directions of applicable states, i.e., state which received aiding. As expected, the x and y channels experienced very similar aiding on average. The table also includes the reduction in standard deviation of the V-INS navigation state error estimates with the simulation reprogrammed not to estimate accelerometer bias, highlighting the advantage of estimating the INS accelerometer bias in addition to the INS velocity error, even if the reduction is very small.

Table 1. V-INS error reduction with and w/out the accelerometer bias: 10K realizations

	Bias Estimated		Bias not Estimated	
	X-Channel	Y-Channel	X-Channel	Y-Channel
Position Error	42.90%	43.00%	42.86%	42.93%
Position Std Dev	17.33%	17.35%	10.15%	10.16%
Velocity Error	31.73%	31.75%	31.42%	31.62%
Velocity Std Dev	14.81%	14.81%	6.19%	6.19%
Accelerometer Bias	0.001%	0.005%	0%	0%
Accelerometer Bias Std Dev	0.001%	0.001%	0%	0%

Constrained/Known Flight Path Demonstration (Phase 3).

The constrained aircraft flight path used in the simulated scenario allows for the demonstration of the increased aiding available when the flight path is known and correlation between the INS position error and velocity is considered. In the simulated scenarios, the aircraft maintains the wings-level, constant speed and altitude, and east direction of the measurement epoch for the entire one-hour flight. As discussed in Section 3.1 pg. 61, this method required exact knowledge of the flight path and is, therefore, not always practical. Figure 23 displays a single realization of the V-INS x-direction navigation error states (and standard deviation) compared to the "free"-INS. The y-direction plots are not shown, but the results are the same.

The reduction in error is substantial, considerably more than when the position velocity correlation is not considered. The correlation present between the position error and velocity error provide an estimate of the INS position error; therefore, unlike the earlier simulations, there is an immediate reduction in the estimated position error following the measurement epoch. Essentially, the system is able to "back out" the position error that accumulated for the first half of the scenario from the ground speed estimate. Accordingly, the x-direction position error estimate standard deviation decreased by 80%, significantly more than the modest 17% reduction realized earlier when the flight path was considered unknown.

There is also a reduction in the horizontal velocity error and accelerometer bias, since the LR estimator accounts for the known flight path, which also reduces the overall position growth.
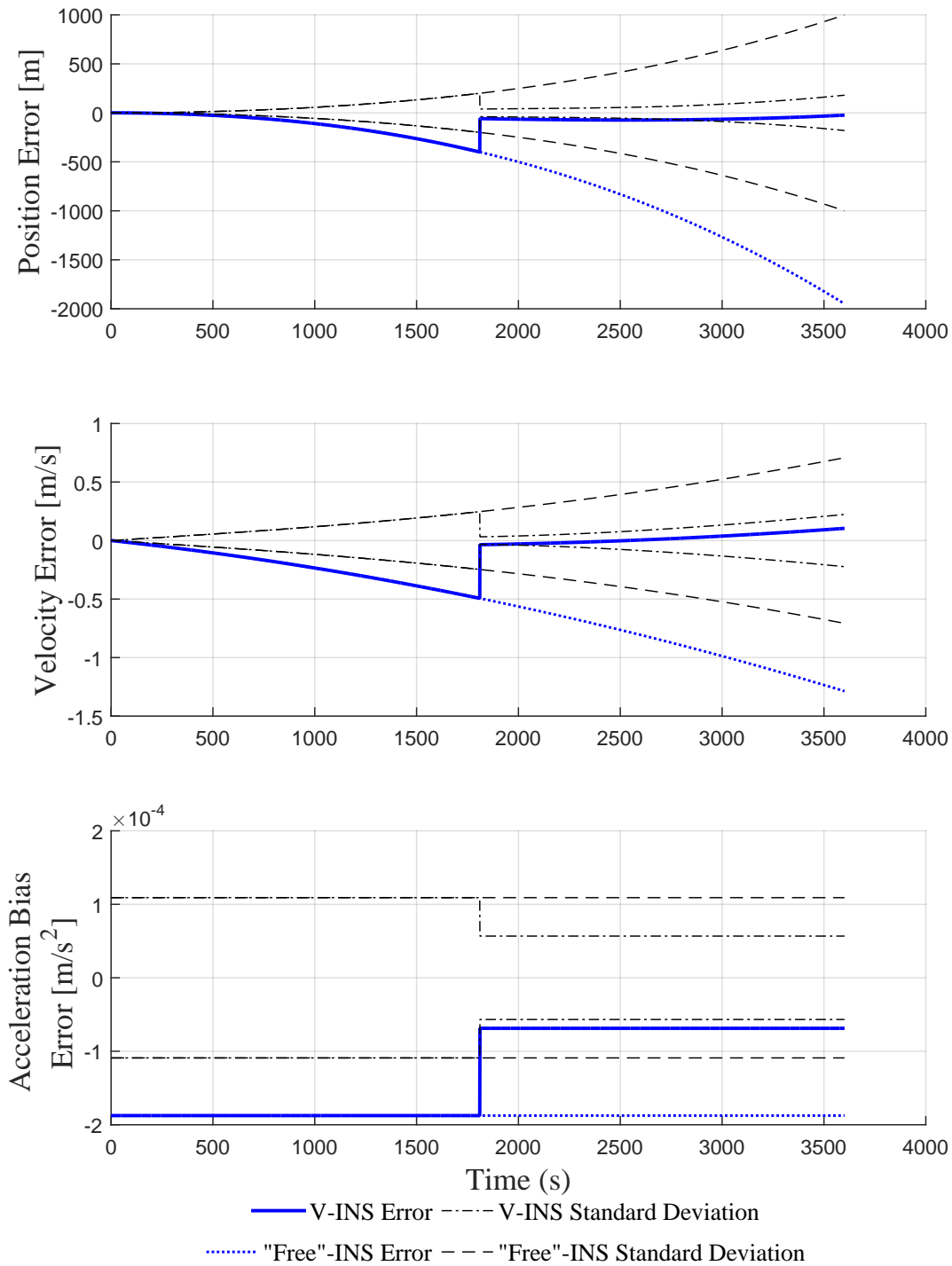
Figure 23. V-INS Aiding when Position/Velocity Error Correlation is Present: x-direction

Additional Measurement Epochs (Phase 4).

As mentioned in Section 3.1 pg. 63, additional measurement epochs provide greater aiding to the INS. This result is apparent from Figure 24 and Figure 25, which demonstrates the error reduction realized in the six-measurement epoch simulation for the x-direction and y-direction, respectively. Examining the plot, the velocity plot, the measurement epochs are clearly demarcated by the abrupt drop in error and standard deviation at roughly 514 second intervals. By the end of the flight, the position standard deviations is 60% reduced compared to the "free"-INS, much greater than the modest 17% reduction realized for a single measurement epoch.

The application of multiple measurement epochs in an operational environment may not be possible due to the risk of pilot task saturation. However, any additional measurement epoch conducted along the flight path will reduce the overall horizontal position error. The scenario considers six measurement epochs, but even a single additional epoch, providing it is not too close to the first, will provide significant additional error reduction.

Tactical-Grade INS (Phase 5).

The final round of simulations demonstrated the V-INS system using a tactical-grade INS, which accumulated horizontal position error at a rate of 100 km/hr, and as Figure 26 illustrates, the "free"-INS horizontal position errors grew to 100 km by the end of the scenario. Like the baseline scenario, this simulation considered only a single measurement epoch, and the results were promising. The V-INS position error standard deviation was reduced by 17.9 km, or 17.9%, slightly better than the 17.3% reduction obtained using the navigation-grade INS. In Figure 27, the velocity error standard deviation was reduced by 15.7%, also slightly better than the 14.8% reduction achieved using the navigation grade INS. Examining Figure 28, it is clear that the accelerometer bias estimate is significantly improved over the navigation-grade scenario, where the aiding was very slight. The ac-

celerometer bias standard deviation was reduced by 8.95%. The increased accuracy in the horizontal accelerometer bias estimates when a tactical-grade INS is used is due to the significantly greater error in the aircraft velocity estimate and contributes its slightly increased performance. The proposed V-INS method could, therefore, also prove useful in aircraft with tactical-grade inertial systems.
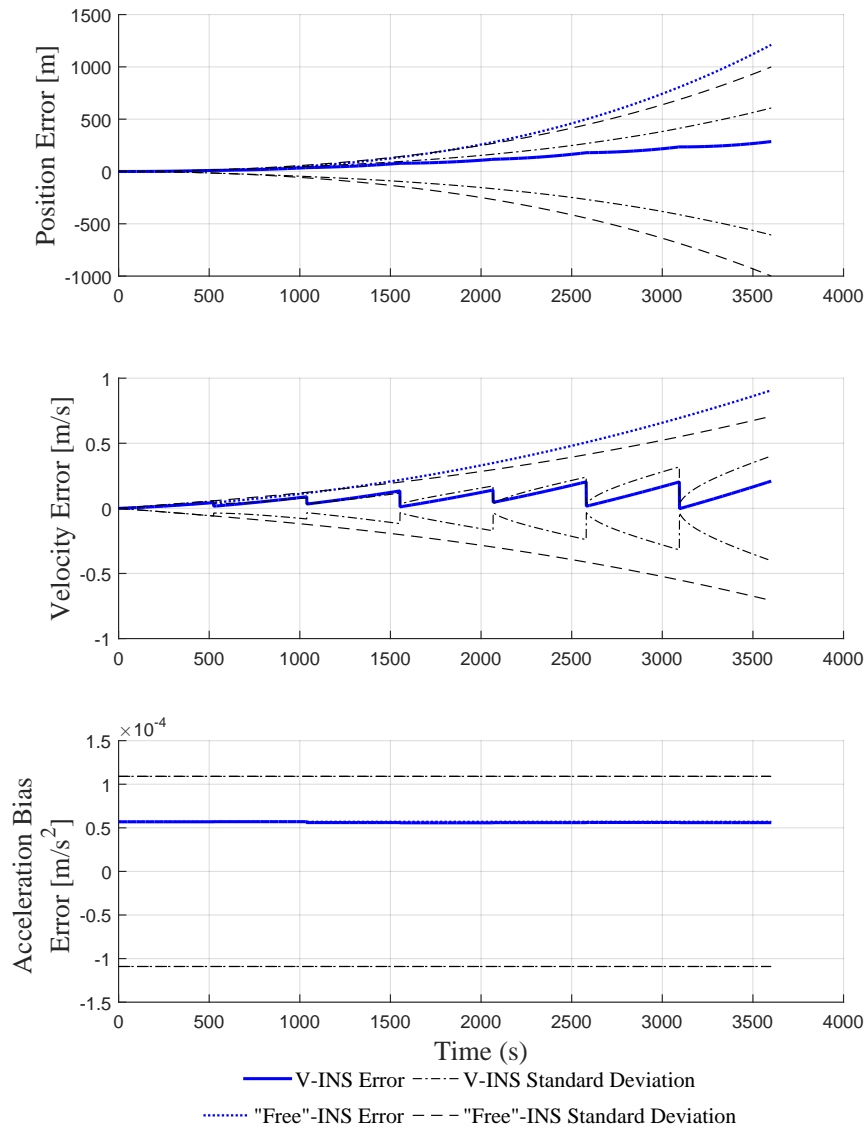

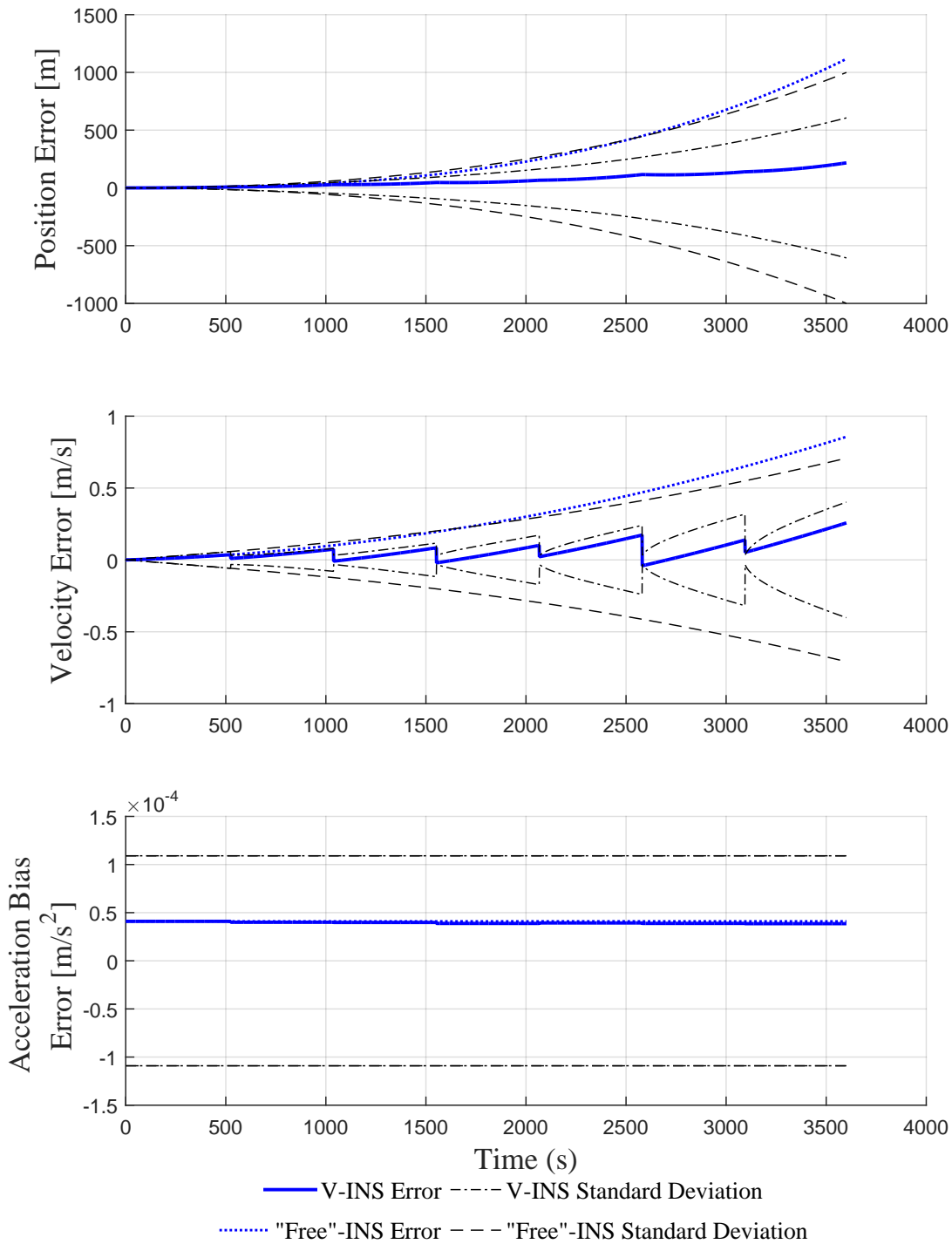Figure 24. "Free"-INS and V-INS error comparison with six measurement epochs: x-direction

Figure 25. "Free"-INS and V-INS error comparison with six measurement epochs: y-direction

Scenario Comparison.

Table 2 compares the V-INS attributes under the varied simulated scenarios including the baseline scenario (navigation grade INS with a single measurement epoch), the baseline scenario with position/velocity correlation considered, a navigation-grade INS with multiple measurement epochs, and finally, a with a single measurement epoch using a tactile-grade INS. Only the x-direction is shown; the y-direction exhibits near equal aiding for all scenarios. Using multiple measurement epochs provides a clear benefit, as does a contained flight path where the position/velocity error correlation may be considered; however, these scenarios may not be practical.

Table 2. Reduction in estimate error and standard deviation among simulated scenarios (x-direction)

	Nav-Grade INS			Tactical-Grade INS
	One Epoch	One Epoch [1]	Multi Epochs	One Epoch
Position Error	42.90%	80.52%	81.46%	44.79%
Position Std Dev	17.35%	81.86%	39.26%	17.85%
Velocity Error	31.46%	62.60%	76.23%	32.78%
Velocity Std Dev	14.81%	68.38%	43.20%	15.69%
Accelerometer Bias	0.001%	13.83%	0.005%	9.73%
Accelerometer Bias Std Dev	0.001%	30.53%	0.001%	8.95%

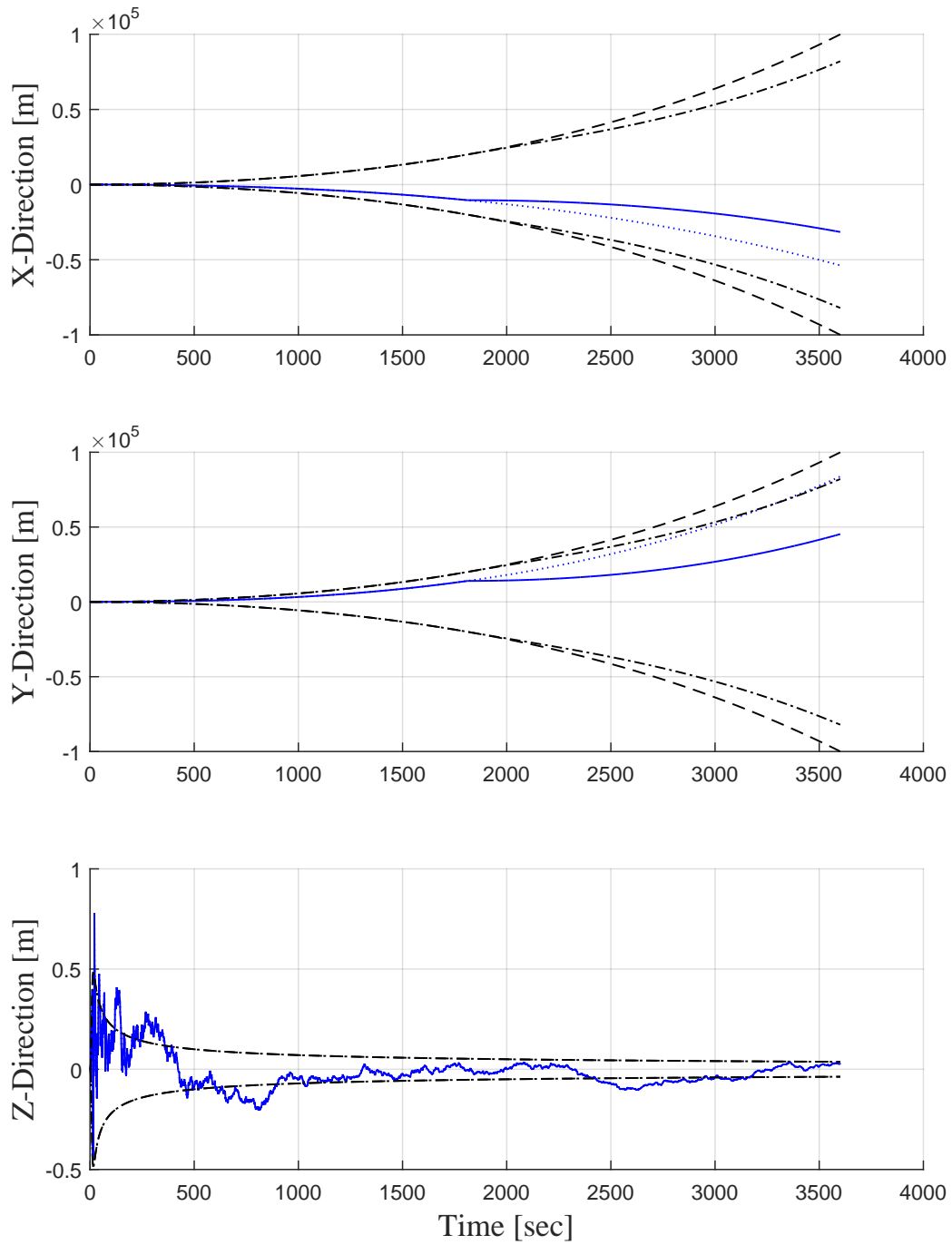[1]with position/velocity error correlation

Figure 26. Propagated tactical-grade V-INS positioin error (solid) and standard deviation (dot-dash) compared to the "Free"-INS position error (dotted) and standard deviation (dashed).
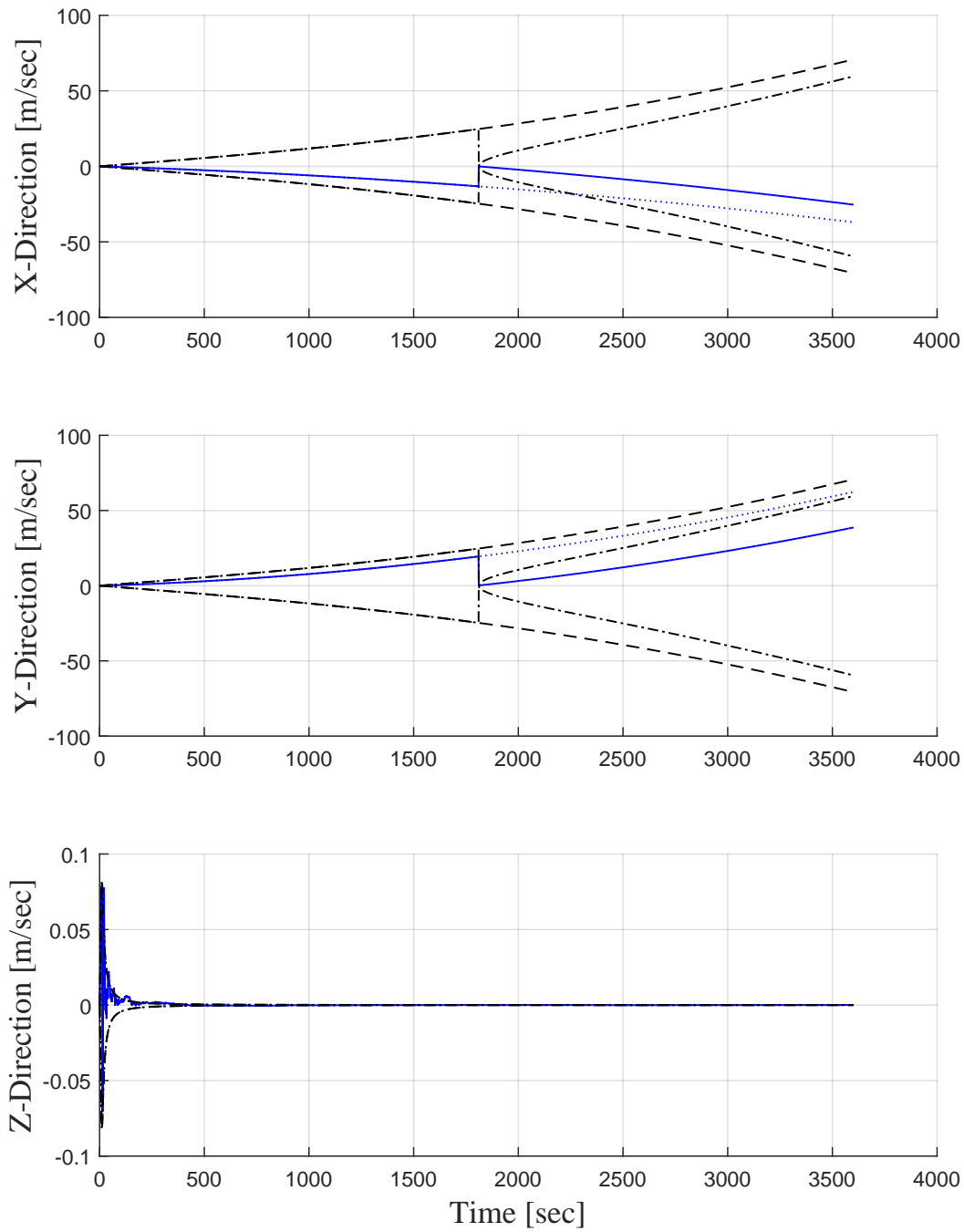
Figure 27. Propagated tactical-grade V-INS velocity error (solid) and standard deviation (dot-dash) compared to the "Free"-INS velocity error (dotted) and standard deviation (dashed).
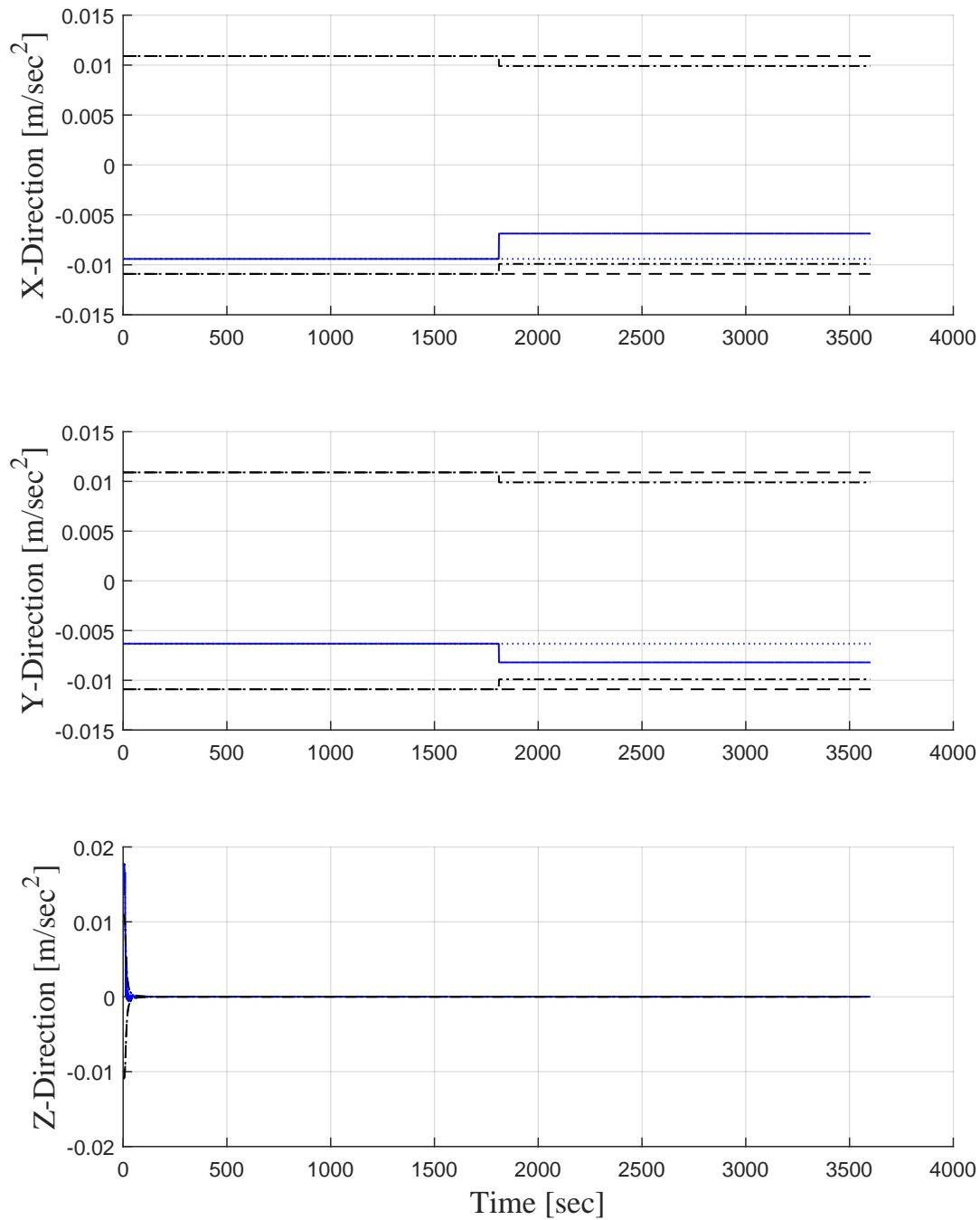
Figure 28. Propagated tactical-grade V-INS accelerometer bias error (solid) and standard deviation (dot-dash) compared to the "Free"-INS velocity error (dotted) and standard deviation (dashed).

89

V. Conclusion

Despite the predominance of the GPS in navigation, our nation's leaders have made it clear that the country needs alternatives. What makes inertial navigation such a promising alternative—and also sets it apart from other modern navigation technologies—is its total self-containment, passiveness, and insusceptibility to RF attack and environmental factors. Alone, the INS is not tenable, but its shortcoming, namely debilitating drift, can be overcome through aiding. Many aiding methods exists, but vision aiding was the focus of this research. In addition to its relatively low cost, employing E/O systems enables the INS to maintain its passive nature emitting no RF.

This work introduced a new, operated-assisted V-INS navigation method based on a modified measurement model for aiding an INS using bearings-only measurements taken over time of a stationary, but unknown ground, feature. An estimate of INS velocity error and accelerometer bias is readily obtained from the measurements, which then allows more accurate future potion estimates by reducing the growth in the INS horizontal position error. A basic navigation scenario simulation was used to demonstrate the novel V-INS aiding concept. The simulation results demonstrated significant improvement of navigation state estimates over time and also a reduction of predicted navigation state estimation uncertainty. At the end of a one-hour flight, a single vision-aiding session conducted at halftime enabled a 17% reduction in the horizontal position uncertainty over the free-running INS estimate. In addition, other variations of the V-INS method were explored demonstrating varying degrees of aiding, including conducting multiple measurement epochs, constraining the flight path to allow position and velocity error correlation, and using a higher error, tactical-grade INS.

The important theoretical development is the unconventional converted measurements method of linearization that makes possible accurate linear state estimation. In addition, an important element of the V-INS navigation method is keeping a human in the loop, thus

avoiding the potential false matches that plague autonomous, computer vision based feature trackers/ATR. However, this does not limit the V-INS navigation method to piloted aircraft, as many unmanned aircraft have downward facing cameras monitored real-time by remote human operators, so, when operationally feasible, their navigation performance could be enhanced using the V-INS method.

The rapid employability of our V-INS is enticing. It requires no maturation of technology and may be implemented on current aircraft, manned and unmanned, without the need for additional hardware. Thus, unlike many new navigation technologies with prospects in the mid and long-terms, it could fill a short-term operational need. In theory, minor updates to the on-board navigation computer are all that is required and implementation cost is relatively low.

The method appears feasible, but more work is required to assess true real-world benefit. Accordingly, continued research should evaluate the method using a more robust dynamics model that does not limit the aircraft trajectory to wings-level, constant altitude flight. In addition, if an accurate INS error model exists, the method could be modified to employ the Kalman filter to achieve the INS update, as opposed to the ad-hoc, direct subtraction/replacement method that was employed in this research. Different flight paths would alter the percentage of error reduction achieved with the V-INS; although, it would not effect the ground speed estimate. The sensor error, specifically error induced by the barometer and E/O also require a more rigorous analysis. In addition, a thorough reexamination of the latest advances in autonomous visual INS research should be accomplished, as well as inquiry into the capabilities of current E/O systems, e.g. the Sniper targeting pod.

If possible, the aiding algorithms should be validated using real flight data consisting of digital imagery and unaided INS output and using a truth reference such as GPS data. Assuming the method proves successful using flight data, actual hardware integration and flight testing is the logical next step.

Future research could also focus on relevant human factors. The error induced by a human operator manually tracking the ground feature on a digital display should be characterized. Furthermore, the accuracy and practicality of allowing the E/O system to track a human-identified and selected feature (e.g., using the Sniper targeting pod's point tracking feature) is worth exploring as it might remove much of the human error.

Appendix A.

1.1 Measurement Equation Linearization

The error terms of the V-INS measurement equation, Equation (63), are linearized, yielding Equation (64), using conventional perturbation analysis: Consider a general non-linear function, $f(x)$. The argument of the function equals its calculated value (e.g., from the navigation computer), which is its true value plus some error. Thus, $f(x_c) = f(x + \delta x)$. An linear approximation of the function may thus be made by $f(x) \approx f(x_c) - \frac{\mathrm{d}f}{\mathrm{d}x}\Big|_x \delta x$. The linearization is performed on Equation (63) as follows:

After rearranging,

$$\begin{pmatrix} x \\ y \end{pmatrix} - \begin{pmatrix} x_p \\ y_p \end{pmatrix} = \frac{z - z_p}{\begin{pmatrix} 0 & 0 & 1 \end{pmatrix} (\mathbf{C}_b^n) \begin{pmatrix} x_f \\ y_f \\ -f \end{pmatrix}} \begin{bmatrix} 1 & 0 & 0 \\ 0 & 1 & 0 \end{bmatrix} (\mathbf{C}_b^n) \begin{pmatrix} x_f \\ y_f \\ -f \end{pmatrix}$$

To aid readability, let $\mathbf{z}$ equal the RHS of the above equation and apply the following substitutions:

$$u = z - z_p,$$

$$v = \begin{pmatrix} 0 & 0 & 1 \end{pmatrix} (\mathbf{C}_b^n)_c \begin{pmatrix} x_{fm} \\ y_{fm} \\ -f \end{pmatrix},$$

$$\text{and} \quad \mathbf{w} = \begin{bmatrix} 1 & 0 & 0 \\ 0 & 1 & 0 \end{bmatrix} \mathbf{C}_b^n \begin{pmatrix} x_f \\ y_f \\ -f \end{pmatrix}.$$

Thus,

$$\mathbf{z} = \frac{u}{v} \cdot \mathbf{w},$$

Next, employing the perturbing technique to linearize yields

$$\mathbf{z}(z, \mathbf{C}_b^n, \mathbf{x}_f) \approx \mathbf{z}(z_c, \mathbf{C}_{bc}^n, \mathbf{x}_{fc}) - \left.\frac{\partial \mathbf{z}}{\partial z}\right|_z \delta z - \left.\frac{\partial \mathbf{z}}{\partial \mathbf{C}_b^n}\right|_{\mathbf{C}_n^b} \delta \mathbf{C}_b^n - \left.\frac{\partial \mathbf{z}}{\partial \mathbf{x}_f}\right|_{\mathbf{x}_f} \delta \mathbf{x}_f$$

where the subscript c indicates a value provided by the baro-aided "free" INS taken at face

value and where $\mathbf{x}_f \equiv \begin{pmatrix} x_f \\ y_f \\ -f \end{pmatrix}$; $\mathbf{x}_{fm} = \mathbf{x}_f + \begin{pmatrix} \delta x_f \\ \delta y_f \\ 0 \end{pmatrix}$. The derivative terms are evaluated as

follows:

$$\left.\frac{\partial \mathbf{z}}{\partial z}\right|_z = \frac{\frac{\partial \mathbf{u}}{\partial z}}{v} \cdot \mathbf{W}$$

$$= \frac{1}{\begin{pmatrix} 0 & 0 & 1 \end{pmatrix} \mathbf{C}_b^n \begin{pmatrix} x_f \\ y_f \\ -f \end{pmatrix}} \begin{bmatrix} 1 & 0 & 0 \\ 0 & 1 & 0 \end{bmatrix} \mathbf{C}_b^n \begin{pmatrix} x_f \\ y_f \\ -f \end{pmatrix}$$

$$\left.\frac{\partial \mathbf{z}}{\partial \mathbf{C}_b^n}\right|_z = \frac{\partial \left(\frac{u}{v}\right)}{\partial \mathbf{C}_b^n} \cdot \mathbf{w} + \frac{u}{v} \cdot \frac{\partial \mathbf{w}}{\partial \mathbf{C}_b^n}$$

$$= -\frac{u}{v^2} \cdot \frac{\partial v}{\partial \mathbf{C}_b^n} \cdot \mathbf{w} + \frac{u}{v} \frac{\partial \mathbf{w}}{\partial \mathbf{C}_b^n}$$

$$= \frac{z - z_p}{\begin{pmatrix} 0 & 0 & 1 \end{pmatrix} \mathbf{C}_b^n \begin{pmatrix} x_f \\ y_f \\ -f \end{pmatrix}} \begin{bmatrix} 1 & 0 & 0 \\ 0 & 1 & 0 \end{bmatrix} \begin{pmatrix} x_f \\ y_f \\ -f \end{pmatrix}$$

$$- \frac{z - z_p}{[\begin{pmatrix} 0 & 0 & 1 \end{pmatrix} \mathbf{C}_b^n \begin{pmatrix} x_f \\ y_f \\ -f \end{pmatrix}]^2} \begin{pmatrix} 0 & 0 & 1 \end{pmatrix} \begin{pmatrix} x_f \\ y_f \\ -f \end{pmatrix} \begin{bmatrix} 1 & 0 & 0 \\ 0 & 1 & 0 \end{bmatrix} \mathbf{C}_b^n \begin{pmatrix} x_f \\ y_f \\ -f \end{pmatrix}$$

$$\frac{\partial \mathbf{z}}{\partial \mathbf{x}_f}\bigg|_{\mathbf{x}_f} = \frac{\partial \left(\frac{u}{v}\right)}{\partial \mathbf{x}_f} \cdot \mathbf{w} + \frac{u}{v} \cdot \frac{\partial \mathbf{w}}{\partial \mathbf{x}_f}$$

$$= -\frac{u}{v^2} \cdot \frac{\partial v}{\partial \mathbf{x}_f} \cdot \mathbf{w} + \frac{u}{v} \frac{\partial \mathbf{w}}{\partial \mathbf{x}_f}$$

$$= \frac{z - z_p}{\begin{pmatrix} 0 & 0 & 1 \end{pmatrix} \mathbf{C}_\mathrm{b}^\mathrm{n} \begin{pmatrix} x_f \\ y_f \\ -f \end{pmatrix}} \begin{bmatrix} 1 & 0 & 0 \\ 0 & 1 & 0 \end{bmatrix} \mathbf{C}_\mathrm{b}^\mathrm{n}$$

$$+ \frac{z - z_p}{\left[\begin{pmatrix} 0 & 0 & 1 \end{pmatrix} \mathbf{C}_\mathrm{b}^\mathrm{n} \begin{pmatrix} x_{fm} \\ y_{fm} \\ -f \end{pmatrix} \right]^2} \begin{pmatrix} 0 & 0 & 1 \end{pmatrix} \mathbf{C}_\mathrm{b}^\mathrm{n} \begin{bmatrix} 1 & 0 & 0 \\ 0 & 1 & 0 \end{bmatrix} \mathbf{C}_\mathrm{b}^\mathrm{n} \begin{pmatrix} x_f \\ y_f \\ -f \end{pmatrix}$$

Appendix B.

2.1 Linear Regression Converted Measurement Covariance

The linear regression implemented at the end of each measurement epoch relies on the converted measurement and its error covariance, $\mathbf{R_x}$ and $\mathbf{R_y}$. It is derived from the measurement equation, Equation (80) or Equation (81), and is dependent on the E/O sensor pixel error, E/O focal length, aircraft altitude, the ground feature location, and the estimates of the INS error provided by the "free"-INS KF. The derivation for the x and y directions is identical, but this derivation considers the x-direction only. From Equation (83),

$$\mathbf{R} = \mathbf{R}_1 + h^2 \mathbf{R}_2$$

where

$$\mathbf{R}_1 = E[\mathbf{v}_1 \cdot \mathbf{v}_1^{\mathrm{T}}], \quad \mathbf{R}_2 = E[\mathbf{v}_2 \cdot \mathbf{v}_2^{\mathrm{T}}],$$

and

$$\mathbf{v}_1 = \begin{pmatrix} \mathbf{m}_{1_0}^{\mathrm{T}} \delta \mathbf{x}_0 - \mathbf{m}_{1_1}^{\mathrm{T}} \delta \mathbf{x}_1 \\ \mathbf{m}_{1_0}^{\mathrm{T}} \delta \mathbf{x}_0 - \mathbf{m}_{1_2}^{\mathrm{T}} \delta \mathbf{x}_2 \\ \vdots \\ \mathbf{m}_{1_0}^{\mathrm{T}} \delta \mathbf{x}_0 - \mathbf{m}_{1_L}^{\mathrm{T}} \delta \mathbf{x}_L \end{pmatrix}_{L \times 1} , \quad \mathbf{v}_2 = \begin{pmatrix} \left(\frac{\delta x_f}{f}\right)_0 - \left(\frac{\delta x_f}{f}\right)_1 \\ \left(\frac{\delta x_f}{f}\right)_0 - \left(\frac{\delta x_f}{f}\right)_2 \\ \vdots \\ \left(\frac{\delta x_f}{f}\right)_0 - \left(\frac{\delta x_f}{f}\right)_L \end{pmatrix}_{L \times 1}$$

thus

$$\mathbf{R}_1 = E[\begin{pmatrix} \mathbf{m}_{1_0}^{\mathrm{T}}\delta\mathbf{x}_0 - \mathbf{m}_{1_1}^{\mathrm{T}}\delta\mathbf{x}_1 \\ \mathbf{m}_{1_0}^{\mathrm{T}}\delta\mathbf{x}_0 - \mathbf{m}_{1_2}^{\mathrm{T}}\delta\mathbf{x}_2 \\ \vdots \\ \mathbf{m}_{1_0}^{\mathrm{T}}\delta\mathbf{x}_0 - \mathbf{m}_{1_L}^{\mathrm{T}}\delta\mathbf{x}_L \end{pmatrix} (\mathbf{m}_{1_0}^{\mathrm{T}}\delta\mathbf{x}_0 - \mathbf{m}_{1_1}^{\mathrm{T}}\delta\mathbf{x}_1, \mathbf{m}_{1_0}^{\mathrm{T}}\delta\mathbf{x}_0 - \mathbf{m}_{1_2}^{\mathrm{T}}\delta\mathbf{x}_2, \cdots, \mathbf{m}_{1_0}^{\mathrm{T}}\delta\mathbf{x}_0 - \mathbf{m}_{1_L}^{\mathrm{T}}\delta\mathbf{x}_L)]$$

(93)

The terms $\delta\mathbf{x}_0$, $\delta\mathbf{x}_1$, ..., $\delta\mathbf{x}_L$ are the "free"-INS navigation state estimation errors; thus, the "free"-INS KF yields estimates of theses estimation errors: $\delta\hat{\mathbf{x}}_0$, $\delta\hat{\mathbf{x}}_1$, ..., $\delta\hat{\mathbf{x}}_L$. Hence, $\delta\mathbf{x}_\ell = \delta\hat{\mathbf{x}}_\ell + \mathbf{e}_\ell$ for $\ell = 0,\ 1,\ ..., L$, where $\mathbf{e}_\ell$ is the KF estimation error. Accordingly, $\mathbf{v}_{\mathbf{x}_1}$ may be written as the sum of two vectors: $\mathbf{v}_{\mathbf{x}_1} = \mathbf{v}_{\mathbf{1}_1} + \mathbf{v}_{\mathbf{1}_2}$, where

$$\mathbf{v}_{1_1} = \begin{pmatrix} \mathbf{m}_{1_0}^{\mathrm{T}}\delta\hat{\mathbf{x}}_0 - \mathbf{m}_{1_1}^{\mathrm{T}}\delta\hat{\mathbf{x}}_1 \\ \mathbf{m}_{1_0}^{\mathrm{T}}\delta\hat{\mathbf{x}}_0 - \mathbf{m}_{1_2}^{\mathrm{T}}\delta\hat{\mathbf{x}}_2 \\ \vdots \\ \mathbf{m}_{1_0}^{\mathrm{T}}\delta\hat{\mathbf{x}}_0 - \mathbf{m}_{1_L}^{\mathrm{T}}\delta\hat{\mathbf{x}}_L \end{pmatrix} \quad \text{and} \quad \mathbf{v}_{1_2} = \begin{pmatrix} \mathbf{m}_{1_0}^{\mathrm{T}}\mathbf{e}_0 - \mathbf{m}_{1_1}^{\mathrm{T}}\mathbf{e}_0 \\ \mathbf{m}_{1_0}^{\mathrm{T}}\mathbf{e}_0 - \mathbf{m}_{1_2}^{\mathrm{T}}\mathbf{e}_1 \\ \vdots \\ \mathbf{m}_{1_0}^{\mathrm{T}}\mathbf{e}_0 - \mathbf{m}_{1_L}^{\mathrm{T}}\mathbf{e}_L \end{pmatrix}$$

(94)

from which we have $\mathbf{R}_1 = \underbrace{\mathbf{v}_{1_1}\mathbf{v}_{1_1}^{\mathrm{T}}}_{\mathbf{R}_{\mathbf{1}_1}} + \underbrace{E[\mathbf{v}_{1_2}\mathbf{v}_{1_2}^{\mathrm{T}}]}_{\mathbf{R}_{1_2}}$. $\mathbf{R}_{1_2}$ is found as follows:

$$\mathbf{R}_{1_2} = E[\mathbf{v}_{1_2}\cdot\mathbf{v}_{1_2}^{\mathrm{T}}] = E[\begin{pmatrix} \mathbf{m}_{1_0}^{\mathrm{T}}\mathbf{e}_0 - \mathbf{m}_{1_1}^{\mathrm{T}}\mathbf{e}_0 \\ \mathbf{m}_{1_0}^{\mathrm{T}}\mathbf{e}_0 - \mathbf{m}_{1_2}^{\mathrm{T}}\mathbf{e}_1 \\ \vdots \\ \mathbf{m}_{1_0}^{\mathrm{T}}\mathbf{e}_0 - \mathbf{m}_{1_L}^{\mathrm{T}}\mathbf{e}_L \end{pmatrix} \cdot (\mathbf{m}_{1_0}^{\mathrm{T}}\mathbf{e}_0 - \mathbf{m}_{1_1}^{\mathrm{T}}\mathbf{e}_0, \mathbf{m}_{1_0}^{\mathrm{T}}\mathbf{e}_0 - \mathbf{m}_{1_2}^{\mathrm{T}}\mathbf{e}_1, ..., \mathbf{m}_{1_0}^{\mathrm{T}}\mathbf{e}_0 - \mathbf{m}_{1_L}^{\mathrm{T}}\mathbf{e}_L)]$$

(95)

The elements of the matrix $\mathbf{R}_{1_2}$ are

$$\mathbf{R}_{1_2(i,j)} = E[(\mathbf{m}_{1_0}^{\mathrm{T}}\mathbf{e}_0 - \mathbf{m}_{1_i}^{\mathrm{T}}\mathbf{e}_i) \cdot (\mathbf{m}_{1_0}^{\mathrm{T}}\mathbf{e}_0 - \mathbf{m}_{1_j}^{\mathrm{T}}\mathbf{e}_j)], \quad \text{for } i = 1, \ ..., L; \ j = i, \ ..., L \qquad (96)$$

which are calculated using the covariance, $\mathbf{P}_{i,j} \triangleq E[\mathbf{e}_i \cdot \mathbf{e}_j^{\mathrm{T}}]$, from the V-INS KF and noting that $\mathbf{P}_{i,j} = \mathbf{P}_{j,i}^{\mathrm{T}}$:

$$\mathbf{R}_{1_2(i,j)} = \mathbf{m}_{1_0}^{\mathrm{T}}\mathbf{P}_0\mathbf{m}_{1_0} - \mathbf{m}_{1_0}^{\mathrm{T}}\mathbf{P}_{0,j}\mathbf{m}_{1_j} - \mathbf{m}_{1_i}^{\mathrm{T}}\mathbf{P}_{0,i}^{\mathrm{T}}\mathbf{m}_{1_0} + \mathbf{m}_{1_i}^{\mathrm{T}}\mathbf{P}_{i,j}\mathbf{m}_{1,j} \qquad (97)$$

Finally, to complete the derivation,

$$\mathbf{R}_2 = E[\begin{pmatrix} \left(\frac{\delta x_f}{f}\right)_0 - \left(\frac{\delta x_f}{f}\right)_1 \\ \left(\frac{\delta x_f}{f}\right)_0 - \left(\frac{\delta x_f}{f}\right)_2 \\ \vdots \\ \left(\frac{\delta x_f}{f}\right)_0 - \left(\frac{\delta x_f}{f}\right)_L \end{pmatrix} \left(\left(\frac{\delta x_f}{f}\right)_0 - \left(\frac{\delta x_f}{f}\right)_1, \left(\frac{\delta x_f}{f}\right)_0 - \left(\frac{\delta x_f}{f}\right)_2, \ ..., \ \left(\frac{\delta x_f}{f}\right)_0 - \left(\frac{\delta x_f}{f}\right)_L \right)]$$

$$(98)$$

which simplifies to

$$\mathbf{R}_2 = \frac{\sigma_c^2}{f^2} \cdot \begin{bmatrix} 2 & 1 & \cdots & 1 \\ 1 & 2 & \ddots & \vdots \\ \vdots & \ddots & \ddots & 1 \\ 1 & \cdots & 1 & 2 \end{bmatrix}_{L \times L} \qquad (99)$$

Bibliography

1. Ben-Afia, Amani, Lina Deambrogio, Daniel Salós, Anne-Christine Escher, Christophe Macabiau, Laurent Soulier, and Vincent Gay-Bellile. "Review and classification of vision-based localisation techniques in unknown environments". *IET Radar, Sonar & Navigation*, 8(9):1059–1072, 2014.

2. Britting, Kenneth R. *Inertial Navigation Systems Analylsis*. John Wiley & Sons, 1971.

3. Brown, Robert Grover and P Y C Hwang. *Introduction to Random Signals and Applied Kalman Filtering*. Wiley, 2012.

4. Crassidis, Jl and Jl Junkins. *Optimal estimation of dynamic systems*. CRC Press LLC, Boca Raton, 2004. ISBN 13: 978-1-4398-3986-7 (eBook - PDF).

5. Divis, Dee Anne. "U.S. Secretary of Defense Wants to Move Past GPS to MEMS–Based Navigation, PNT Experts Doubtful". *Inside GNSS (Online)*, 2015. URL `http://www.insidegnss.com/node/4553`.

6. Fletcher, J, M Veth, and J Raquet. *Real-time fusion of image and inertial sensors for navigation*. Technical report, AFIT, WPAFB, OH, 2007.

7. Fuentes-Pacheco, Jorge, José Ruiz-Ascencio, and Juan Manuel Rendón-Mancha. "Visual simultaneous localization and mapping: a survey". *Artificial Intelligence Review*, 43(1):55–81, 2015.

8. George, Michael and Salah Sukkarieh. "Inertial navigation aided by monocular camera observations of unknown features". *Proceedings - IEEE International Conference on Robotics and Automation*, 3558–3564, Apr 2007.

9. Giebner, M G. *Tightly-coupled image-aided inertial navigation system via a kalman filter.* Masters thesis, AFIT, WPAFB, OH, 2003.

10. Hartley, Richard and Andrew Zisserman. *Multiple View Geometry in Computer Vision.* Cambridge university press, 2003.

11. Honeywell International Inc. "AM-250 Barometric Altimeter". A60-0810-000-001 datasheet, Dec 2008.

12. Hyten, John. "NDIA Luncheon Speech", May 2015. URL `http://www.afspc.af.mil/library/speeches/speech.asp?id=758`. Remarks by General John Hyten at the May 2015 NDIA Luncheon, Peterson AFB, CO.

13. Jones, E. S. and S. Soatto. "Visual-inertial navigation, mapping and localization: A scalable real-time causal approach". *The International Journal of Robotics Research*, 30(4):407–430, jan 2011.

14. Lerro, Don and Yaakov Bar-Shalom. "Tracking with de-biased consistent converted measurements versus EKF". *IEEE Transactions on Aerospace and Electronic Systems*, 29(3):1015–1022, 1993.

15. Lindbergh, Charles A. and Fitzhugh Green. *We.* G.P. Putnam's Sons, New York, 1927.

16. Magree, Daniel and Eric N Johnson. "A Monocular Vision-aided Inertial Navigation System with Improved Numerical Stability". *Proceedings of the AIAA Guidance Navigation and Control Conference, Kissimmee, Florida*, 6–2015. 2015.

17. Maybeck, P S. *Stochastic Models, Estimation, and Control*, volume 2. Academic Press, 1982.

18. Maybeck, Peter S. *Stochastic Models, Estimation, and Control*, volume 1. Academic press, 1982.

19. Mirabile, Anthony T. *Pilot-Assisted Inertial Navigation System Aiding Using Bearings-Only Measurements Taken Over Time.* Masters thesis, AFIT, 2015.

20. Mirabile, Anthony T. "Pilot-Assisted INS Aiding Using Bearings-Only Measurements Taken Over Time". *Proceedings of the 28th International Technical Meeting of the Sattelite Division of Navigation (ION GNSS+ 2015).* Tampa, Florida, 2015.

21. Mueller, F. K. *A History of Inertial Guidance.* Technical report, VITRO CORP of America, 1963.

22. Mutlu, G. *The Navigation Potential of Ground Feature Tracking.* Masters thesis, AFIT, 2009.

23. Nielsen, Michael. *Development and Flight Test of A Robust Optical-Inertial Navigation System Using Low-Cost Sensors.* Masters thesis, AFIT, WPAFB, OF, 2008.

24. Panahandeh, Ghazaleh and Magnus Jansson. "Vision-Aided Inertial Navigation Based on Ground Plane Feature Detection". *Mechatronics, IEEE/ASME Transactions on,* 19(4):1206–1215, 2014. ISSN 1083-4435.

25. Polat, M. *INS Aiding by Tracking An Unknown Ground Object.* Masters thesis, AFIT, WPAFB, OH, 2002.

26. Porter, A E. *INS Aiding Using Passive, Bearings-Only Measurements of an Unknown Stationary Ground Object.* Masters thesi, AFIT, WPAFB, OH, 2003.

27. Potter, Leslie S. *The Navigation of the Air.* Harper and Brothers, New York and London, 1931.

28. Quarmyne, James. *Inertial Navigation System Aiding Using vision.* Masters thesis, AFIT, WPAFB, OH, 2014.

29. Quarmyne, James and Meir Pachter. "Inertial navigation system aiding using vision". *American Control Conference (ACC), 2014*, 85–90. IEEE, 2014.

30. Ratches, James A. "Review of current aided/automatic target acquisition technology for military target acquisition tasks". *Optical Engineering*, 50(7):072001–072001, 2011.

31. Relyea, A L. *Covariance analysis of vision aided navigation by bootstrapping*. Masters thesis, AFIT, WPAFB, OH, 2012.

32. Sazdovski, Vasko and P. M G Silson. "Inertial navigation aided by vision-based simultaneous localization and mapping". *IEEE Sensors Journal*, 11(8):1646–1656, 2011.

33. Shelton, William. "Integrating Air, Space & Cyberspace Capabilities". Washington, DC, Sep 2013. Remarks by General Shelton at the AFA Air and Space Technology Exposition.

34. Simon, D. *Optimal State Estimation: Kalman, H Infinity, and Nonlinear Approaches*. Wiley, 2006.

35. Stevens, Frederick. "Aiding the Inertial Navigation System". *Navigation*, 6(3):166–174, 1958.

36. Titterton, David and John Weston. *Strapdown Inertial Navigation Technology*, volume 17 of *Radar, Sonar and Navigation Series*. IET, second edition, 2004.

37. Tuma, A D. *Automated Driftmeter Fused with Inertial Navigation*. Masters thesis, AFIT, WPAFB, OH, 2014.

38. United States. Dept. of the Air Force. *Air navigation (AF Manual 51-40)*, volume v.1. Air Training Command, Washington, DC, 1959.

39. VectorNav Technologies, LLC . "Inertial Measurement Units and Inertial Naviga-
   tion". (Online Article), 2015. URL `http://www.vectornav.com/support/library/`
   `imu-and-ins`.

40. Veth, M J. *Fusion of imaging and inertial sensors for navigation.* Phd dissertation,
   AFIT, 2006.

REPORT DOCUMENTATION PAGE

Form Approved
OMB No. 0704–0188

1. REPORT DATE *(DD–MM–YYYY)*	2. REPORT TYPE	3. DATES COVERED *(From — To)*
26–03–2016	Master's Thesis	Sept 2014 — Mar 2016

4. TITLE AND SUBTITLE

Visual-INS Using a Human Operator and Converted Measurements

5a. CONTRACT NUMBER

5b. GRANT NUMBER

5c. PROGRAM ELEMENT NUMBER

6. AUTHOR(S)

Montgomery, Turner J, Capt

5d. PROJECT NUMBER

15G454D, 16G113

5e. TASK NUMBER

5f. WORK UNIT NUMBER

7. PERFORMING ORGANIZATION NAME(S) AND ADDRESS(ES)

Air Force Institute of Technology
Graduate School of Engineering and Management (AFIT/EN)
2950 Hobson Way
WPAFB OH 45433-7765

8. PERFORMING ORGANIZATION REPORT NUMBER

AFIT-ENG-MS-16-M-036

9. SPONSORING / MONITORING AGENCY NAME(S) AND ADDRESS(ES)

Air Force Research Laboratory
Attn: Dr. Stewart DeVilbiss
2241 Avonics Dr. bldg 620
WPAFB, OH 45433
Phone: (312)798-4413
Email: stewart.devilbiss.1@us.af.mil; stewart.devilbiss@afit.edu

10. SPONSOR/MONITOR'S ACRONYM(S)

AFRL/RYWN

11. SPONSOR/MONITOR'S REPORT NUMBER(S)

12. DISTRIBUTION / AVAILABILITY STATEMENT

DISTRIBUTION STATEMENT A:
APPROVED FOR PUBLIC RELEASE; DISTRIBUTION UNLIMITED.

13. SUPPLEMENTARY NOTES

This work is declared a work of the U.S. Government and is not subject to copyright protection in the United States.

14. ABSTRACT

A method human operated INS aiding is explored in which the pilot identifies and tracks a ground feature of unknown position over a short measurement epoch using an E/O sensor. One then refers to Visual-INS. In contrast to current research trends, a human operator is entrusted with visually tracking the ground feature. In addition, a less conventional measurement linearization technique is applied to generate "converted" measurements. A linear regression algorithm is then applied to the converted measurements providing an estimate of the INS horizontal velocity error and accelerometer biases. At the completion of the measurement epoch, the INS is corrected by subtracting out the estimated errors. Aiding the INS in this manner provides a significant improvement in the accuracy of the INS-provided aircraft navigation state estimates when compared to those of a free/unaided INS. A number of scenario are simulated including with and without a constrained flight path, with single vs. multiple ground feature tracking sessions, and with a navigation vs. tactical grade INS. Applications for this autonomous navigation approach include navigation in GPS denied environments and/or when RF emitting/receiving sensors are undesirable.

15. SUBJECT TERMS

Vision-Aided Inertial Navigation, Driftmeter, Targeting Pod, Kalman Filter, Simulation, Bearing Measurements

16. SECURITY CLASSIFICATION OF:

a. REPORT	b. ABSTRACT	c. THIS PAGE
U	U	U

17. LIMITATION OF ABSTRACT

U

18. NUMBER OF PAGES

116

19a. NAME OF RESPONSIBLE PERSON

Dr. Meir Pachter, AFIT/ENG

19b. TELEPHONE NUMBER *(include area code)*

(937) 255-3636, x7247; meir.pachter@afit.edu

Standard Form 298 (Rev. 8–98)
Prescribed by ANSI Std. Z39.18